Année 2013 N° d'ordre : 41196

Université Lille1 Sciences et Technologies
Laboratoire Génie Civil et géo-Environnement
École Doctorale Sciences Pour l'Ingénieur

THÈSE

pour l'obtention du grade de
Docteur de L'Université Lille1 Sciences et Technologies
spécialité Génie Civil – Géotechnique

NUMERICAL STUDY OF THE THERMO-ACTIVE PILES BEHAVIOR IN COHESIONLESS SOILS

---

par

Maria Elizabeth SURYATRIYASTUTI

présentée et soutenue publiquement **le 30 septembre 2013**
devant le jury constitué de :

Président :	Roger FRANK	Professeur, École des Ponts ParisTech
Rapporteurs :	Lyesse LALOUI	Professeur, EPFL Suisse
	Fabrice EMERIAULT	Professeur, INP Grenoble
Examinateurs :	Isam SHAHROUR	Professeur, Université Lille1
	Farimah MASROURI	Professeur, Université de Lorraine - ENSG
	Sébastien BURLON	Ingénieur de recherche, IFSTTAR
Directeur de thèse :	Hussein MROUEH	Professeur, Université Lille1

ACKNOWLEDGMENTS

My deepest gratitude goes first and foremost to my research director, Prof. Hussein MROUEH, who fully entrusted me to undertake this doctoral research project and welcomed me very warmly to his research team. My extended gratitude goes to Dr. Sébastien BURLON who also supervised me all along this research. It is an honor for me to have two excellent tutors with two complementary viewpoints: scientific and practical. Without their clear guidance, continuous encouragement and openness towards my opinions, I would not have completed my PhD dissertation. I also thank to them for the knowledge transfer, fruitful discussions and helpful advices that kept me persistently enthusiastic about this research.

I would like to sincerely thank Prof. Roger FRANK, the president of International Society for Soil Mechanics and Geotechnical Engineering, who gave me the honor of chairing my PhD Committee. I also express my gratitude to Prof. Lyesse LALOUI and Prof. Fabrice EMERIAULT for their attentive review on my manuscript despite their huge responsibilities elsewhere. I also want to thank Prof. Farimah MASROURI for her interest to examine my research. My appreciation also extends to Prof. Isam SHAHROUR, the director of LGCgE where I am affiliated, not only for agreeing to be part of the jury but also for being available anytime to discuss about my work's difficulties.

I would like to express my respectful gratitude to all my jury for their constructive remarks that enriched the quality of my PhD dissertation. I did truly benefit from their professional experiences through the priceless discussion during my defense.

Thank you to all the colleagues and partners in the ANR project « GECKO » in which this doctoral research takes part: ECOME, BRGM, IFSTTAR, CETE Nord Picardie, LEMTA–Université de Lorraine and EPFL. My particular thanks go to Jean-Baptiste BERNARD (ECOME), Julien HABERT (CETE Nord Picardie) and Charles MARAGNA (BRGM) for the idea exchanges and data sharing.

I wish to express my very special thanks to my colleagues who granted their time for the proofreading of my research's work, either for the thesis or the published articles: Anti, Riza, Johanes, Faten, Jesse, and Irene.

Over the last three years in the LGCgE, I was supported by friendly familial relationships and interesting scientific exchanges with the PhD colleagues, permanent lecturers/researchers and administrative staffs, whom I thank warmly. I think particularly to Wei and Hind with whom I shared the ups and downs of PhD's life and to Yustian by whom I learned a lot of soil and foundation behaviors. My warm thanks also extend to the teaching colleagues in the department « Licence/Master » at Polytech'Lille with whom I worked with pleasure between research and teaching.

My acknowledgments would not be complete without expressing my profound gratitude to all my former teachers in Civil Engineering Department, University of Indonesia who constantly encourage me to pursue my academic career. More specifically, I want to thank Prof. Irwan KATILI, the Chief of Civil Engineering Department, for all what he has done.

I have to thank François. His support both scientifically and personally have provided the serenity during this thesis' completion.

Finally, I am indebted to my parents, my big family and my beloved best friends in Jakarta, Indonesia for their endless love and infinite understanding. This thesis belongs to them.

to my beloved parents,

my two favorite Lecturers/Researchers ever…

ABSTRACT

The recent technology for the heating/cooling building system, known as thermo-active piles, has effectively reduced the land use area and drilling cost by incorporating the vertical closed-loop heat exchanger pipes into the pile foundations. The heat transfer principle remains the same with the conventional ground heat exchanger system: an extraction of the steady ground temperature during winter and a recharge of the ground thermal energy during summer. Indeed, the energy transfer in the thermo-active pile system is becoming more complex owing to the thermo-hydro-mechanical interaction between the ground, the aquifer, the concrete pile, and the overlying building. Recently in France, the implementation of this novelty faces some difficulties due to the lack of understanding about the potential impact of seasonal temperature cycles on the environmental sustainability and the structural safety. Considering those concerns, this thesis conducts the study of the thermo-active piles behavior and their interaction with the structure and the environment in the intention to optimize the geotechnical design of such piles according to the French design standard for the deep foundations.

First of all, a study of the physical phenomena occurring in the entire system under the thermo-hydro-mechanical interactions is conducted. Since the ratio of the pile diameter to the pile length is very small, the temperature variations in the pile affect mainly the pile axial response. Thus, the study interest is narrowed to the impact of temperature cycles on the pile bearing capacity by paying a particular attention on modeling the soil–structure interaction with finite difference method. A set of three-dimensional numerical models is performed to understand the thermo-active piles response located in cohesionless soil with consideration of several loading stages and various restraint conditions. The first model concerns a single thermo-active pile subjected to a single thermal load, the second deals with a single thermo-active pile under combined axial mechanical and cyclic thermal loads, and the third one is related to the thermo-active piles located in a group of piles to observe the influence on the other classical bearing piles. The need to properly render the cyclic plasticity behavior in such piles is provided by modeling the interface elements at the soil–pile contact zone using the laboratory-developed law named ‘Modjoin’ law. Otherwise, the load transfer *t–z* method in one-dimensional model can be an alternative solution in the practical geotechnical design, but no *t–z* law that takes into account the cyclic fatigue effects exists yet. This study carries out a development of the existing *t–z* law by integrating the nonlinearity condition and cyclic hardening rules.

Keywords: numerical modeling, three-dimensional model, soil–pile interface, nonlinearity, thermo-mechanical loading, cyclic loading, thermo-active piles

RÉSUMÉ

Les pieux énergétiques constituent une technique récente permettant d'une part le chauffage et la climatisation de bâtiments et assurant d'autre part le rôle de fondations profondes. Cette technique consiste à mettre en place dans des fondations profondes classiques un système échangeur de chaleur. Le principe de transfert de chaleur est similaire à celui utilisé pour des systèmes échangeurs de chaleur conventionnels : un fluide caloporteur permet d'extraire de l'énergie thermique du sol durant l'hiver et d'en injecter durant l'été. Dans le cas de pieux énergétiques, l'interaction entre le sol, le pieu et la structure ne fait pas seulement appel à des considérations mécaniques mais exigent de tenir compte d'aspects thermiques et hydrauliques, ce qui rend relativement complexe la compréhension globale du comportement d'un pieu énergétique. Actuellement, en France, la réalisation effective de pieux énergétiques rencontre un certain nombre de difficultés qui sont en partie liées à une connaissance insuffisante des effets des cycles de température sur la pérennité d'un système de fondations constitué de pieux échangeurs de chaleur. L'objectif de ce mémoire est d'apporter quelques éclairages sur ce sujet, notamment dans le but de contribuer, à terme, à l'élaboration de règles de calcul simples de la portance des fondations profondes énergétiques.

Tout d'abord, une synthèse des phénomènes physiques régissant l'interaction thermo-hydro-mécaniques mis en jeu est présentée. Ensuite, considérant le rapport entre le diamètre d'un pieu et sa longueur suffisamment faible, les travaux réalisés se focalisent essentiellement sur les problématiques liées à l'allongement et au raccourcissement du pieu dans sa direction axiale. Différentes modélisation numériques sont effectuées par la méthode des différences finies pour étudier la réponse de pieux énergétiques dans des terrains sans cohésion en tenant compte de différentes conditions aux limites. Le premier modèle est relatif à un pieu énergétique isolé soumis à une seule charge thermique. Le second traite d'un pieu énergétique isolé soumis à une charge axiale mécanique et des variations de température. Le troisième porte sur le comportement des pieux énergétiques appartenant à un groupe de pieux. L'analyse porte en particulier sur l'interaction entre ces pieux et les autres pieux classiques. Dans tous les cas, afin de rendre compte correctement des effets cycliques, l'interface sol-pieu est modélisée par la loi 'Modjoin' développée au LGCgE. Enfin, un modèle unidimensionnel basé sur la méthode de courbes de transfert de type *t–z* est mis en œuvre. Une loi *t–z* prenant en compte les effets de chargements cycliques est mise au point. Elle permet notamment de gérer la non-linéarité des phénomènes cycliques et de rendre compte de différents types d'écrouissage.

Mots-clés: modélisation numérique, calcul tridimensionnel, interface sol–pieu, non-linéarité, chargement thermomécanique, chargement cyclique, pieu énergétique

TABLE OF CONTENTS

LIST OF FIGURES

LIST OF TABLES

NOMENCLATURE

Greek symbols

α	hardening function in the constitutive laws of interface behavior (Section1.4.2.3)	
α	parameter controlling the slope of the proposed *t–z* function	m
α_T	thermal expansion coefficient	°C^{-1}
β	parameter controlling the amplitude of peak of strain hardening for the monotonic part in the proposed *t–z* function	kPa
β^c	parameter controlling the rate of kinematic hardening in the Modjoin law	–
β_m	coefficient of compressibility	Pa^{-1}
γ	shear deformation	μdef
γ	parameter controlling the rate of strain hardening for the monotonic part in the proposed *t–z* function	m
γ^c	parameter controlling the amplitude of kinematic hardening in the Modjoin law	kPa/m
δ	parameter controlling the rate of loading in the proposed *t–z* function	–
ΔT	temperature gradient	°C
ε	deformation	μdef
ε	parameter controlling the rate of cyclic hardening in the proposed *t–z* function	m
η	turtuosity factor	
θ	water content	%
λ	plastic multiplier in the constitutive laws of interface behavior	
λ_T	thermal conductivity of material	W/m °C
μ	coefficient of friction	
ν	Poisson's ratio	
ξ	parameter controlling the rate of cyclic degradation in the proposed	–

	t–z function	
ρ	parameter controlling the amplitude of cyclic degradation in the proposed *t–z* function	–
ρ_c	density of material	kg/m^3
σ	stress	kPa
σ_n	normal stress in interface	kPa
τ	shear stress	kPa
φ	friction angle	°
ψ	water potential head	m
Ψ	dilation angle	°
ω	annual radial frequency ($2\pi/365$)	°
ϕ	porosity factor	

Roman letters

a	air content	%
a_c	parameter controlling the rate of phase change (conractancy–dilatancy) in the Modjoin law	–
A	area	m^2
ADR	parameter controlling the rate of isotropic hardening in the Modjoin law	–
B	width of rectangular pile	m
B_r	width of raft	m
c	cohesion	kPa
c_T	specific heat extraction of solid mineral	J/kg °C
C_v	volumetric heat capacity	J/m^3°C
COP	coefficient of performance of the heat pump	
d	damping depth	m
D	pile diameter	m
D_θ	isothermal diffusivity	m^2/s
D_T	thermal diffusivity	m^2/s
DR	parameter controlling the amplitude of isotropic hardening in the Modjoin law	–
E	Young's modulus	MPa

E_M	Menard's pressuremeter modulus	MPa
f	surface yield limit function	
g	potential plastic function	
g	gravitational acceleration	9,8 m/s^2
G	shear modulus	MPa
GP	group pile without cap	
H	total soil moisture potential (used only in Chapter 1.2)	m
H	pile length (used throughout Chapter 2 to 5)	m
J_2	second deviatoric stress invariant	
k_b	slope for the bearing stress vs. base displacement in the Frank & Zhao law	
k_n	normal stiffness of interface	MN/m
k_s	shear stiffness of interaface	MN/m
k_t	slope for the shaft friction vs. displacement in the Frank & Zhao law	
k_w	hydraulic conductivity	m/s
K	bulk modulus	MPa
K_h	head axial fixity	
K_{ps}	soil–pile relative stiffness	
K_{rs}	raft–soil stiffness	
L	length	m
L_v	Latent heat	J/kg
n	number of cycles (used throughout Chapter 2 to 5)	
N	normal force	kN
p	pore pressure	kPa
p	mean principal stress of soil in p–q space	kPa
p_{LM}	Menard's pressure limit	MPa
P	applied force	kN
$\overline{P}$	mean applied force	kN
P_W	applied mechanical working load	kN
P_{HP}	heat pump power	kW
q	deviatoric stress of soil in p–q space	kPa
$\vec{q}$	flux	W/m^2
q_b	bearing stress	MPa

q_s	shaft friction	kPa
Q	external force	MPa
$\dot{Q}$	heat energy	W
r	pile radius	m
$\dot{r}$	internal volumetric heat	W/m^3
R_c	kinematic hardening function in the Modjoin law	
R_{max}	isotropic hardening function in the Modjoin law	
SP	single pile	
t	time	s
t_r	thickness of raft	m
T	temperature	°C
T_{ave}	annual mean ground temperature	°C
u_n	normal displacement of interface	m
u_t	tangential displacement of interface	m
$\vec{v}$	velocity / flow	m/s
w	axial displacement	m
w_b	tip or base displacement	m
z	depth	m

Subscripts

$_{atm}$	atmospheric
$_b$	pile base
$_h$	pile head
$_l$	liquid phase
$_s$	pile shaft
$_s$	solid mineral
$_v$	vapor phase
$_w$	water components

Superscripts

^{e}	elastic part
^{mec}	mechanical loading
^{n}	combined loading (working load + cyclic thermal load)
^{p}	plastic part
th	thermal loading

NB: The sign convention used throughout this dissertation is the usual convention in soil mechanics, i.e. compression is positive.

GENERAL INTRODUCTION

The construction of thermo-active piles has grown fast over the last 30 years as a result of the forthcoming increase in the fuel energy cost. As a part of ground heat exchanger (GHE) system, this technology consists of circulating a heat carrier fluid inside a pile foundation which will exchange the heat energy with the surrounding ground. This technology is addressed to produce both heating and cooling of the building in accordance with the seasonal energy demand, using the ground as a heat source in the winter and as a heat sink in the summer. Therefore, the fluid circulating in the piles is set to vary from –10°C to +35°C of the steady ground temperature (Kavanaugh 2010; Laloui and Di Donna 2011). Accordingly, the pile foundations act as structural bearing and heat exchanger elements, supporting not only the permanent and transient loads of the overlying structure but also a cycle of temperature loads injected in the foundation.

As the ground is a porous medium, the heat transfer process in the thermo-active pile system reveals a complex thermo-hydro-mechanical coupling. The issue of heat transfer in a saturated or unsaturated soil is highlighted in the first place. Since the transfer is related to the types of the soil, the soil permeability, and the soil hydraulic gradient; the heat transfer in the system can be considered in two phenomena: (i) the conduction phenomenon between the pile and the ground and (ii) the advection phenomenon carried by the groundwater flow, with respect to the very little contribution of the evaporation and solar radiation phenomena. The additional stress induced by temperature variations in the pile foundations is regarded as the second major issue. The foundations undergo a combined thermo-mechanical loading and thus alter the pile behavior, in particular at the soil–pile interface (Bourne-Webb *et al.* 2009; Laloui *et al.* 1999). Consequently, the design and the dimensioning of this type of foundations should carefully consider the additional thermal stress.

Recently in France, the design of thermo-active foundations has been the major discussion among the geotechnical experts, concerning the interaction problems between the foundations, the surrounding ground, and the upper-structure. Despite the successful number of thermo-active pile installations in European countries such as in Austria, Switzerland, Germany and UK (Adam and Markiewicz 2009; Brandl 2006; Katzenbach *et al.* 2008; Pahud and Hubbuch 2007a), the uptake of this technology in France has not been commercialized yet due to concerns in the construction codes about the potential impact of temperature cycles on the geotechnical performance. Over the long-term thermal operation, the environmentalists concern about the sustainability of the ground energy while the building's insurers concern about the safety of the structural foundation. On the one hand, an over-heated ground or a frozen ground during seasonal thermal operation may develop if the energy balance of the system is failed to achieve. On the other hand, the expansion and contraction of the piles under temperature variations may cause several detrimental effects in the foundation system. It is therefore necessary to ensure that the cycles of temperature injected in the piles will not change (i) the ground soil characteristics, i.e. the ground temperature equilibrium and the groundwater level, and (ii) the load-bearing pile capacity, i.e. the foundation settlement, the allowable concrete stresses, and the bearing resistance.

Based on the actual condition in France, this PhD research intends to respond to those concerns in the intention to optimize the design of the thermo-active piles according to the French design standard for the deep foundations. The study is divided into two major works: the understanding of the physical interaction phenomena in the system and the analyses of the thermo-active piles behavior with numerical modeling methods. Chapter 1 summarizes the state of the art of the thermo-active foundations to identify the principal needs in the geotechnical design of such piles. The energy transfer and the related thermo-hydro-mechanical interaction in the system are presented. A particular attention is paid to the review of modeling the geotechnical capacity of piles under cyclic thermo-mechanical loading. Two modeling approaches are proposed (one-dimensional and three-dimensional) and the existing constitutive laws under cyclic loadings for both approaches are presented.

Thereafter, the study focuses on numerical modeling of the thermo-active piles behavior. Several study limitations are made for the sake of simplicity, such as only thermo-mechanical coupling is considered for the axially loaded piles located in a saturated granular soil. To beginning with, Chapter 2 presents a simplified thermal diffusion analysis of a thermo-active pile to the surrounding soil over a single thermal load. In the first stage, an internal diffusion inside the pile is modeled to determine the temperature produced in the pile and at the pile perimeter in contact with the ground soil. The influence of the different types of absorber pipe as well as the seasonal phases of thermal loading is discussed. In the second stage, macro-scale diffusion between the pile and the surrounding soil is performed using a thermo-mechanical coupling analysis to observe the effect of temperature gradient on the pile behavior.

Approaching reality in the construction industry, this research study has a particular interest on the soil–pile interaction design of the thermo-active piles by modeling interface elements at the soil–pile contact zone. Considerations of the combined loads (i.e. mechanical working and thermal loads) as well as the cyclic fatigue effects during thermal cycles are taken into account. In line with those interests, the need of using an appropriate behavior law under cyclic loading arises together with the demand of using a practical tool in dimensioning the foundations. Therefore, a constitutive law of soil–pile interface behavior developed in the laboratory, the Modjoin law, is employed in the 3D analysis of the thermo-active piles behavior. Through this sophisticated law with the help of a finite difference code, the soil–pile–structure interaction analyses of a single thermo-active pile (in Chapter 3) and of thermo-active piles within a group of piles (in Chapter 4) are conducted. In Chapter 5, a development of a proposed *t–z* cyclic function using the load transfer method is presented. The proposed function is then implemented into a computer program in order to analyze the behavior of a single thermo-active pile in 1D. Results of the two modeling approaches are compared to show the capability of the two behavior laws in rendering the cyclic fatigue phenomena. In the end, the numerical results in terms of the percentage of change in pile behavior induced by temperature variations can estimate the range of safety margin for the geotechnical design of the thermo-active piles.

CHAPTER 1
THERMO-ACTIVE PILES: PHYSICAL PROCESS AND GEOTECHNICAL CHALLENGES*

1.1 Introduction

A recent technology for the heating/cooling building system, well-known as thermo-active piles, which integrates the structural foundations of buildings with the vertical closed-loop heat exchanger pipes has successfully became the innovative perfection of the ground heat exchanger (GHE) systems (Figure 1.1). Compared to the conventional GHE systems, the thermo-active piles give benefits in preventing the groundwater pollution vis-à-vis the open loop system, reducing the land area use vis-à-vis the horizontal closed-loop system and economizing the drilling cost vis-à-vis the vertical closed-loop system (Brandl 2006). Moreover, the thermal conductivity of concrete pile foundations is two times higher than that of backfill grout (Brandl 2006), which leads this technology to produce a higher output energy among the other GHE systems.

Like every GHE system, the thermo-active piles exchange heat with the ground by using the earth as a heat source in the winter or a heat sink in the summer. The ground soil, in where lies the geothermal energy, has a relatively steady temperature of approximately 10–15 °C within the depth of 10–20 m in most European countries (i.e. shallow geothermal energy) (Brandl 2006; Saner 2001). To satisfy the double needs in heating and cooling the buildings throughout the year, the heat carrier fluid circulating inside the exchanger pipes is usually set at 11–19 °C above the steady ground temperature in the summer mode and at 6–8°C below the steady ground temperature in the winter mode (Kavanaugh 2010). The fluid should contain an anti-freeze solution

* Some of the materials presented in this chapter have been published in [SUR 14], [SUR 13c] and [SUR 12a] as listed in Appendix C

(i.e. propylene glycol) in order to avoid freezing at the pipes inclination angle and should also contain additives to prevent corrosion at the valves or the heat pump (Brandl 2006). The vertical closed-loop exchanger pipes inserted inside the concrete piles are generally made from high density polyethylene (HDPE), which functions to transport the circulating fluid to the heat pump. This latter increases the fluid temperature level to a usable room temperature with a small amount of electricity input (Lund *et al.* 2004). For each kWh of heating output, only 0,22–0,3 kWh of electricity is required to operate the heat pump (Saner 2001). Finally, the heat produced from the heat pump is then distributed to the building via the collective heating/cooling pipe works embedded in the floors or walls of the buildings.

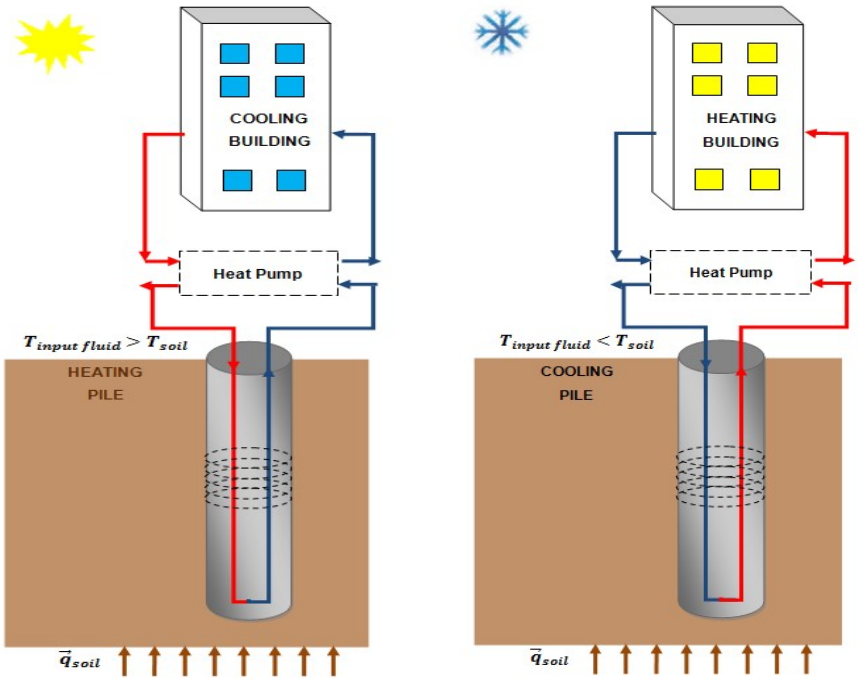

Figure 1.1 – Schema of energy transfer in the thermo-active pile system (Suryatriyastuti *et al.* 2012)

Since the inception of this technology in 1984 in Austria, the implementation of such foundations has been realized in several European construction projects, such as: the high-rise Main Tower in Frankfurt (Ennigkeit and Katzenbach 2001; Katzenbach *et al.* 2008), the Dock Midfield terminal at Zurich airport (Pahud and Hubbuch 2007a; Pahud and Hubbuch 2007b), the Lainzer Tunnel in Vienna (Adam 2008; Markiewicz *et al.* 2005), and the One New Change complex in London that has successfully delivered the heating/cooling for urban city (Crawley *et al.* 2011; Devriendt *et al.* 2012). In line with

the interests of GHE systems to provide an environmentally friendly technology, the installation of thermo-active piles in UK has recorded 4294 tones of annual CO_2 saved in 2011 (Boranyak 2013). Moreover, in the context of the heat production capacity, a thermo-active pile foundation can extract the ground energy of approximately 80 W/m during the seasonal energy storage system (Boënnec 2008) depending on the soil conditions and the pile length (Brandl 2006). The system efficiency can reach up to 5,1 of the heat pump's *COP* (Pahud and Hubbuch 2007a) and thus reduces the running and life-cycle costs (Brandl 2013). For example, the Zurich airport reported the cost saving up to €36900 relative to the conventional system with the annual thermal cost of €0,04/kWh (Pahud and Hubbuch 2007a).

Despite their remarkable benefits, the thermo-active piles technology still leaves several issues in geotechnical viewpoint. The thermal transfer between fluid, concrete and soil depends strongly on the hydrological properties of soil and thus generates the thermo-hydro-mechanical interaction between the soil and concrete. For 1°C of increased temperature, the pile axial stress increases of approximately 100–200 kPa and the shaft friction mobilized at the soil–pile interface varies in the range of –2,1 to +2,5 kPa between the upper-half and the lower-half of the pile (Amatya *et al.* 2012; Bourne-Webb *et al.* 2009; Laloui *et al.* 2006). Any restraint applied at the pile extremity and any permanent load of structure applied at the pile head will change the values of the thermally-induced stress (Amatya *et al.* 2012; Bourne-Webb *et al.* 2009). It is worth mentioning that the injected fluid temperature varies over the season so the pile foundation system undergoes cyclic thermal loads that may degrade the soil–pile capacity. Besides, a design standard that takes into account the thermal interaction within the foundation system has not been established yet (Knellwolf *et al.* 2011) thus leads to the cautious and inefficient geotechnical dimensioning (Boënnec 2009).

Based on the state of the art of the thermo-active piles presented above, in the first time this chapter will discuss about the physical transfer process within the system, then derive the additional mechanical stress induced by the thermo-hydro transfer in the foundations, and finally describe the approach methods used in this study in order to better designing the geotechnical capacity of the thermo-active piles.

1.2 Physical process of energy transfer in the thermo-active foundations

Heat transfer within the thermo-active pile systems is a very complex thermodynamic process. Heat convection flows through the fluid circulating in the exchanger pipes, heat conduction occurs within the concrete piles and also the soil grains, heat advection comes through the groundwater flow, vapor diffusion and latent heat during the evaporation–condensation cycles of the groundwater might only be possible in partially-saturated or unsaturated soil, and evaporation–radiation at the soil surface contributes very little to the transfer (Suryatriyastuti *et al.* 2012). The process depends on the type of the soil and its water content, the presence of groundwater and the soil hydraulic gradient. This study takes a consideration that the heat transfer in thermo-active pile system can be simplified into two phenomena: the conduction phenomenon between the pile–the ground and the advection phenomenon carried by the groundwater flow.

1.2.1 Thermo-hydro-mechanical properties

1.2.1.1 Intrinsic properties

The heat flux is transmitted principally by thermal conductivity λ_T and volumetric heat capacity C_v of the transfer medium. Volumetric heat capacity indicates the ability of a substance to store heat energy, which is a product of material density ρ_c with specific heat extraction c_T. These properties are strongly related to the mineral compositions of the soil (i.e. solid mineral "*s*" or water liquid "*w*") and the porosity factor ϕ, as given in equations 1.1–1.2.

$$C_v = (1-\phi)(\rho_c c_T)_s + \phi(\rho_c c_T)_w \quad [1.1]$$

$$\lambda = (1-\phi)(\lambda_T)_s + \phi(\lambda_T)_w \quad [1.2]$$

The ratio of thermal conductivity to the volumetric heat capacity is called thermal diffusivity $D_T = \lambda_T/C_v$, which refers to a value of the diffusion rate of a material. For

heat advection flux and vapor flux, hydraulic conductivity k_w, potential head ψ, and latent heat L_v are the other major properties that govern the transfer. The values of heat transfer properties depend on the type and size of grains, the water content θ and the air content a. For example, moist or saturated soil has a thermal capacity greater than that of dry soil since the thermal conductivity of dry soil is about five times lower than that of saturated soil (Riederer *et al.* 2007). Otherwise, granular soil has a hydraulic conductivity approximately three orders of magnitude greater than fine soil due to their larger grain size (Deru and Kirkpatrick 2001). The values of hydraulic and thermal properties of soil according to the soil type are summarized in Table 1.1.

Table 1.1 – Thermal and hydraulic properties in soil (Riederer *et al.* 2007)

Soil type	*Hydraulic conductivity* k_w *(m/s)*	*Thermal conductivity* λ_T *(W/m K)*		*Volumetric heat capacity* C_v *(MJ/m³K)*	
		Non saturated	*Saturated*	*Non saturated*	*Saturated*
Clay	$10^{-8} – 10^{-10}$	0,2 – 0,3	1,1 – 1,6	0,3 – 0,6	2,1 – 3,2
Silt	$10^{-5} – 10^{-8}$	0,2 – 0,3	1,2 – 2,5	0,6 – 1,0	2,1 – 2,4
Sand	$10^{-3} – 10^{-4}$	0,3 – 0,4	1,7 – 3,2	1,0 – 1,3	2,2 – 2,4
Rock	$10^{-1} – 10^{-3}$	0,3 – 0,4	1,8 – 3,3	1,2 – 1,6	2,2 – 2,4

1.2.1.2 Ground temperature

In the uppermost few meters, the ground temperature T varies with time and depth at the heterothermal zone of soil (Burger *et al.* 1985). The variation with time $T(t)$ is generally caused by external temperature (i.e. air temperature and solar radiation) while the propagation in depth $T(z)$ is related to the heat flux and internal terrestrial heat in the soil. The variation of ground temperature forms a sinusoidal function as expressed in the following equation (Hillel 2004):

$$T(z,t) = T_{ave} + A_0 e^{-\frac{z}{d}} \left(\sin\left(\omega t - \frac{z}{d} \right) \right) \qquad [1.3]$$

where T_{ave} and A_0 denote the annual mean ground temperature and the maximum annual amplitude of ground temperature, respectively. d indicates a damping depth of the

annual fluctuation which is given by $d = (2D_h/\omega)^{1/2}$, where D_T is thermal diffusivity of soil and ω is annual radial frequency ($2\pi/365$).

Fluctuation in ground temperature diminishes with depth and becomes steady to the annual mean ground temperature at the soil neutral zone, in where the shallow geothermal energy lies (Burger *et al.* 1985). In European countries, the steady annual mean ground temperature is on the order of 10–15°C beneath 10 m of depth (Brandl 2006; Saner 2001). More than 50 m below the surface, the ground temperature increases regularly with depth with a deep geothermal gradient of 3°C per 100 m (Saner 2001).

1.2.1.3 Groundwater flow

Soil with moving groundwater propagates heat much faster than that without groundwater flow and, therefore, increases the specific heat extraction/injection capacity up to 15–50% (Ma and Grabe 2010; Riederer *et al.* 2007; Saner 2001). Indeed, a sufficiently large groundwater flow of approximately 35 m/year conducts to a natural thermal regeneration of soil (Fromentin *et al.* 1999; Riederer *et al.* 2007) that is advantageous for the thermo-active pile system. The amount of heat extracted during winter no longer depends on the amount of heat injected during summer, thus the equilibrium of ground temperature is guaranteed (Laloui and Di Donna 2011). In this case, the surrounding soil will not be affected by thermal volumetric variations. However, ground water flow can also have a negative effect if subsoil thermal energy storage is intended during system operation, as the stored heat is then carried away (Hofinger *et al.* 2010).

The groundwater flow changes due to the variation of water content (i.e. hydraulic gradient) and temperature in both liquid and vapor phases. In general, the flow due to hydraulic gradient is greater than the flow arising from the temperature gradient, for both very dry (unsaturated) and very wet (saturated) media (Hadley and Eisenstadt 1955; Philip and de Vries 1957). The water content variation is led by the isothermal diffusivity D_θ while the temperature variation is controlled by the thermal diffusivity D_T. When the soil is saturated, all pores are full of water and participate in the water transport. In this case, only the liquid transfer is counted in the groundwater flow. When

the soil is desaturated, the water movement takes place through thinner and thinner pores and using more tortuous ways. Hence, the liquid diffusivity tends to play the most important role in saturated soil while the vapor diffusivity is dominant in unsaturated soil (Philip and de Vries 1957). It is therefore important to separate distinctly the groundwater movement in the liquid and vapor transfer for the case of saturated soil and unsaturated soil.

Liquid flow in saturated soil

In liquid phase, the movement of groundwater v_l is governed by the Darcy's law. Darcy stated that the flow is a product of the hydraulic conductivity k_w with the hydraulic gradient as expressed in equation 1.4. In hydrogeology, the hydraulic gradient is approximated by the finite difference ratio $\Delta H/\Delta l$, where H is the total soil moisture potential: $H = \psi + z$. ψ is the pressure potential (matric potential in units of length) and z is the elevation above a reference plan. The segment of length Δl along the streamlines can have any orientation in space, even against gravity, depending on the direction of the flow.

$$\vec{v}_l = -k_w \, grad\, H = -k_w \, grad\left(\psi(\theta,T) + z\right) \qquad [1.4]$$

The liquid flow can be derived in the following relation (Deru and Kirkpatrick 2001; Parlange *et al.* 1998; Piechowski 1999):

$$\vec{v}_l = -k_w \left(\frac{\partial \psi}{\partial \theta} grad\theta - \frac{\partial \psi}{\partial T} gradT - 1 \right) \qquad [1.5]$$

$$\vec{v}_l = -D_{\theta l} grad\theta - D_{Tl} gradT - k_w \qquad [1.6]$$

where $D_{\theta l}$ and D_{Tl} denote the isothermal and thermal liquid diffusivity, respectively.

Vapor flow in unsaturated soil

Movement in vapor phase v_p is the diffusion of water vapor in the air-filled pores which generally takes place in unsaturated soil. The flow can be approximated by modifying

the diffusion law of Fick as below (Deru and Kirkpatrick 2001; Parlange *et al.* 1998; Piechowski 1999):

$$\vec{v}_v = -D_{\theta v}\, grad\theta - D_{Tv}\, gradT \qquad [1.7]$$

where $D_{\theta v}$ and D_{Tv} indicate the isothermal and thermal vapor diffusivity, respectively. The two vapor diffusivities are related to the vapor diffusivity at atmospheric condition D_{atm}, the turtousity factor η, the air content a, the gas pressure (g/RT), and also the vapor pressure ρ_v and water pressure ρ_w. The derivation of the two vapor diffusivities is given in the following equations 1.8–1.10 (Deru and Kirkpatrick 2001; Parlange *et al.* 1998; Piechowski 1999).

$$D_{\theta v} = \eta a D_{atm} \frac{g}{RT} \frac{\rho_v}{\rho_w} \frac{\partial \psi}{\partial \theta} \qquad [1.8]$$

$$D_{Tv} = \frac{\eta a D_{atm}}{\rho_w} \frac{\partial \rho_v}{\partial T} \qquad [1.9]$$

$$D_{atm} = 2290\left(1 + \frac{T}{273}\right)^{1.75} \qquad [1.10]$$

1.2.2 Energy conservation

1.2.2.1 In the soil

If the surrounding soil has a substantial moving groundwater, the heat advection transfer cannot be ignored. The energy conservation in the thermo-active pile system should take into account the soil hydraulic gradient, i.e. the liquid flow in saturated soil and the vapor flow in unsaturated soil. In some cases, latent heat could be produced in unsaturated soil by the change in water phase.

It is worth mentioning that the flow due to temperature gradient is not significant thus can be neglected. Therefore, the energy conversation in saturated soil with a substantial moving groundwater can be estimated by the following relation:

$$C_v \frac{\partial T}{\partial t} = div\left(\lambda\, grad\, T\right) - \rho_l c_l k_w\, grad\psi\, grad\, T - \rho_l c_l k_w\, grad\, T \qquad [1.11]$$

where ρ_l and c_l denote the mass density and specific heat extraction for the water in liquid phase.

In unsaturated soil with a substantial moving groundwater, the energy conservation can be expressed by:

$$C_v \frac{\partial T}{\partial t} = div\left(\lambda\, grad\, T\right) - \rho_v c_v \left(D_{\theta v}\, grad\, \theta\right) grad\, T - L_v\, div\left(D_{\theta v}\, grad\, \theta\right) \qquad [1.12]$$

where ρ_v and c_v denote the mass density and specific heat extraction for the water in vapor phase.

If there is no groundwater flow in the surrounding soil, the heat transfer in the thermo-active pile system is limited to pure heat conduction, with an addition of vapor latent transfer only in partially-saturated or unsaturated soil. Equations 1.13 and 1.14 are used to solve the energy conservation in saturated and unsaturated soil, respectively.

For saturated soil without groundwater flow:

$$C_v \frac{\partial T}{\partial t} = div\left(\lambda\, grad\, T\right) \qquad [1.13]$$

and for unsaturated soil without groundwater flow:

$$C_v \frac{\partial T}{\partial t} = div\left(\lambda\, grad\, T\right) - L_v\, div\left(D_{\theta v}\, grad\, \theta\right) \qquad [1.14]$$

1.2.2.2 In the concrete pile

The incorporation of the geothermal system into the structural and civil works of the building should be designed to satisfy not only the mechanical equilibrium but also the energy equilibrium. The thermal energy provided by the concrete thermo-active piles

should equal the thermal energy extracted from the ground soil as given in equation 1.15. This energy conservation will help to determine the required number of thermo-active piles, which is governed by equation 1.16.

$$\dot{Q}_{soil} = \dot{Q}_{concrete} \quad [1.15]$$

$$\int (\vec{q} C_v \, dl)_{soil} = \int \left(n_{pile} \vec{q} C_v \, dl\right)_{concrete} \quad [1.16]$$

where $\dot{Q}$ indicates the thermal energy, $\vec{q}$ denotes the heat flux, n_{pile} is the number of thermo-active piles installed, and l is the length of material.

According to equation 1.16, the energy production is strongly related to the properties of the transfer media and the length of surface contact between the transfer media. 1 kW of heating needs the surface of concrete structures in contact with soil roughly between 20 m^2 in saturated soil and 50 m^2 in dry sand (Brandl 2006). More precisely, a pile with diameter of 30–50 cm can extract the ground thermal energy of 40–60 W/m while the one with diameter larger than 60 cm can extract 35 W/m^2 of earth contact area (Brandl 2006).

1.2.2.3 In the building

The quantity of energy production in the building depends strongly on the efficiency of the heat pump, which is defined by the coefficient of performance (*COP*) or the ratio of the output energy to the input electricity energy. The *COP* is generally ranging from 3,0 to 6,0. The higher the number is, the better the efficiency produces. However, for economic reasons, a value of $COP > 4$ should be achieved (Lund *et al.* 2004). Therefore, the usable room temperature should not exceed 35–45°C and the extraction temperature in the exchanger pipes should not fall below 0°C (Brandl 2006). As a consequence, this novel technology tends to be limited to a low range temperature of 0–50°C.

Conservation energy between the building system and the thermo-active pile system is given in equation 1.17, where P_{HP} denotes the heat pump power. This latter indicates

the electricity input energy to operate the heat pump, which is equal to the output energy produced divided by the heat pump's *COP*.

$$\dot{Q}_{building} = \dot{Q}_{piles} + P_{HP} = \dot{Q}_{piles} + \frac{\dot{Q}_{building}}{COP} \quad [1.17]$$

1.3 Geotechnical challenges: Temperature induced change in mechanical behavior of the foundation

In thermodynamic viewpoint, the incorporation of the shallow geothermal system into the structural and civil works of the building has proved to be beneficial. This study will be hereafter limited to the remaining problems in geotechnical viewpoint concerning the detrimental effects in mechanical resistance of foundation systems due to temperature injected.

If a free concrete pile is heated, the pile will expand. The elongation of the pile due to heating relative to the initial length, which is generally known as thermal deformation ε^{th}, is equal to the gradient temperature applied ΔT multiplied by the thermal expansion coefficient of concrete α_T (Equation 1.18).

$$\varepsilon^{th} = \frac{\Delta L}{L} = \alpha_T \, \Delta T \quad [1.18]$$

As a result, the state of deformation in the concrete pile will change as below:

$$\varepsilon = \varepsilon^{e} + \varepsilon^{th} \quad [1.19]$$

where ε^{e} indicates the elastic deformation of the concrete pile. Due to the restraint of the overlying structure and the surrounding soil, the concrete pile cannot have a free thermal expansion or contraction. Interaction within the structures leads to the additional thermal stress in the concrete piles, which is governed by the elasticity law of Hooke as expressed in equation 1.20. For the sake of clarity, a compressive force resulting from the normal stress of the pile σ is taken as positive according to the

convention in soil mechanics. This additional thermal stress will be then transferred to the ground by the mobilized shaft friction or end bearing at the soil–pile interface.

$$\sigma = E\left(\varepsilon - \varepsilon^{th}\right) = E\left(\varepsilon - \alpha_T \Delta T\right) \qquad [1.20]$$

Furthermore, the thermo-active piles are subjected not only to thermal stress induced by temperature variations in heat exchanger elements but also to mechanical stress caused by the static weight of the upper structure. Observations from in-situ thermo-active piles installed at EPFL, Switzerland (Laloui *et al.* 2006) and Lambeth College, UK (Bourne-Webb *et al.* 2009) have noted that the expansion of a heated pile results in a pile head heave and an increase in axial stress. The increased axial stress modifies the mobilization of shaft friction, where the end bearing stress increases and the friction mobilized at the upper-half of the pile decreases. A cooled pile has an opposite response of the heated pile: an increase in pile settlement and a reduction in axial stress. Due to the pile contraction, the end bearing stress reduces and the friction mobilized at the upper-half of the pile increases. However, the changes in axial stress and shaft friction depend strongly on the end-restraint condition between the pile and the overlying structure (Amatya *et al.* 2012; Bourne-Webb *et al.* 2009). The change in pile mechanical behavior under temperature variations is best described in Figure 1.2.

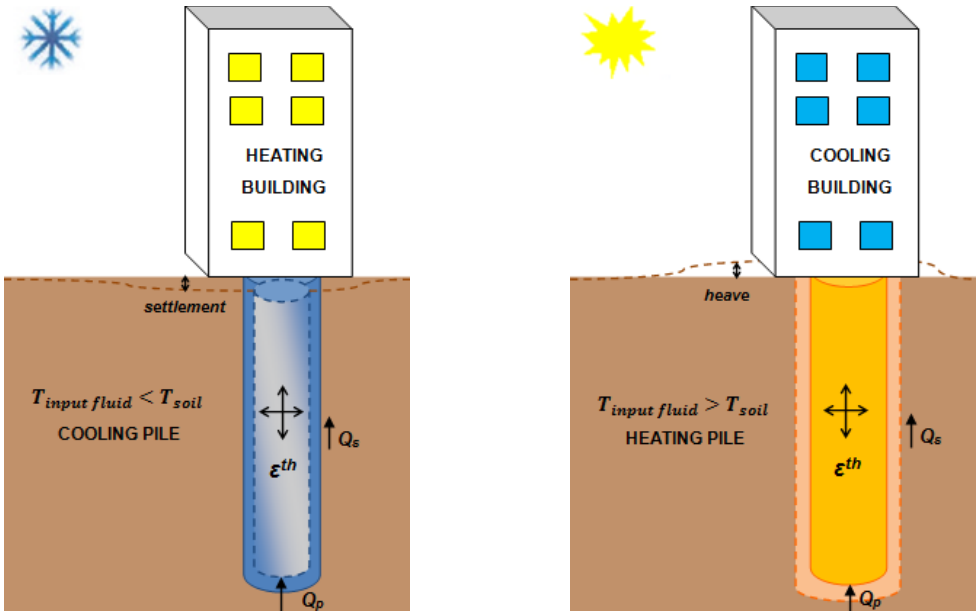

Figure 1.2 – Contraction and expansion of the thermo-active pile

Nevertheless, since the capacities to dissipate the heat in clayey soil and in sandy soil are dissimilar, the impact on the mechanical behavior of the thermo-active piles located in those two types of soil will not be the same.

1.3.1 Thermo-active piles located in clayey soil

When a soil is heated, all of the constituents dilate including the solid skeleton and pore water, but the expansion of the water is greater than that of the pore space. According to experimental tests conducted in previous research studies, heating prior to loading of the normally consolidated clays produces contraction while that of over consolidated clays produces dilation. Hence, thermal volumetric deformation depends strongly on the stress history or the over consolidation ratio (Campanella and Mitchell 1968; Cekerevac and Laloui 2004).

In drained condition, a temperature change of 1°C may produce an excess in pore pressure of approximately 1,5% of the mean effective pressure (Campanella and Mitchell 1968). But, the pre-consolidation pressure decreases non-linearly with increased temperature, which corresponds to the decrease of the yield limits in an isotropic plane with increased temperature (Cekerevac and Laloui 2004; Laloui 2001). Through triaxial tests with controlled temperature up to 90°C, the friction angle at critical state can remain independent with temperature change but the elastic modulus increases slightly of approximately 4 kPa with a temperature change of 68° in normally consolidated clay (Cekerevac and Laloui 2004). In undrained condition where the pore water cannot escape, there can be no volume change due to temperature variation. However, experimental results showed that the failure of clays in undrained condition is reached at temperature values between 70–90°C caused by an increase in pore pressure. This latter leads to an effective main stress drop under constant total stress conditions and thus attains the critical state line (Hueckel and Pellegrini 1989).

Generally, clayey soil has a low permeability due to their pore sizes so the groundwater velocity in clays is relatively low. Therefore, the heat advection transfer by groundwater flow is insignificant compared to the heat conduction in soil grains. As a result, clays will undergo a significant temperature gradient that leads to an additional volumetric

deformation and thus causes variation in the pore pressure. The relationship between the groundwater *v* and the pore pressure *p* in the function of gradient temperature ΔT is expressed in equation 1.21:

$$\left(\beta_m\right)_x \frac{\partial p}{\partial t} - \left(\alpha_T\right)_x \frac{\partial T}{\partial t} + div\,\vec{v} = 0 \qquad [1.21]$$

where *x* indicates the mineral composition of soil related to its porosity factor and β_m and α_T denote the coefficient of compressibility and thermal expansion, respectively. Refer to the mechanical equilibrium state in soil as given in equation 1.22, an increase in temperature causes an increase in pore water pressure and thus a decrease in the effective stress, which can induce clay's swelling.

$$div\,\overline{\overline{\sigma}} - grad\ p + \rho g = 0 \qquad [1.22]$$

In the case of the thermo-active piles, this condition is favorable; both the pile and the soil are subjected to thermal deformations, so the relative displacements between the soil and the pile are small. Hence, the temperature-induced additional stress at the soil–pile interface is not remarkable. Furthermore, since the maximum temperature injected in the thermo-active pile system is below 50°C, the clayey soil around the thermo-active piles will effectively remain in the thermo-elastic condition without a change in soil properties. However, under normally consolidated condition, the changes in clay volume with temperature variations may lead to a compaction during temperature increase and an expansion during temperature decrease. Thus, over the long-term seasonal operation of the thermo-active piles, clayey soil may have cyclic volume change and cyclic swelling of the mass which may degrade the soil resistance.

1.3.2 Thermo-active piles located in sandy soil

Because sandy soil has a high permeability, the groundwater will rapidly diffuse the imposed pile temperature through heat advection transfer phenomenon. In this case, the thermal gradient in sandy soil is very small. The soil will not undergo additional thermal volumetric deformation, only the concrete piles will undergo such a deformation.

Hence, this is the unfavorable case scenario for the thermo-active pile system; the additional stress induced by the temperature variation is all concentrated in the concrete piles and at the soil–pile interface.

Since the ratio between the pile diameter and the pile length are very small, the pile radial movements induced by temperature variations can be neglected in comparison with the thermally induced axial movements of the pile. The axial movements *w* of the pile are not uniform with depth, as given in equation 1.23, and strongly relates to the shaft friction mobilized in contact with soil (Laloui *et al.* 2003).

$$\varepsilon = \frac{\Delta w}{dz} = \varepsilon^{e} + \varepsilon^{th} \qquad [1.23]$$

The repartition of normal force *N* in the pile with depth related to the axial deformation ε is given in equation 1.24 as follows:

$$N = EA\left(\varepsilon - \varepsilon^{th}\right) \qquad [1.24]$$

where *E* is the Young's modulus of the pile and *A* is the pile area. With regard to the mechanical interaction of the soil and pile, the unit friction mobilized q_s at the pile shaft can be obtained from equation 1.25:

$$q_s = \frac{EA}{\pi D}\frac{\Delta\varepsilon}{dz} \qquad [1.25]$$

where *D* indicates the pile diameter, $\Delta\varepsilon$ the variation of deformation at the upper part and lower part of the pile in a concerned layer *dz*.

With regard to the seasonal temperature variations in the thermo-active piles, the change in axial movement, normal stress, and shaft friction mobilized in the concrete piles will change cyclically and thus may lead to the degradation of pile axial capacity. For example, over the cooling phase, the progressive decrease in axial stress may lead to the concrete tensile stress and also the downdrag (i.e. negative shaft friction). Hereafter, the study will focus on the axial capacity analysis of the thermo-active piles located in sandy soil under combined mechanical and cyclic thermal loadings.

1.4 Axial capacity under cyclic loading in cohesionless soil using the soil–pile interaction analysis

One of important issue in analyzing the axially loaded piles is modeling the interaction between the pile and the soil adjacent to the pile shaft, where shaft friction represents the main part in the axial capacity of the piles. In addition, under repeated loading such the one in the thermo-active pile system, a progressive shear stress degradation occurs due to the gradual densification of the sand layer close to the structural surface in the zone called soil–pile interface (Mortara 2008). Therefore, it is important to quantify such degradation at the soil–pile interface zone in order to predict the loss of the pile axial capacity.

While in-situ experiences are the best way to determine the axial capacity of piles, numerical modeling can give a good prediction of the pile behavior only if the soil–pile interface is correctly modeled. There exist two modeling approaches: the first one is using finite element method in a complex three-dimensional (3D) model and the other one is using load transfer method in a simplified one-dimensional (1D) model. The first permits to model any constitutive soil model (e.g. linear/nonlinear, elastic/elastoplastic) in taking into account the whole interaction of the pile, the surrounding soil, and the upper structure. The second is the simplest method by dividing the pile into a number of segments supported by discrete springs which represent the soil resistance at each pile shaft element and at the pile base. Both the simplified one-dimensional or complex three-dimensional models require the definition of behavior law of soil–pile interface.

To properly model the thermo-active pile behavior, the consideration of cyclic plasticity into fatigue is necessary. Four basic assumptions of an incremental plasticity model are as follows: yield condition, flow rule, consistency condition, and hardening rule (Lemaitre *et al.* 2009) as shown in Figure 1.3. The yield surface defines the boundary recognition between elastic–elastoplastic regions and the flow rule controls the plastic increment in the yield surface. The consistency condition shows that during any plastic loading by reversing the load direction, the behavior of the material is always elastic as the root of the hardening rules. Two common viewpoints for yield surface from the

hardening rules are isotropic hardening and kinematic hardening. The kinematic hardening determines the load removing or the inverse loading while the isotropic hardening is able to handle any proportional and non-proportional loading but is not able to draw the stress-strain hysteresis loop under cyclic loading.

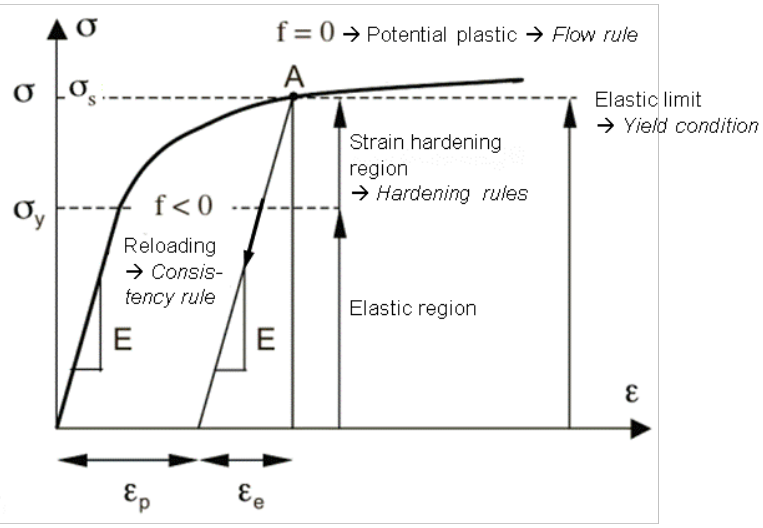

Figure 1.3 – General schema of elastoplasticity model (Lemaitre *et al.* 2009)

1.4.1 Cyclic behavior of the soil–pile interface

Generally speaking, the seasonal thermal contraction and dilatation in the thermo-active piles can be equated with a two-way cyclic axial loading. A number of experimental investigations has been carried out to study the response of piles under cyclic axial loading. Holmquist and Matlock (1976) stated that two-way cyclic loading results in a dramatic reduction in the pile load capacity much more than that in the case of one-way cyclic loading. Besides, they pointed out that the reduction in shaft friction reaches up to 75% in the case of extremely large displacement amplitudes. Data collected by Bea *et al.* (1980) showed a remarkable increase in pile head settlement with the number of cycles that causes a reduction in load capacity. On the other hand, Bjerrum (1973) and Bea *et al.* (1980) indicated that the more rapid the rate of loading is, the greater the pile capacity becomes. In cohesionless soil, as the number of cycle increases, the interface response becomes stiffer while the rate of stiffening decreases (Desai *et al.* 1985; Fakharian and Evgin 1997). The sand densification produced by cyclic loading

increases the dilative behavior of interface, thus allowing a significant recovery of shear stress in the post-cyclic stage (Mortara *et al.* 2007).

Poulos found that under two-way axially cyclic loading, the reduction in material volume leads to the reduction in normal stress and consequently to the reduction in shear stress mobilized between the shaft and the soil (Poulos 1982; Poulos 1989). According to these facts, Poulos concluded that the degradation in shaft resistance depends not only on the reduction in shear stress mobilized as a function of absolute cyclic slip displacement but also on the reduction in normal effective stress due to volumetric strain during cyclic shearing (Fakharian and Evgin 1997; Uesugi and Kishida 1991). The former component may become more significant in less compressible soils whereas the latter component may dominate in compressible soils.

On the other hand, Lemaitre and Chaboche (2009) defined various phenomena of degradation in materials due to cyclic fatigue effects under cyclic loading, such as:

- Under an imposed non-symmetrical strain, a mean stress relaxation phenomenon appears, which indicates a progressive increase/decrease in stress with cycles (Figure 1.4a)
- Under an imposed non-symmetrical stress, the phenomena of strain ratcheting or strain accommodation can be found. Ratcheting refers to the progressive accumulation of plastic strain during cycles (Figure 1.4b) while accommodation is the stabilization of plastic strain after certain cycles (Lemaitre *et al.* 2009).

1.4.2 Soil–pile interaction analysis in 3D approach

In three-dimensional model of axially loaded pile, problems can arise if the elements representing the soil around the pile are too large. To overcome the problem, it is important to either use thin solid elements in the soil adjacent to the pile shaft and/or use interface elements (Potts and Zdravkovic 2001). Several models of interface elements will be described below with the presentation of constitutive laws of interface behavior.

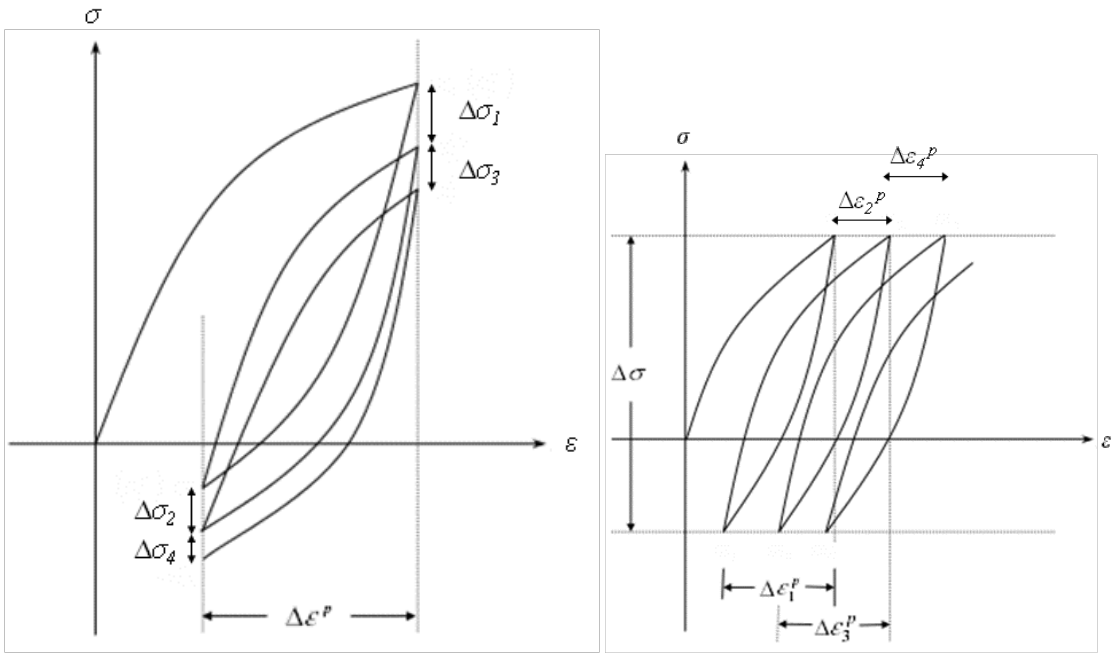

(a) Mean stress relaxation ***(b) Strain ratcheting***

Figure 1.4 – Cyclic behavior under non-symmetrical loading (Lemaitre *et al.* 2009)

1.4.2.1 Interface elements at the soil–pile contact zone

Zero thickness elements

Goodman *et al.* (1968) has the one who founded an element of 4 nodes with 8 degrees of freedom called element “GTB”. This element is based principally on joint element. It is then considered to a virtual material associated to a constitutive law, such stresses and relative movements between the nodes. The relative movements are the principal variable of deformation, which is obtained by the relation to the absolute displacements using the matrix of interpolation function (Cao 2010; Said 2006).

Another type of this element is called element “LRH”, which consists of spring connections to link the opposite nodes (De Gennaro and Frank 2005; Herrmann 1978; Said 2006). Contact points between the two contact bodies are divided in two. Each pair of nodes provides two virtual springs which represent the tangential stress and the normal stress at the surface contact (Figure 1.5a). These springs are expressed by a matrix of rigidity that control sliding and separation between the contact bodies (Cao

2010; Said 2006). The continuity of displacements at the interface is governed by the constitutive laws (e.g. elastoplastic laws, incremental laws, *etc.*). The failure condition, such as slip or separation, is governed by constitutive failure criteria (e.g. Mohr-Coulomb criterion, Drucker Prager criterion, *etc.*). A combination of the advantages in the elements "GTB" and "LRH" is compiled in the macro-element, well-known as "LKI". The "LKI" element consists of two elements of "GTB" as shown in Figure 1.5b (Kaliakin and Li 1995; Said 2006).

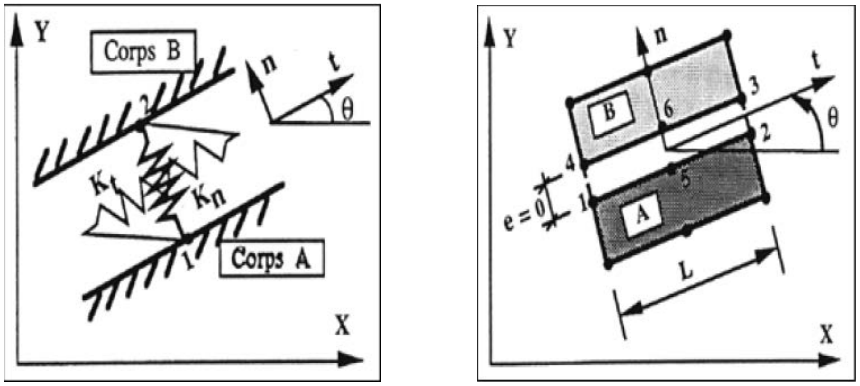

(a) Element LRH ***(b) Element LKI***

Figure 1.5 – Zero-thickness element (Cao 2010)

Thin layer elements

Thin layer element was first developed by Desai *et al.* (1984) who found that the response of the interface should be governed by an appropriate constitutive model. The formulation of this type of element is based on the assumption that the interface can be replaced by an equivalent solid element with a small thickness. The contact surface is modeled using rectangular isoperimetric elements, which is characterized by a high aspect ratio (ratio of the largest dimension of element *L* to its smallest dimension *t*) and constitutive mechanical behavior laws at the contact zone. The associated behavior laws must be valid both in the parallel direction to the shear stress and in the perpendicular direction to the normal stress (De Gennaro and Frank 2005).

In the case of bidimensional element, a classic isoparametric element has 8 nodes as shown in Figure 1.6. This element presents four points of integration (i.e. point of Gauss). The element is inclined at a relative angle α from the axis x_1 of the global

coordinate system. The relationship between global stress and strain related to local stress and strain is given in equations 1.26–27 (De Gennaro and Frank 2005).

$$\begin{pmatrix}\sigma_n\\ \tau\end{pmatrix} = T_\sigma \begin{pmatrix}\sigma_{11}\\ \sigma_{22}\\ \tau_{12}\end{pmatrix} = \begin{bmatrix}\sin^2\alpha & \cos^2\alpha & -2\sin\alpha\cos\alpha\\ -\cos\alpha\sin\alpha & \cos\alpha\sin\alpha & \cos^2\alpha-\sin^2\alpha\end{bmatrix}\begin{pmatrix}\sigma_{11}\\ \sigma_{22}\\ \tau_{12}\end{pmatrix} \quad [1.26]$$

$$\begin{pmatrix}\varepsilon_n\\ \gamma\end{pmatrix} = T_\varepsilon \begin{pmatrix}\varepsilon_{11}\\ \varepsilon_{22}\\ \gamma_{12}\end{pmatrix} = \begin{bmatrix}\sin^2\alpha & \cos^2\alpha & -2\sin\alpha\cos\alpha\\ -\cos\alpha\sin\alpha & \cos\alpha\sin\alpha & \cos^2\alpha-\sin^2\alpha\end{bmatrix}\begin{pmatrix}\varepsilon_{11}\\ \varepsilon_{22}\\ \gamma_{12}\end{pmatrix} \quad [1.27]$$

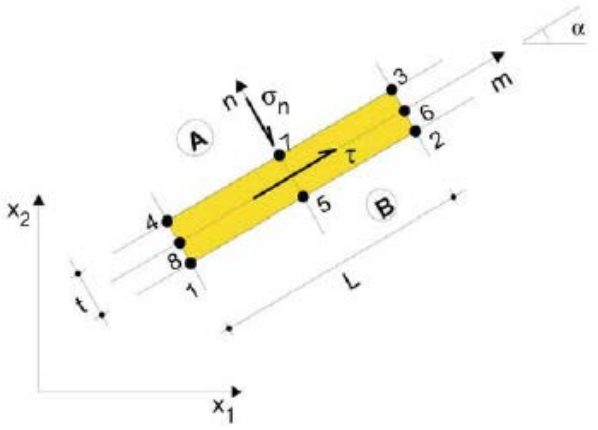

Figure 1.6 – Thin layer elements with 8 nodes (De Gennaro and Frank 2005)

1.4.2.2 Constitutive law of soil–pile interface behavior

Soil–pile interface is a zone of contact between the pile surface and the soil surface which plays an important role on kinematic continuity governed by deformation gradient (De Gennaro and Frank 2005). Modeling a bidimensional element of interface will allow localizing the relative movements and ensuring the continuity of stresses between two different solids. The definition of the thickness of interface element is so various depending on soil characteristics and inclusion, which can modify significantly the characteristics of the behavior. Since the exact thickness of the interface zone is not known, displacement increments are often employed instead of strains.

Elastic behavior

When an interface is subjected by a given soil–pile relative movement, the kinematic

variables that can be measured directly are the normal displacement u_n and the tangential displacement u_t. In general, the elastic behavior is defined by an incremental relationship between the two elastic displacements and stresses as given in the following equation:

$$\begin{pmatrix} d\sigma_n \\ d\tau \end{pmatrix} = \begin{bmatrix} k_n & 0 \\ 0 & k_t \end{bmatrix} \begin{pmatrix} du_n^e \\ du_t^e \end{pmatrix} \quad [1.28]$$

where σ_n and τ and denote the normal and shear stress, respectively. k_n and k_t are normal stiffness and shear stiffness of interface that can be determined from direct shear tests.

Plastic behavior

Incremental plastic displacements are computed generally by using a flow rule based on the plastic potential as follows:

$$\begin{pmatrix} du_n^p \\ du_t^p \end{pmatrix} = \lambda \begin{pmatrix} \dfrac{dg}{d\sigma_n} \\ \dfrac{dg}{d\tau} \end{pmatrix} \quad [1.29]$$

where λ indicates a scalar factor of proportionality, well-known as a plastic multiplier, and g represents the plastic potential function. If the plastic potential function g is assumed to be the same as yield function f, then the interface behavior follows the associative flow rule of plasticity. Otherwise, the interface follows the non-associative flow rule.

The most common criterion to define the plasticity region is the Mohr-Coulomb failure criterion. The surface yield limit f describing the elasticity limit with the associated isotropic hardening is expressed in equation 1.30, where φ_i and c_i denote the friction angle and cohesion factor of interface. The cohesion factor is zero ($c \approx 0$) for the interface located in sandy soil (i.e. cohesionless soil).

$$f = |\tau| + \sigma_n \tan\varphi_i - c_i \quad [1.30]$$

When the shear stress attains its failure limit, a plastic condition is reached and the shear stiffness becomes zero. Therefore, a flow rule is added to describe the plastic dilating phase in considering a dilation angle Ψ. Potential plastic *g* is then expressed by equation 1.31.

$$g = |\tau| + \sigma_n \tan \Psi \qquad [1.31]$$

The elastic-perfectly model considers the shear displacements but lack the possibility of considering the plastic deformations before failure. This model is poor in terms of modeling the normal displacements and post-peak behavior of interface, such as a progressive hardening and a phase change (contractancy–dilatancy) during reversal loading in cyclic path.

Presentation of several constitutive laws which take into account the plasticity under cyclic loading will be detailed in the following sections. These constitutive laws concern the behavior of the sand–structure interface.

1.4.2.3 Constitutive law of soil–pile interface behavior under cyclic loading

Hierarchical Single Surface (HISS) model

The hierarchical approach is initially developed by Desai and Fishman (1991) for modeling the soil–rock joints and is then enhanced by Navayogorajah *et al.* (1992) to model the sand–structure interface under cyclic loading. The model allows incorporation of various factors such as nonassociativeness, strain-softening, and static and cyclic loading including a systematic approach for interface roughness. Inclusion of roughness, softening, and cyclic loading are new features of the model proposed herein as shown in Figures 1.7–1.8.

The model has a closed yield surface defined by a continuous yield function *f*, a strain hardening function *r* to describe post peak rigidity, an ultimate limit state by asymptotic stress envelope, non-associative flow rule, reproduction of dilatancy phase, and

variation of asperity angle. Major advantage is that this model can generalize the discontinuity model between two solids.

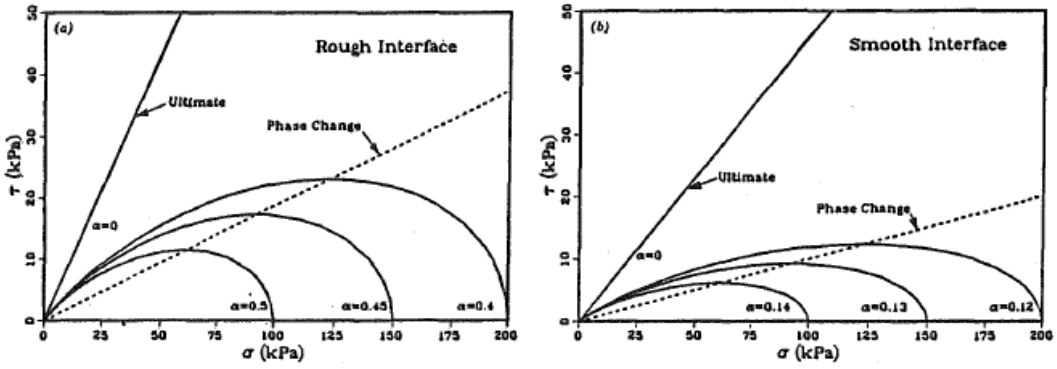

Figure 1.7 – Typical yield and limit surface using HISS for different types of interface roughness (Navayogarajah *et al.* 1992)

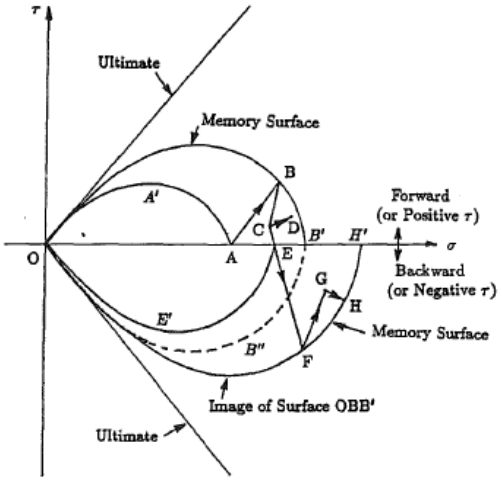

Figure 1.8 – Extension of HISS model to cyclic loading (Navayogarajah *et al.* 1992)

The yield function *f* with the associated flow rule is expressed in equation 1.32. Here, γ indicates the ultimate parameter corresponding to the asymptotic stress states, *n* is called the phase-change parameter because it defines the state in which volumetric strain changes from contractive to dilative, and α governs the hardening function which defines evolution of the yield surface during the deformation. Also, ξ_v and ξ_D are the volumetric and shear plastic displacement, respectively.

$$f = \tau^2 + \alpha\sigma^n - \gamma\sigma^2 \qquad [1.32]$$

$$\alpha = \gamma \exp(-a\xi_v)(1+\xi_D)^{-b} \quad [1.33]$$

The potential function g with a non-associative flow rule is proposed in the following equations by replacing α to α_Q:

$$q = \tau^2 + \alpha_Q \sigma^n - \gamma \sigma^2 \quad [1.34]$$

$$\alpha_Q = \alpha + \alpha_{ph}\left(1-\frac{\alpha}{\alpha_i}\right)\left[1-\kappa\left(1-\frac{r}{r_u}\right)\right] \quad [1.35]$$

Modified Mohr-Coulomb model with the phase transformation state

The model developed by De Gennaro and Frank (2005) has direct links with the Mohr–Coulomb failure criterion but it includes a deviatoric hardening/softening behavior and integrates a phase transformation state (concept of compaction-dilatancy) as shown in Figure 1.9. A modification of the ultimate state condition at large tangential displacements is proposed which allows accounting the change in granular volume during shearing. Since the constitutive model is devoted to model the behavior of sand–structure interface, the failure condition is given by the Mohr-Coulomb criterion in neglecting cohesion as follows:

$$\tau_f = \tan\varphi_f \sigma_n = \mu_f \sigma_n \quad [1.36]$$

where φ_f is the friction angle of the interface at failure and μ_f is the coefficient of friction. Such a hardening phase could either tend to a plateau (for loose interfaces) or evolves into strain-softening and then lean towards a final plateau corresponding to the ultimate state (for dense interfaces).

The yield surface f is governed by the Mohr–Coulomb failure criterion with an addition of the hardening/softening function that gives the evolution of the mobilized friction coefficient during loading (Equation 1.37).

$$f = \tau - \mu(u_t^p)\sigma_n = 0 \quad [1.37]$$

The hardening/softening function is distinguished according to the types of interface. Loose interfaces have typically a continuous hardening which leads to a progressive mobilization of the coefficient of friction μ until reaching the ultimate value at constant volume $\mu_f = \mu_r$. For dense interfaces, the coefficient of friction increases toward μ_p throughout hardening phenomenon and then decreases to the asymptotic ultimate value μ_r. The plastic potential function is given in equation 1.38 while the flow rule to reproduce dilatancy phase is expressed in equation 1.39.

$$g = \tau + \mu_c \sigma_n \ln\left(\frac{\sigma_n}{\sigma_o}\right) \qquad [1.38]$$

$$D = \frac{\mathrm{d}u_n^p}{\mathrm{d}u_t^p} = \mu_c - \mu \qquad [1.39]$$

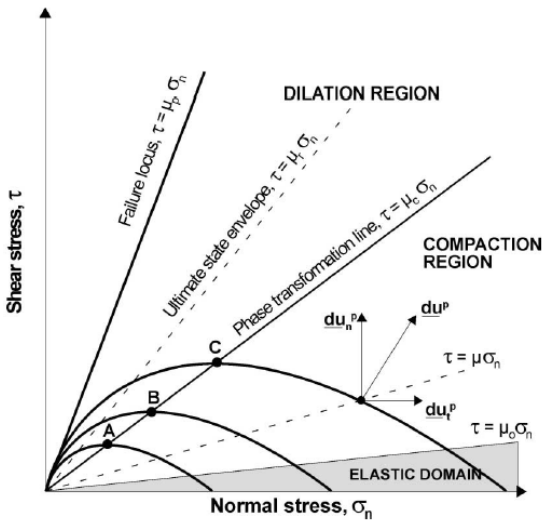

Figure 1.9 – Elastoplasticity region in De Gennaro & Frank model (De Gennaro and Frank 2005)

Two surfaces model with rotational hardening

A 2-D constitutive model for interface behavior between sand and solid inclusions under cyclic loading is developed based on two-surface elastoplasticity (Mortara *et al.* 2002) as shown in Figure 1.10. It is formulated in terms of interface stresses and displacements and the interface is represented as a continuum surface subjected to kinematic discontinuities.

The main characteristics of this model are defined by the linear elastic behavior, the conical isotropic plastic surface, the hardening/softening rule for the isotropic surface, the distinct flow rules for hardening and softening, the cyclic conical surface subjected to rotational hardening, the bounding hardening modulus for the cyclic conical surface, and a continuous variation of the flow rule with densification. The model is based on the experimental results obtained from laboratory direct shear interface tests conducted under both constant normal load (CNL) and constant normal stiffness (CNS) conditions.

The conical isotropic plastic surface f where α is the associate softening-hardening function is expressed in the following equation:

$$f = \sqrt{\tau^2} - \alpha\sigma_n = 0 \qquad [1.40]$$

The extension of the static model to cyclic conditions has been obtained by adding a second plastic mechanism, constituted by an angular shaped yield domain inside the isotropic one. The simplest approach is to consider a rotational motion of the cyclic domain with a rotation angle θ.

The cyclic conical surface is defined as follows:

$$f_0 = \sqrt{\bar{\tau}^2} - \alpha_0\bar{\sigma}_n = 0 \qquad [1.41]$$

where $\bar{\tau}$ and $\bar{\sigma_n}$ are the stresses in a reference system attached to the kinematic mechanism and rotated by an angle θ.

The flow rule of the model is non-associated and is represented by a bilinear relation in the stress–dilatancy diagram $\eta = ad + b$. The plastic potential with the non-associated flow rules is given by:

$$g = \sqrt{\tau^2} - \frac{b}{1+a}\sigma_n\left[1 + a\left(\frac{\sigma_n}{\sigma_c}\right)^{\frac{1+a}{a}}\right] = 0 \qquad [1.42]$$

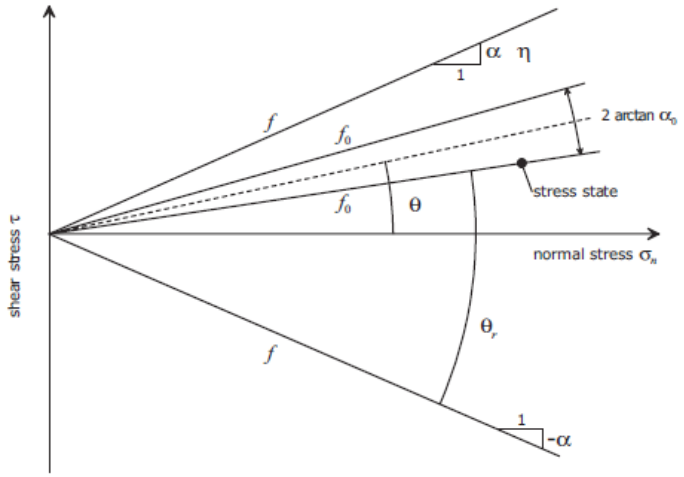

Figure 1.10 – Two surfaces model in cyclic loading by Mortara *et al.* (2002)

1.4.2.4 A particular laboratory-developed law: Modjoin law

Modjoin is a constitutive law of interface behavior under cyclic loading within the framework of elastoplasticity using the concept of bounding surface, which is belonging to zero-thickness interface elements (Shahrour and Rezaie 1997). The relationships governing the cyclic plastic behavior of the interface should describe that the interface has an elastic behavior and also contractive-dilative behavior for each loading reversal. The function should draw the evolution of contracting–dilating phase not only under monotonic loading but also during cyclic loading. These required phenomena are modeled in the Modjoin law by two families of surface: the first one is the bounding surface including the limit resistance of the interface and the second one is the cyclic surface enclosing the domain of yielding (Figure 1.11).

The bounding surface f_l with the associated isotropic hardening function $R_{\max}$ are defined by equations 1.43–1.44 as follows:

$$f_l = |\tau| + \sigma_n R_{\max} \qquad [1.43]$$

$$R_{\max} = \tan\varphi + DR\left(1 - e^{ADR\,u_{tr}^{p}}\right) \qquad [1.44]$$

where $R_{\max}$ is governed by the friction angle of soil φ and cumulative plastic tangential

displacement u_{tr}^{p}. *DR* and *ADR* are the control parameters which indicate respectively the amplitude and the rate of isotropic hardening. The parameter *DR* controls the hardening or softening of a material according to the type of surrounding soil. The positive value of *DR* gives a hardening behavior of the interface in a dense soil while the negative value gives a softening behavior of the interface in a loose soil.

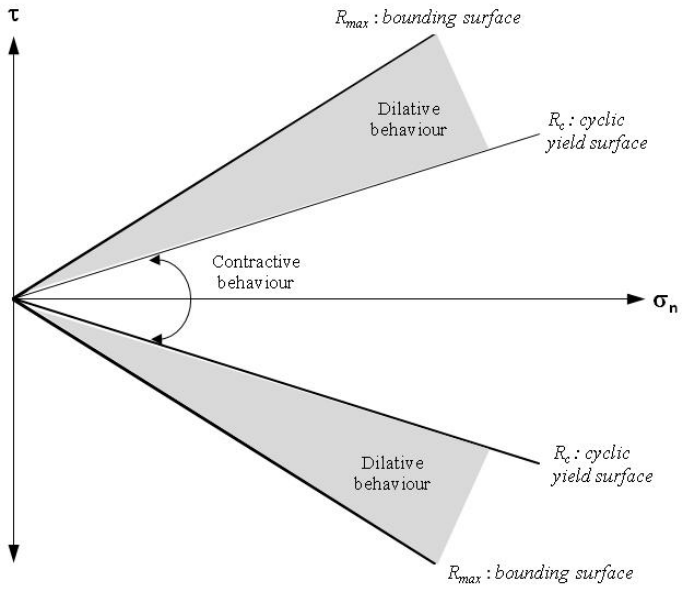

Figure 1.11 – Schematic illustration of Modjoin model (Shahrour and Rezaie 1997)

The cyclic surface f_c with the associated kinematic hardening function R_c are given in equations 1.45 and 1.46, which are governed by the parameters γ_c, β_c, and λ. γ_c controls the amplitude of peak and β_c is the velocity of kinematic hardening. The greater the value of γ_c is, the interface becomes more rigid with a greater hardening. λ denotes the plastic multiplier.

$$f_c = \left|\tau - \sigma_n R_c\right| \qquad [1.45]$$

$$dR_c = \lambda\left(\gamma_c \left|R_{\max} - R_c\right|^{\beta_c}\right) \qquad [1.46]$$

Finally, the flow rule to reproduce the contracting phase followed by the dilating phase is given in equations 1.47 and 1.48. This rule depends on the actual plastic tangential displacement u_{tc}^{p}, the dilation angle Ψ, and the velocity of phase change a_c.

$$\frac{\partial g}{\partial \sigma_n} = \left(\tan \Psi - \left| \frac{\tau - \sigma_n R_c}{\sigma_n} \right| \right) e^{-a_c u_{tc}^p} \qquad [1.47]$$

$$\frac{\partial g}{\partial \tau} = \frac{\tau}{|\tau|} \qquad [1.48]$$

The Modjoin law incorporates soil non-homogeneity, nonlinearity, cyclic degradation, post-peak softening-hardening, and interface dilatancy. Recently, the Modjoin law has been enhanced to control cyclic degradation phenomena such as stress relaxation, strain ratcheting, and strain accommodation (Cao 2010). Figure 1.12 shows the response of the Modjoin interface compared to a direct shear test performed in CETE Nord Picardie under imposed symmetrical displacement. Depending on the choice of parameters, the Modjoin law can render several cyclic degradation phenomena as shown in Figure 1.13.

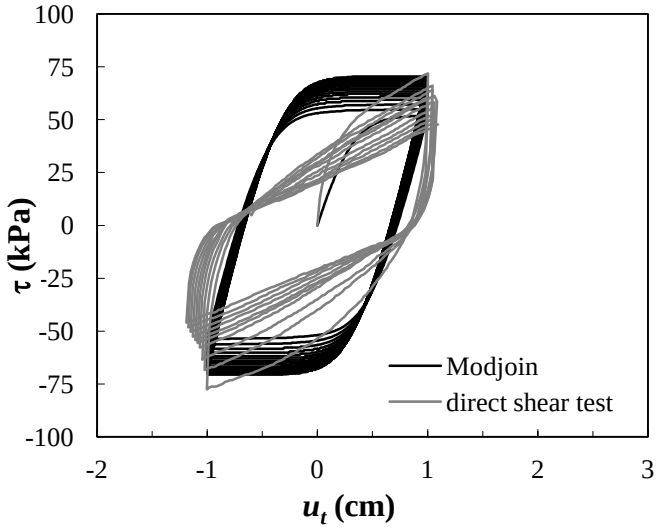

Figure 1.12 – Comparison of interface behavior under symmetrical displacement

1.4.3 Soil–pile interaction analysis in 1D approach

1.4.3.1 Load transfer method

The load transfer approach, commonly used for the design of piles under axial load, is based on modeling the soil–pile interaction by local laws of mobilized soil–pile resistance, *t*–*z* law (Frank and Zhao 1982). This approach requires dividing the pile into

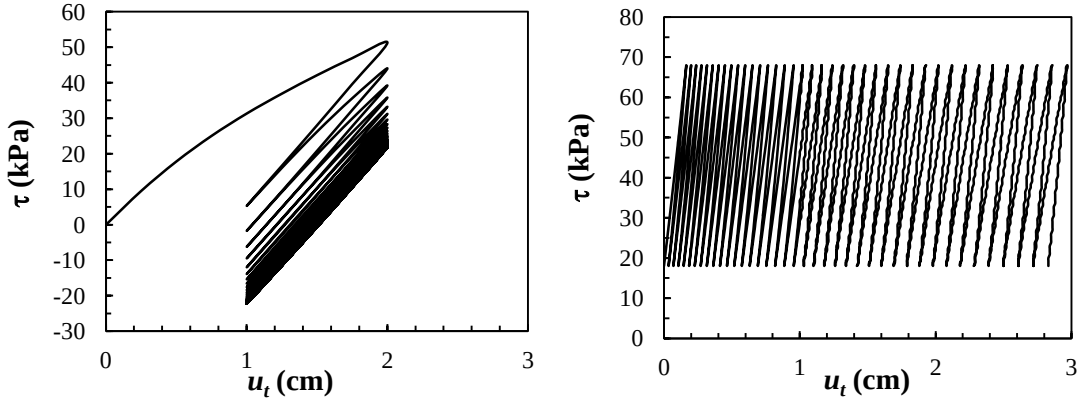

(a) stress relaxation phenomenon *(b) strain ratcheting phenomenon*

Figure 1.13 – Behavior of the Modjoin interface under nonsymmetrical cyclic loading

a number of segments supported by discrete springs, which represent the soil resistance at each shaft element (Poulos and Davis 1980; Reese *et al.* 2006). The movement of the pile at any point in the segment is related only to the shaft resistance at that segment (Poulos and Davis 1980). The differential equation of the mechanical equilibrium of the pile is expressed in the following relation:

$$EA\frac{d^2w}{dz^2} + f_{pile-soil}(z,w) = 0 \qquad [1.49]$$

where *EA* denotes the stiffness of the pile, *E* is the Young's modulus of the concrete pile, *A* is the area of the pile, *w* is the axial displacement according to axe *z*, and $f_{pile\text{-}soil}$ is the *t–z* function relative to the properties of the soil–pile interface. To solve this differential equation, the *t–z* function should govern the relation between the mobilized shaft friction q_s and the soil–pile relative displacement *w* and also between the bearing stress q_b and tip displacement w_b (Frank and Zhao 1982). Resolution of the differential equation is completed by an iterative numerical procedure at each shaft segment by imposing an initial condition at the pile base until the limit condition at the pile head is achieved.

The fundamental requirement of load transfer analysis is the appropriate *t–z* function used to measure local shaft friction and relative displacement of soil–pile. A number of *t–z* curves resulted from in-situ static loading tests has been established and commonly

used in the construction engineering (Coyle and Reese 1966; Coyle and Sulaiman 1967; Reese and O'Neill 1987) but nowadays the *t–z* curves may be obtained via theoretical relationship with the stiffness of the surrounding soil (Kraft *et al.* 1981; Randolph and Wroth 1978). Particularly in France, the *t–z* function was established based on the relation with the pressuremeter test. The Frank and Zhao model (Frank and Zhao 1982) and Monnet model (Monnet and Bernhardt 2000) are the most common functions used in the geotechnical analysis of piles.

1.4.3.2 *t–z* function

Linear elastic perfectly plastic (Frank and Zhao model)

The theoretical function by Frank and Zhao (1982) is presented on the curves of axial friction mobilized q_s–w and bearing stress q_b–w_b (Figure 1.14). The shape of the curves, with two linear parts and a plateau equals the ultimate value, conforms to the behavior often observed in pile in-situ loading tests (Frank and Zhao 1982).

The slopes of first linear branch are related to the Menard's pressuremeter modulus E_M as given in Table 1.2 for bored piles located in fine soils (e.g. clays and limestone) and in granular soils (e.g. sands and rocks). This relation represents a linear elastic behavior until a stress value equal to a half of the ultimate shaft friction value or the ultimate bearing stress. From these stress values on, the slopes become stiffer with a value $k_s/5$ (for the shaft friction) or $k_b/5$ (for the bearing stress) until the ultimate stress values are reached. The third branch is defined by a plateau equal to the ultimate value, which expresses a linear plastic behavior.

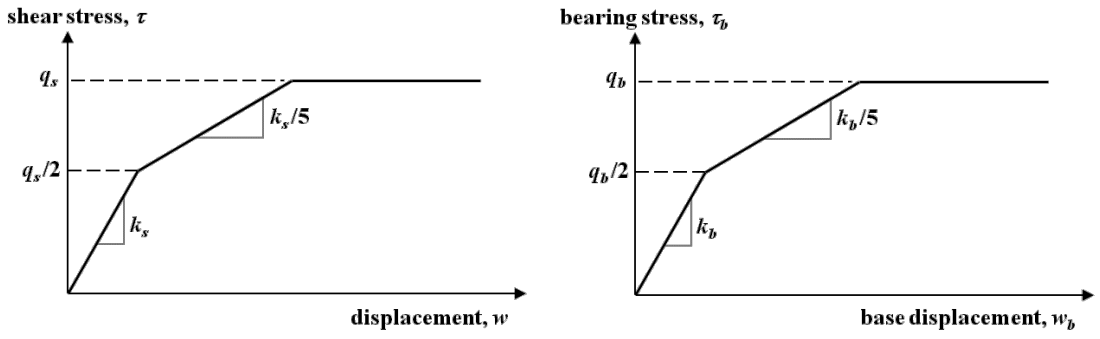

Figure 1.14 – *t–z* curves in Frank and Zhao model (Frank 1995)

Table 1.2 – Frank and Zhao model (Frank 1995)

		Fine soils	*Granular soils*
Shaft friction mobilized	k_s	$2\frac{E_M}{D}$	$0{,}8\frac{E_M}{D}$
End-bearing stress	k_b	$11\frac{E_M}{D}$	$4{,}8\frac{E_M}{D}$

Non linear elastoplastic (Monnet model)

The *t–z* function by Monnet (Monnet and Bernhardt 2000) proposes a nonlinear relationship of mobilized shaft friction and soil–pile relative movement as given in equation 1.50. The function is related to the maximum friction q_s and ultimate displacement w_u which can be estimated by the relation with the pile diameter D and the soil shear modulus G (Equation 1.51). The value of soil shear modulus is taken by the Menard's pressuremeter modulus, for $G = E_M/3\alpha$ where α is the rheological coefficient of Menard. The governed relationship is best described in Figure 1.15.

$$\tau = \frac{q_s w}{w_u}\left(2 - \frac{w}{w_u}\right) \qquad [1.50]$$

$$w_u = q_s \frac{D}{2G} = q_s D \frac{3}{2}\frac{\alpha}{E_M} \qquad [1.51]$$

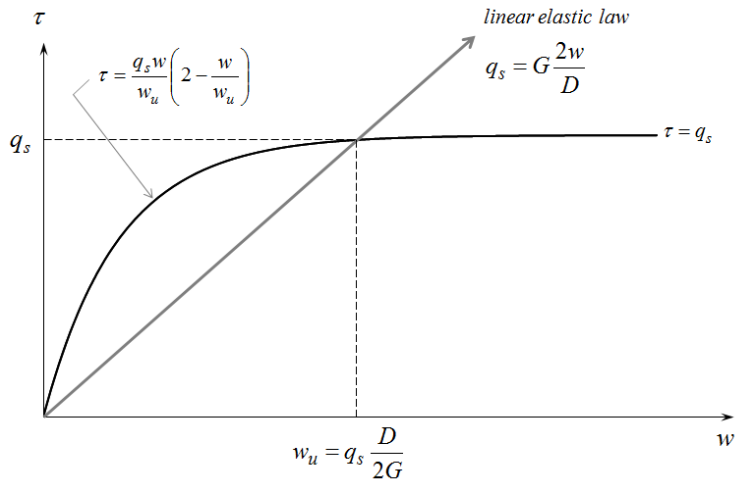

Figure 1.15 – *t–z* curve in Monnet and Bernhardt model (Monnet and Bernhardt 2000)

Linear elastic perfectly plastic adapted to cyclic loading (Thermo-Pile model)

Laboratory of Soil Mechanics in Swiss Federal Institute of Technology Lausanne has worked out on two-way cyclic loading. By adopting the *t–z* curve of Frank and Zhao (1982), they added an unloading curve to draw the reversible behavior of the soil–pile interface as shown in Figure 1.16. The slopes of the three branches of the unloading curve remain equal to the loading curve with respect to the negative value of stress. The behavior of bearing stress is not allowed having a negative value so there is no additional unloading curve in the *q–z* curve. These modified curves are implemented into Thermo-Pile program software, which is designed especially to analyze the response of the thermo-active piles under cyclic thermal loads (Knellwolf *et al.* 2011; Laboratory of Soil Mechanics 2011). However, the function is limited to linear elastoplastic behavior without having a kinematic hardening function.

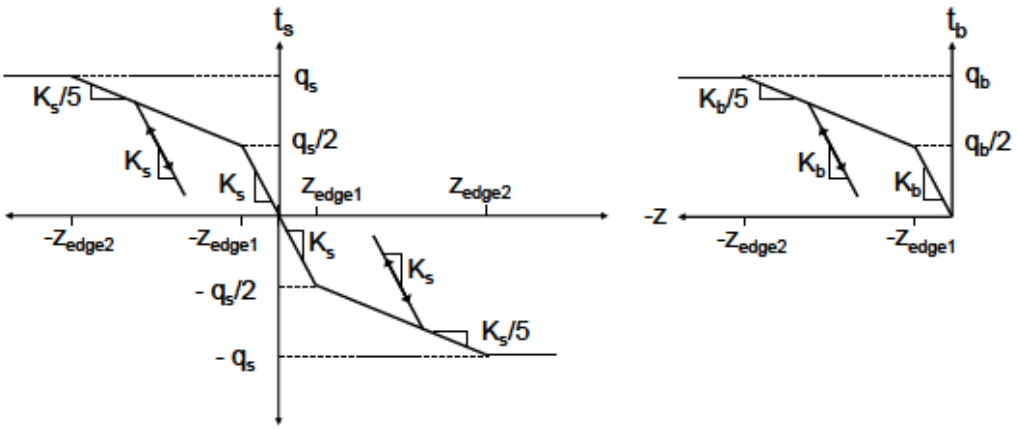

Figure 1.16 – *t–z* curves in the Thermo-Pile program (Knellwolf *et al.* 2011)

Nonlinear elastoplastic adapted to cyclic loading (RATZ model)

Randolph has developed a theoretical *t–z* function under axially cyclic loading and implemented it to RATZ numerical computation program analysis (Randolph 1986; Randolph 2003a). The shape of the curve has no precise theoretical basis but allows a sufficient flexibility to model most aspects of the soil responses, such as nonlinear behavior and strain hardening prior to peak followed by strain-softening after peak (Randolph 2003a). The function consists of a linear elastic part with the initial slope ξ, a

nonlinear parabolic shape which describes the evolution of stress until peak value τ_p followed by strain hardening mechanism, and a strain softening stage where the current value of shaft friction is related to the absolute pile displacement. Initially, the unloading curve will be elastic until yield will occur at some point. The loading – unloading curve is shown in Figure 1.17. Cyclic degradation is taken into account in the model by calculating the accumulated plastic deformation (Chin and Poulos 1992). In its recent version, some extensions are included such as thermal strain in the pile, but it is limited to a single magnitude of the thermal cyclic strains for each analysis.

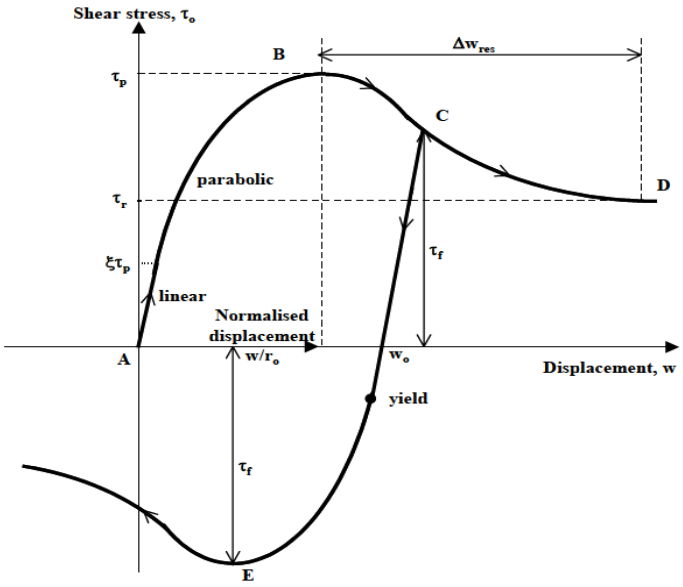

Figure 1.17 – *t–z* curve in the RATZ program (Randolph 2003a)

1.5 Conclusion

This chapter summarizes the problem studied during the PhD research by narrowing the general problems of the thermo-active pile system into the remaining challenges in the geotechnical domain. Due to the heat diffusion between the piles and the ground, additional thermal stress develops in the piles thus changes the mechanical state of the foundation system. The change is strongly related to the type of the surrounding soil, such as clay or sand and saturated or non-saturated. After a comprehensive explanation about the impact of temperature gradient on the mechanical behavior of piles located in

clays and in sands, this research choose to take place in studying the thermo-active piles located in saturated sandy soils.

This chapter also points out the necessity of studying the cyclic response in the soil–pile interface of such piles by modeling correctly the soil–pile interaction using the appropriate behavior law with cyclic plasticity condition. There are two common methods used in the soil–pile interaction modeling: finite element/difference method in three-dimensional approach and load transfer method in one-dimensional approach. The laboratory-developed law, the Modjoin law, is chosen to be employed in the further three-dimensional numerical analyses due to its capability of modeling the cyclic degradation effects such as stress relaxation and strain ratcheting. However, to meet the practical needs in engineering construction, one-dimensional modeling with the load transfer method is regarded as the best way. But, up to the present time, there is not available yet a *t–z* function for the load transfer method that takes into account the kinematic hardening rules to model cyclic degradation under two-way cyclic loading.

CHAPTER 2
THERMAL ANALYSIS: DIFFUSION WITHIN THE THERMO-ACTIVE PILE SYSTEM*

2.1 Introduction

In the case of thermo-active piles located in sandy soil without moving groundwater, the heat transfer process between the fluid circulating in the concrete pile and the surrounding ground produces a heat build-up in the ground around the concrete wall. This latter reduces effectively the thermal performance of thermo-active foundations and causes also the heat or cold accumulation in the ground. Several research studies on the thermal diffusion within the thermo-active piles have been widely developed in the needs to achieve higher energy performance of the exchanger system and energy balance of the ground. Thermal fluid interaction analyses with the convection flow inside the exchanger pipes has been conducted by Loveridge and Powrie (2013), Rouissi *et al.* (2012), and Choi *et al.* (2011) in taking into account the Reynolds, Nusselt, and Prandtl numbers. A coupled heat conduction–advection transfer has been performed by Ma and Grabe (2010) to analyze the influence of the groundwater flow on the thermal efficiency of such pile. Choi *et al.* (2011) and Jalaluddin and Miyara (2012) have compared the continuous and intermittent operation of the heat pump both in numerical and in-situ approaches. They found out that the intermittent operation can alleviate effectively the unbalance cumulative energy around the thermo-active piles thus can stabilize the annual mean ground temperature. In other way, Gao *et al.* (2008) and Hamada *et al.* (2007) have shown that the energy performance of the thermo-active foundations are strongly related to the fluid flow rate injected and the type of absorber

* Some of the materials presented in this chapter have been published in [SUR 13a] and [SUR 13c] as listed in Appendix C

pipes inserted in the pile.

All of the above-described studies have put an interest in increasing the energy performance and efficiency of such foundations. However, the heat concentration around the concrete wall and the change in annual ground temperature profile would effectively cause some detrimental effects in the mechanical stress of the concrete and soil. This chapter deals with a numerical analysis of the transient heat conduction in a thermo-active pile located in a fully-saturated sandy soil, aiming to adequately understand the diffusion occurring in the system and to identify the temperature effect on the mechanical resistance of such pile. The study intends to determine the temperature produced in the pile and at the soil–pile interface, to observe the change in ground temperature profile due to seasonal temperature injected in the pile, and thus to quantify the additional thermal stress carried in the pile. The scope of study is limited to thermal conductive transfer excluding the fluid convection flow and the advection flow of groundwater. The pile is loaded by a single thermal load without any permanent load of the building is included. The results of this chapter will provide the hypotheses for the further mechanical soil–pile interaction analysis.

2.2 Presentation of numerical model

A concrete pile having diameter D 60 cm and length H 15 m is located in the centre of a soil mass. The soil mass boundary dimension is selected after a parametric analysis to ensure an adiabatic boundary condition, with the horizontal radius is set at 15 m from the pile centre and the height of soil mass at 30 m. The mesh is refined around the pile in order to increase the precision in the high strain gradient areas. Four U-shaped absorber pipes are located 10 cm from the outer surface of the concrete pile, which are placed surrounding the pile with a 28 mm outer diameter. The position of the absorber pipes forms an anti-symmetric *I-O-I-O* configuration, with *I* designating the inlet flow and *O* the outlet flow. Figure 2.1 shows the mesh dimension of a complete model while Figure 2.2 shows the cross-section detail of the thermo-active pile.

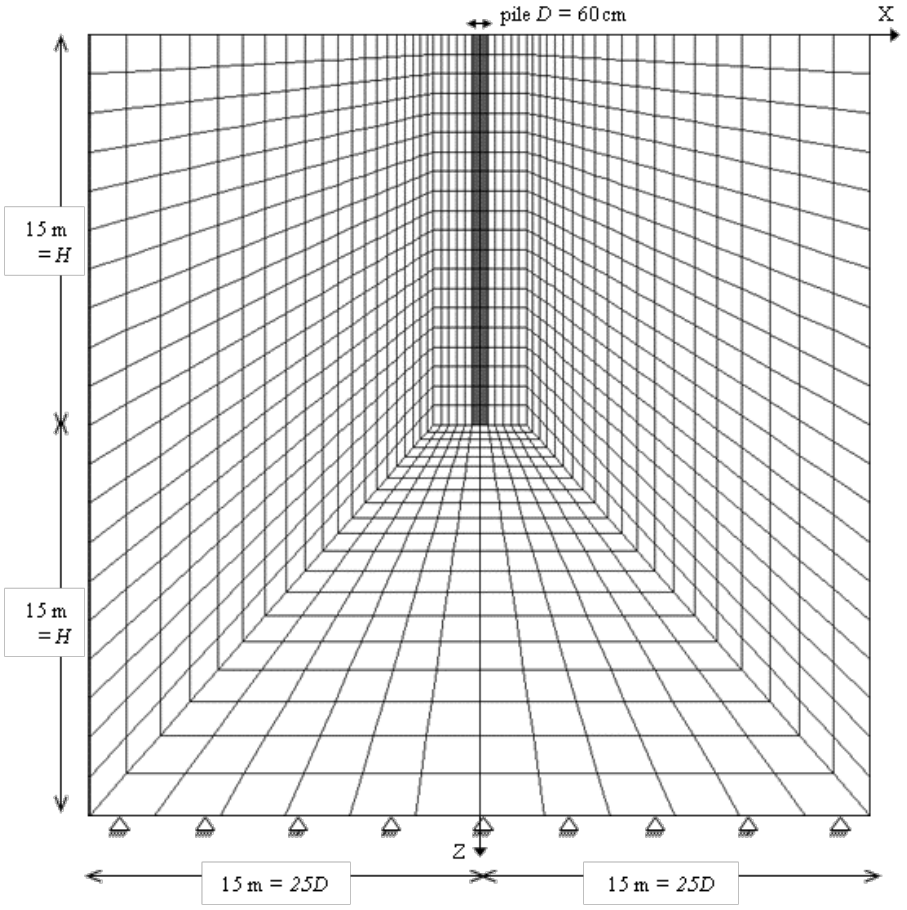

Figure 2.1 – Dimension of the complete model (XZ plane)

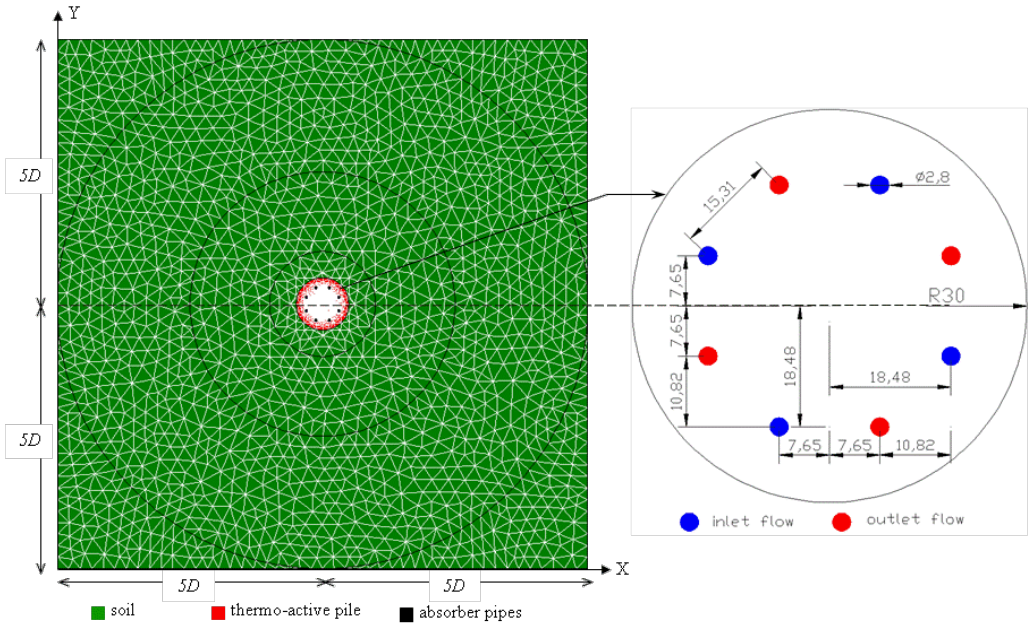

Figure 2.2 – Cross-section detail of a thermo-active pile at XY plane

Both the pile and soil are modeled as solid elements and behave in linear thermo-elastic condition. The absorber pipes are modeled as circular line sources neglecting the heat convection flow inside the pipes. The ground soil is assumed as a fully-saturated sandy soil so that only heat conduction is considered and no advection is modeled. The annual mean ground temperature T_{ave} is set at 14°C. Table 2.1 summarizes the thermo-elastic properties of the materials used in this case study. These properties are assumed not to change with temperature because the gradient of temperature applied in the pile is in the range of ±20°C.

The numerical analysis is conducted in two phases:

(i) a two-dimensional (2D) model to observe the micro-scale diffusion in the thermo-active pile itself (from the absorber pipes to the concrete pile);

(ii) a three-dimensional (3D) model to observe the macro-scale diffusion around the thermo-active pile and the surrounding soil.

Table 2.1 – Thermo-elastic properties of the materials

		Absorber pipes	*Concrete pile*	*Soil*
Material density	ρ_c	960 kg/m^3	2500 kg/m^3	1950 kg/m^3
Thermal conductivity	λ_T	0,42 W/m °C	1,8 W/m °C	1,5 W/m °C
Specific heat extraction	c_T	2000 J/kg °C	880 J/kg °C	800 J/kg °C
Coefficient of thermal expansion	α_T	1,4 ×10^{-4} °C^{-1}	1,2 × 10^{-5} °C^{-1}	5,0 × 10^{-6} °C^{-1}
Bulk modulus	K	–	20 GPa	10 MPa
Shear modulus	G	–	7,5 GPa	3,75 MPa

2.3 Micro-scale diffusion inside the thermo-active pile

This section is devoted to study the diffusion inside the thermo-active pile due to the seasonal heat carrier fluid injected in the absorber pipes aiming to determine the temperature produced in the centre of the pile and at the soil–pile contact zone. In reality, when the heat pump is operating, the temperature of the heat carrier fluid in the inlet and outlet pipes varies with time for very short periods (i.e. a few hours) in accordance with the heat pump power. Also, down with the depth, the fluid temperature

varies forming a V letter between the inlet and outlet pipes (Gao *et al.* 2008; Loveridge and Powrie 2013).

For the sake of simplicity, the numerical analysis is conducted in a two-dimensional approach for a given depth of the pile and at a given input–output fluid temperature. The model takes the viewpoint of a XY plane in a cylindrical coordinate as shown in Figure 2.2. The variation of the fluid temperatures with depth is thus ignored. In this case study, the heat conduction transfer can be evaluated in the radial direction by the following differential equation:

$$C_v \frac{dT}{dt} = \lambda_T \left(\frac{d^2T}{dr^2} + \frac{1}{r}\frac{dT}{dr} \right) \qquad [2.1]$$

This simplified 2D model assumes a constant and continuous heat flux density with time to ensure the performance of the heat pump. According to this assumption, the temperature difference between the inlet and outlet fluids in the model is set constant with time $\Delta T_{in\text{-}out} = c^{te}$. As a part of this ongoing research project, an experimental test of micro thermo-active piles was conducted by ECOME from February 2011 to January 2012. Results of the test show that the temperature difference ΔT between the supply (inlet) fluid and the return (outlet) fluid can be considered constant for one season of loading as shown in Figure 2.3. This experimental result meets a good agreement with the boundary condition used in this numerical study.

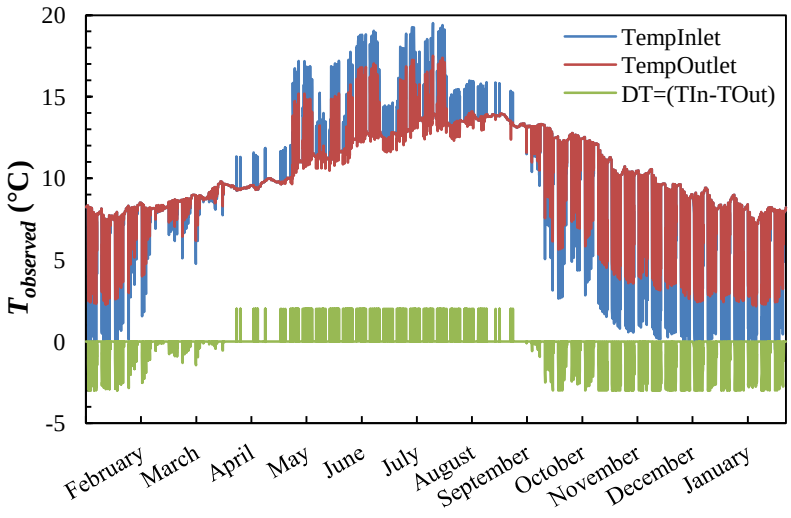

Figure 2.3 – Observation of the temperature in the micro thermo-active piles by ECOME

In the first time, the analysis is conducted in the winter mode with T_{inlet} = 4°C during three months of thermal loading. Considering the energy performance of the heat pump, ΔT is set constant at −3° thus T_{outlet} is set at 7°C. Because of geometry limitations, the initial ground temperature is considered equal to the annual mean ground temperature with time and depth $T_{ini}(z,t) = T_{ave}$. Figure 2.4 shows the radial distribution of the temperature in the thermo-active pile at the end of 3 months of loading. After 3 months of loading, the temperature in the thermo-active pile is relatively uniform on the order of 5,5–6,5°C. Temperature value in the pile centre is 5,65°C and that at the pile perimeter is 6,33°C. These temperatures are approximately equal to the average temperature of the absorber pipes.

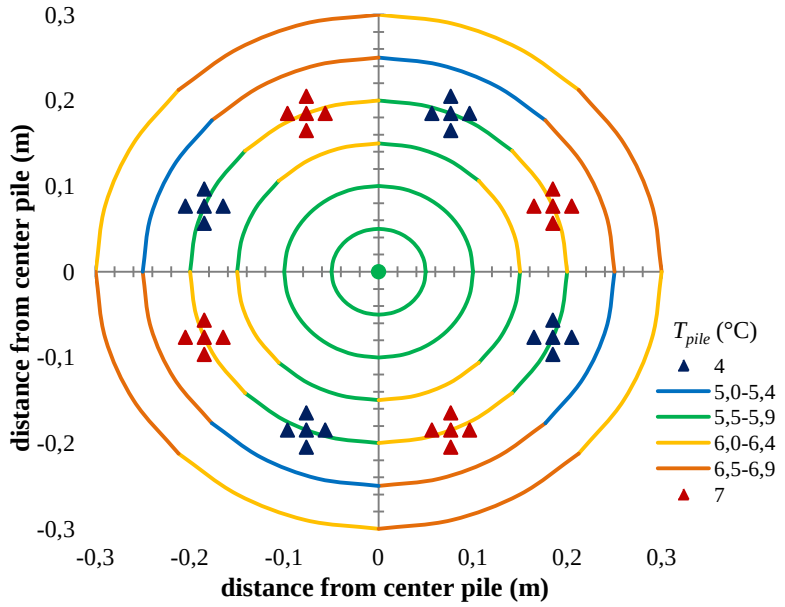

Figure 2.4 – Temperature profile in a thermo-active pile at the end of 3 months of loading

2.3.1 Influence of the types of absorber pipe

In order to study the influence of the absorber pipe on the heat diffusion, three types of absorber pipe configuration are compared. Model A is the reference model as explained in the preceding section. Model B has four U-shaped absorber pipes, like model A, with a symmetric position in the *I-O-O-I* configuration. As for model C, two W-shaped absorber pipes are used with an anti-symmetric *I-O-I-O* configuration. The difference of

configurations between the three models is better shown in Figure 2.5.

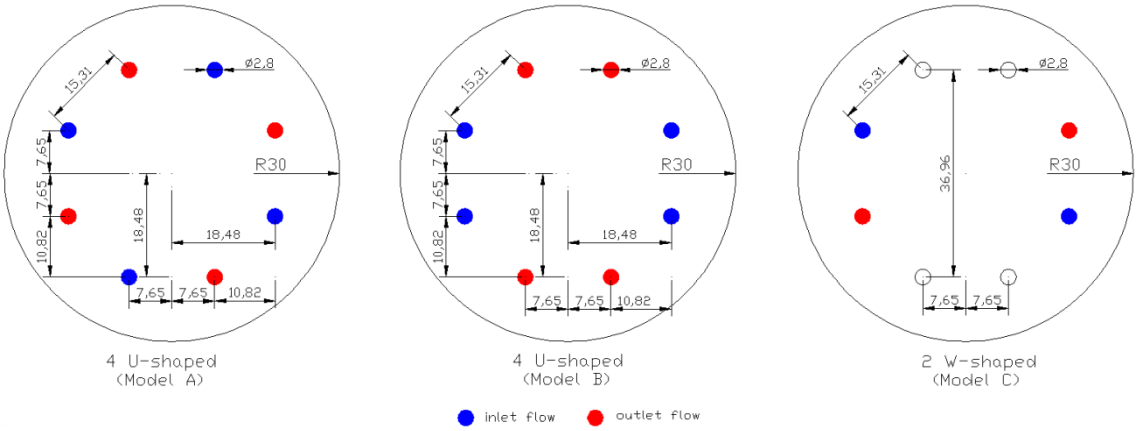

Figure 2.5 – Cross-section details of the different models

Figure 2.6 shows the temperature contour in a radial plan view and Figure 2.7 shows the heat flux density in the pile at the end of 3 months of loading. The figures show that with the same flow rate applied in each model, model A produces the most uniform temperature contour and the most equally distributed flux density over the entire pile section compared to other models. In terms of thermal diffusion, configuration in model A is recommended to avoid an asymmetric concentration of heat in the pile. However, model C with two W-shaped absorber pipes produces the highest average pile temperature as shown in Figure 2.8. According to this result, the W-shaped type is more effective in terms of energy productivity than the U-shaped type.

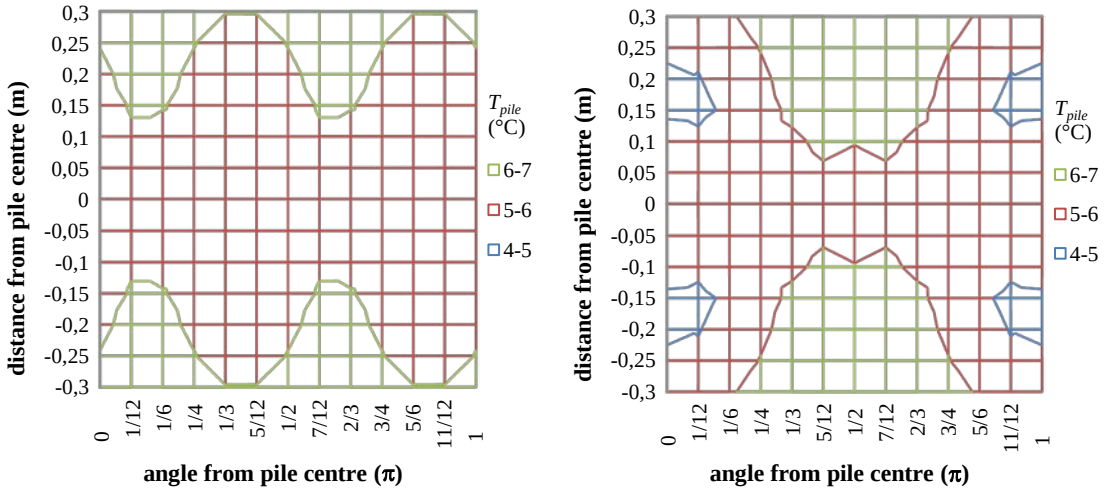

(a) Model A ***(b) Model B***

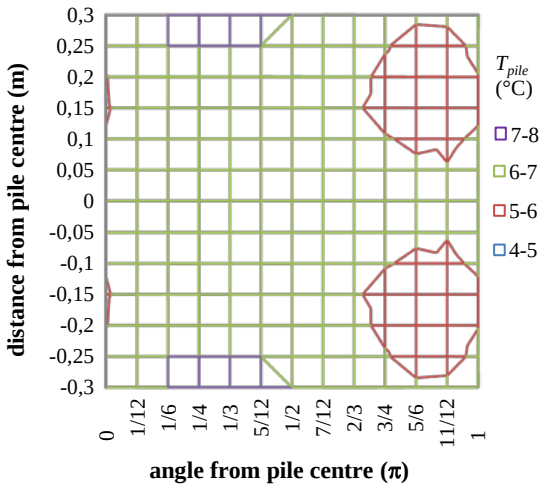

(c) Model C

Figure 2.6 – Temperature contour *T(r,θ)* at the end of 3 months of loading

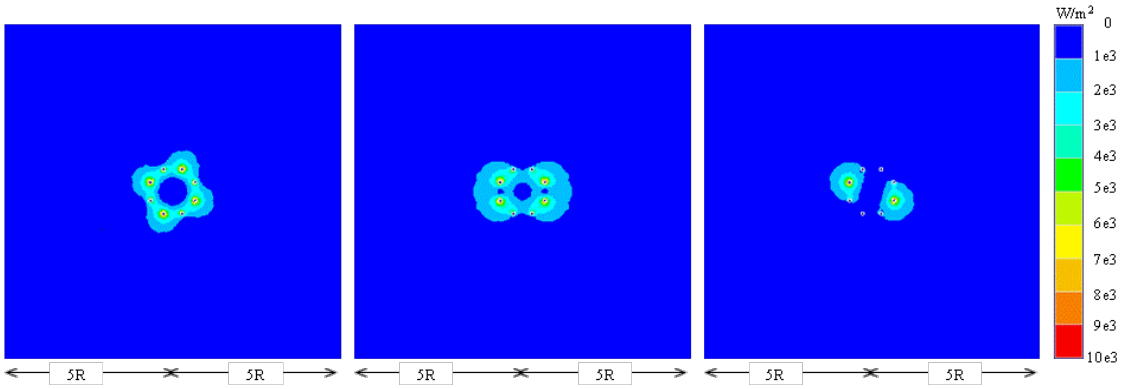

(a) Model A *(b) Model B* *(c) Model C*

Figure 2.7 – Flux density *q(r,θ)* at the end of 3 months of loading

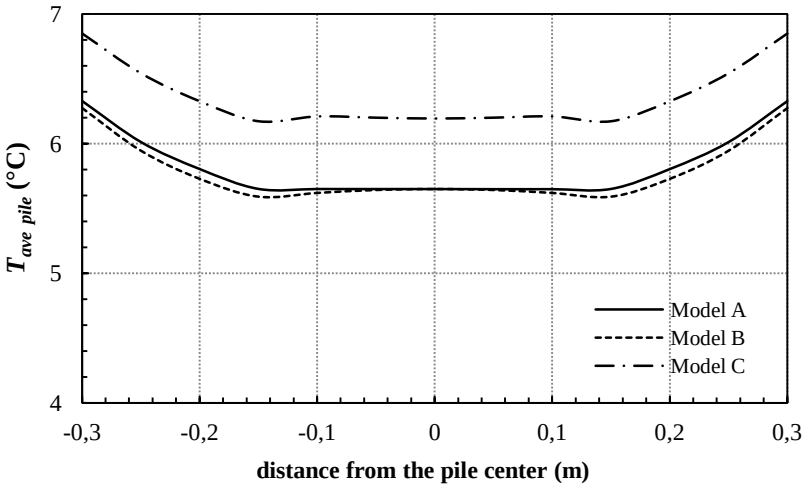

Figure 2.8 – Average pile temperature in radius *T(r)*

2.3.2 Transient diffusion in one year operation

Diffusion in seasonal operation time is analyzed by applying discontinuous thermal loads for every 3 months of loading. During each seasonal operation time, ΔT between inlet flow and outlet flow remains fixed, with respect to the experimental results, in order to maintain the energy efficiency of the heat pump. The design of seasonal fluid is illustrated in Figure 2.9 with ΔT −3°C in the cooling phase and +2°C in the heating phase.

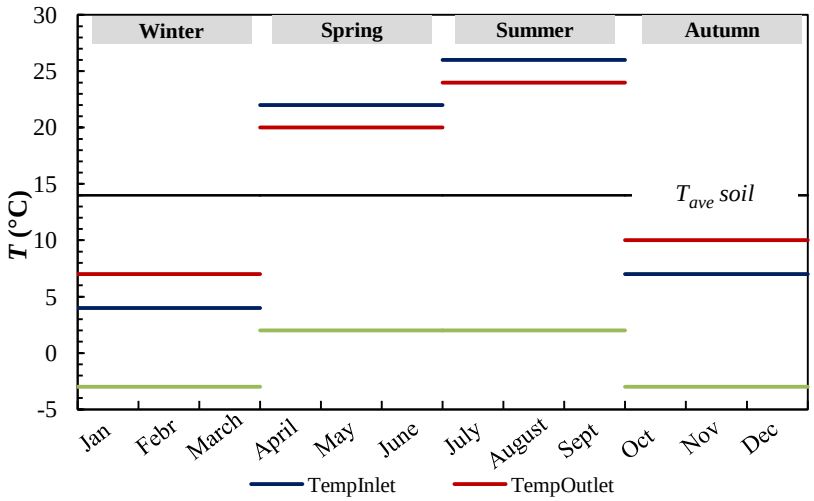

Figure 2.9 – Input design of thermal loading over 1 year operation time

Table 2.2 summarizes the temperature applied in the absorber pipes and the temperature produced in the pile at the end of 3 months of loading. For a better understanding, Figure 2.10 shows the evolution of temperature at the pile centre and at the pile perimeter during three months of thermal loading. For each seasonal thermal loading, the temperatures at the pile centre and at the pile perimeter (i.e. soil–pile interface) vary progressively from the initial ground temperature and then equilibrate steadily to the average temperature of the pipes. Since the temperature difference between the pile centre and the pile perimeter is less than 1°C, it can be concluded that the temperature in the pile is quite homogenous over the entire pile section to the average temperature of the pipes.

Table 2.2 – Temperature in the pile at the end of 3 months of thermal loading in 2D model

Model	*Absorber pipes*		*Pile*		*Representation of season*
	T_{inlet}	T_{outlet}	T_{centre}	$T_{interface}$	
A1	4	7	6,33	5,65	Winter
A2	22	20	20,31	20,88	Spring
A3	26	24	23,92	24,81	Summer
A4	7	10	9,04	8,59	Autumn

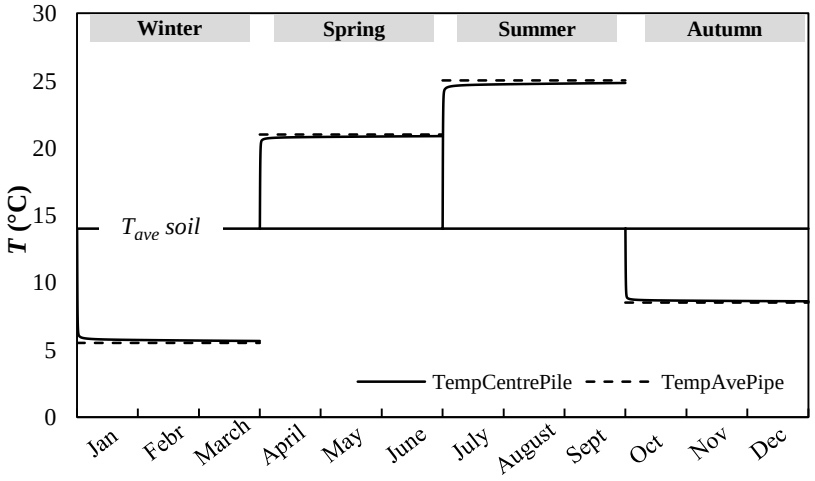

(a) Temperature in the pile centre

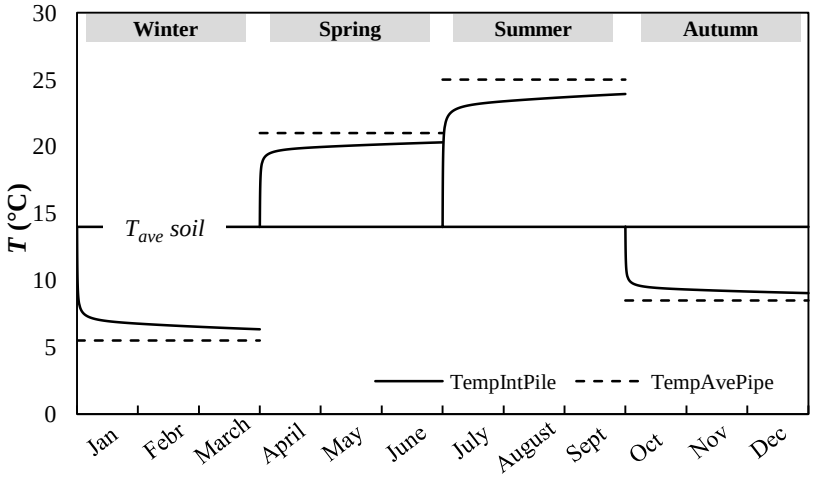

(b) Temperature at the pile perimeter

Figure 2.10 – Pile temperature relative to the average temperature of the absorber pipes

2.4 Macro-scale diffusion of a thermo-active pile to the surrounding sandy soil

After concluding that the pile temperature is equal to the average temperature of the absorber pipes, a three-dimensional analysis of heat conduction between the pile and the surrounding sandy soil is conducted. The 3D numerical model is advantageous for modeling complex geometry with various combined loads. Accordingly, the variation of ground temperature with depth and time *T(z,t)* (previously expressed in equation 1.3) can be taken into account in this study. Analysis is carried out in uncoupled thermo-mechanical model using the finite difference code FLAC^{3D}. Owing to the symmetry of the problem (i.e. load and geometry symmetry), only one-fourth of the complete domain is modeled. Consequently, a null flux is imposed in the symmetrical axes. Only thermal load is applied and no mechanical load coming from the weight of building is taken into account. The thermal loads are applied continuously over a year and homogeneously over the whole pile section with the values of load are recapitulated in Table 2.3.

Table 2.3 – Applied temperature in the thermo-active pile in 3D model

Model	*Pile*	*Absorber pipes*		*Representation of season*
	$T_{ave\text{-}pipes}$	T_{inlet}	T_{outlet}	
A1	5	4	7	Winter
A2	21	22	20	Spring
A3	25	26	24	Summer
A4	9	7	10	Autumn

2.4.1 Change in ground temperature profile

The ground temperature is initially modeled by taking consideration of the surface air temperature and solar radiation in climatic condition as governed by equation 1.3. The annual mean ground temperature T_{ave} is taken as 14°C. The soil mass has internal volumetric heat $\dot{r}$ of 0,001 W/m^3 and terrestrial surface flux $\vec{q}$ at depth 30 m of 0,0544 W/m^2. Figure 2.11 shows in greater clarity the domain of the model with the boundary conditions. The initial ground temperature profile with time and depth is better shown in

Figures 2.12–2.13. The initial ground temperature varies within the uppermost 10 meters and gets steady to the annual mean ground temperature T_{ave} at depth 12–15 meter.

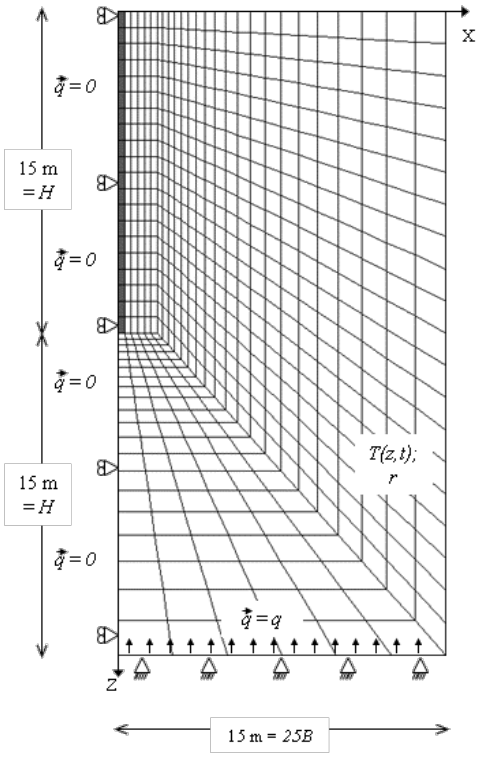

Figure 2.11 – Numerical model

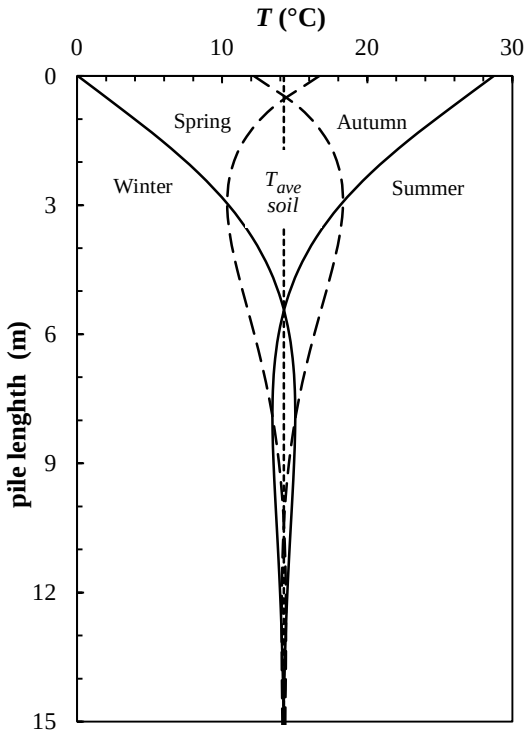

Figure 2.12 – Initial ground temperature profile *T(z)* at a distance *x = D*

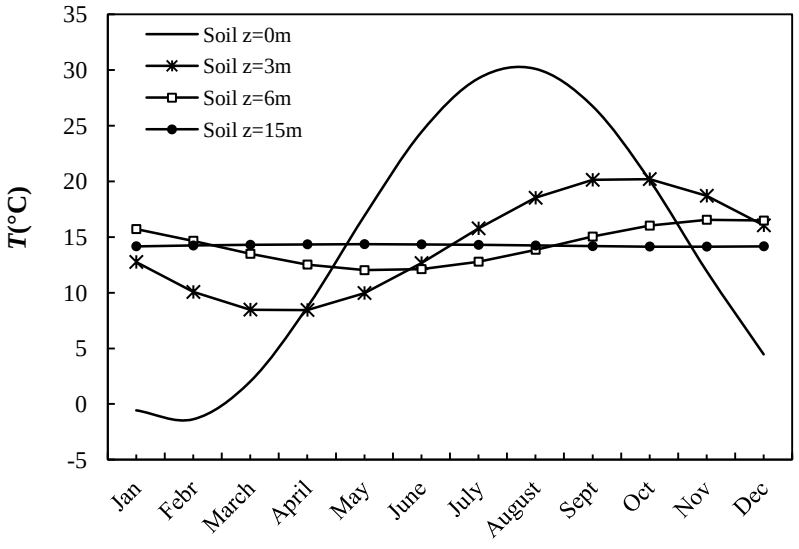

Figure 2.13 – Initial ground temperature profile *T(t)* at different depths of soil

After that, a thermo-active pile is installed in the soil system. The fluid temperature circulating in the pile is applied uniformly along the pile axes and is constant during one season of loading. The values of the seasonal temperature applied in the pile are taken from the results of the 2D modeling, which are equal to the average temperature of the absorber pipes. The system is then subjected to combined sinusoidal ground temperature and seasonal thermo-active pile temperature. Figure 2.14 shows the ground temperature profile after the activation of the thermo-active pile. It can be seen that the ground temperature equilibrium is quite disturbed due to the seasonal thermal loading in the pile. Accordingly, the ground temperature at a depth $z > 10$ m for each season is no longer close to T_{ave}. Furthermore, the ground temperature at a distance of approximately one pile diameter from the pile centre changes completely over the entire depth of a pile length, which becomes much colder in the winter and warmer in the summer. The system has lost the steady-balance ground temperature due to the installation of a thermo-active pile. Also, because the surrounding ground is a granular type, the heat diffusion in soil grains occurs very quickly thus the heat concentration is accumulated around the pile. Figure 2.15 which shows the temperature diffusion contour during a year of loading confirms the presence of heat build-up around the soil–pile contact zone.

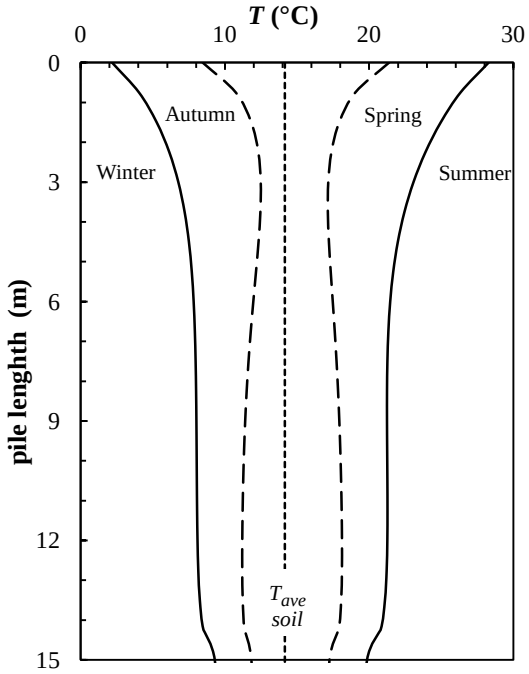

(a) T(z) at a distance 0,6 m from the pile centre (x = D)

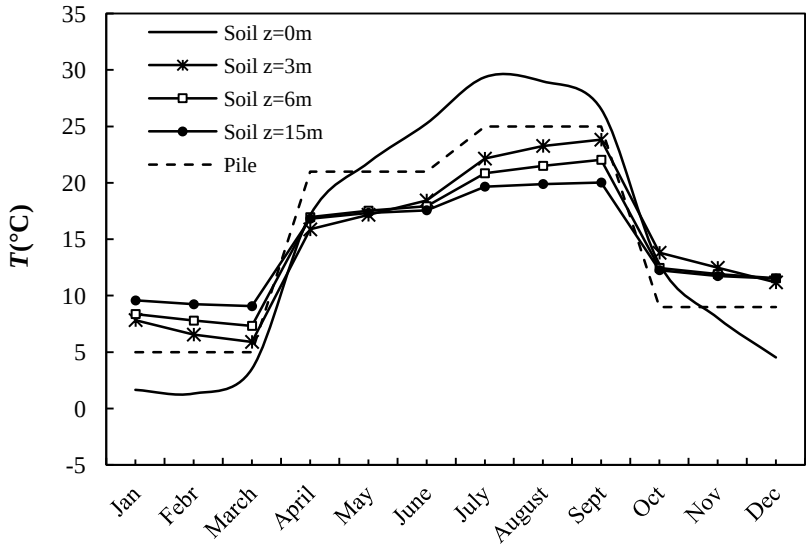

(b) T(t) at different depths of soil

Figure 2.14 – Temperature profile after the installation of a thermo-active pile

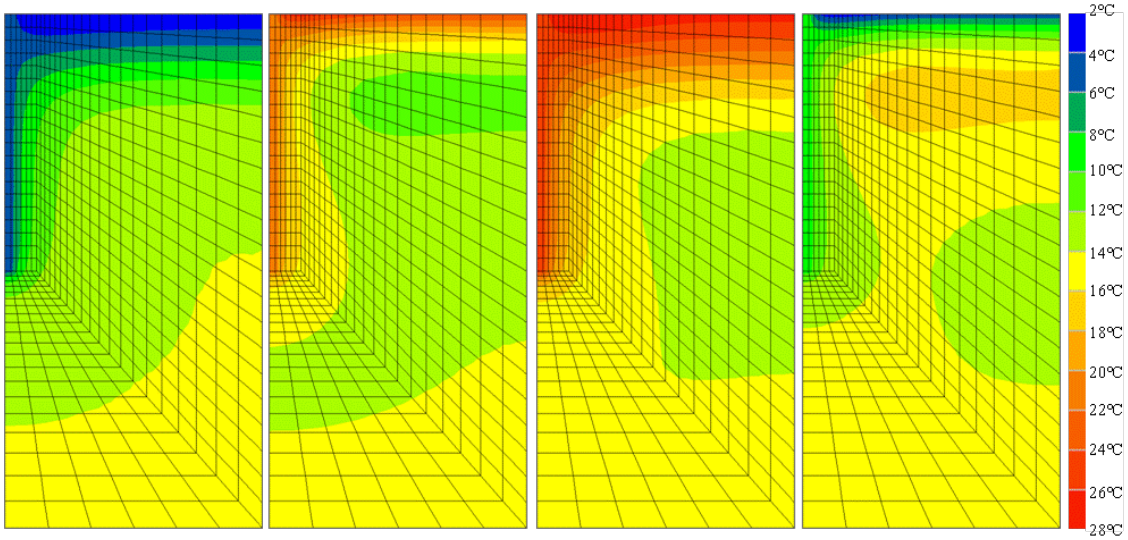

(a) Winter ***(b) Spring*** ***(c) Summer*** ***(d) Autumn***

Figure 2.15 – Temperature diffusion contour at the end of each season of loading

2.4.2 Temperature induced change in pile behavior

This present study considers a pure thermal loading with no service load coming from the upper structure is applied in an attempt to fully understand the effect of temperature on the soil–pile behavior. Since the heat is concentrated around the pile (refer to Figure 2.15), the additional thermal stress is carried mostly by the concrete pile. Figure 2.16

shows the contour of temperature-induced axial displacement according to the diffusion within the system. The radial thermal displacements are relatively insignificant compared to the axial thermal displacements according to the very small ratio of the diameter to the length of the pile. As expected, the change in displacement is greatly found in the concrete pile and at the soil surface and the soil mechanical equilibrium is not affected by the heat diffusion. For the sake of clarity, the positive value represents a downward settlement and the negative value represents an upward heave.

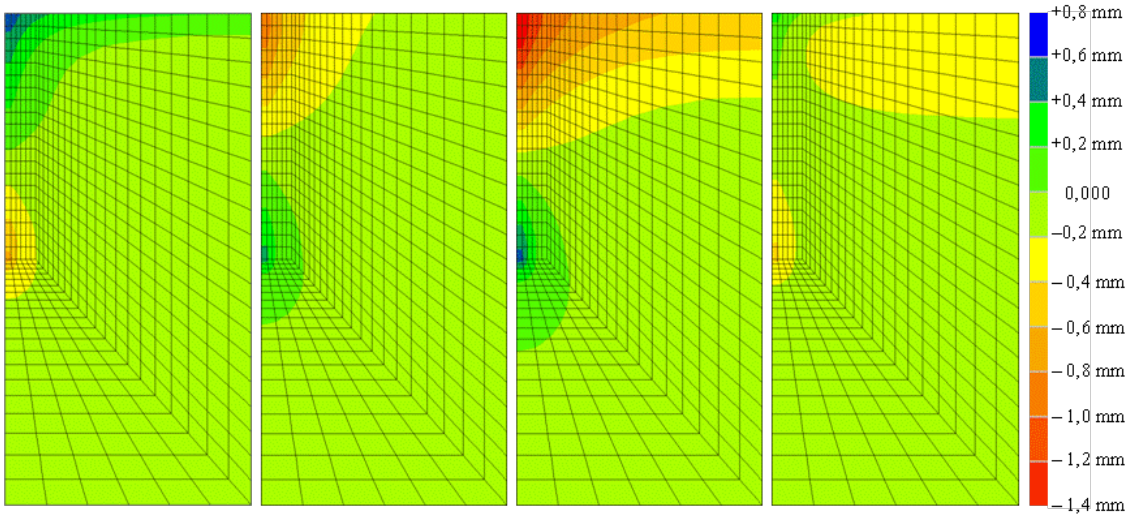

(a) Winter ***(b) Spring*** ***(c) Summer*** ***(d) Autumn***

Figure 2.16 – Contour of temperature-induced displacement at the end of each season of loading

Figure 2.17 shows with a greater clarity the seasonal evolution of the axial thermal displacement at the soil surface and at different depths of the pile. It is clearly seen that over 1 year of thermal loading, the mechanical response of the pile induced by temperature varies following the seasonal temperature variation with $\varepsilon^{th}(t) = \alpha_T \Delta T(t)$. However, over the entire length of the pile, there is a point that does not undergo any change in axial displacement over a year of thermal loading, which is called a null point (Bourne-Webb *et al.* 2013; Bourne-Webb *et al.* 2009; Knellwolf *et al.* 2011). This condition can be found in line with opposite responses in movement of the head and of the base of the pile (Figure 2.18a). This latter is due to the zero restraint at the pile head so the pile can move freely. The thermal displacement of the pile can be translated into thermal deformation based on the applied thermal gradient in the pile as shown in

Figure 2.18b. Because the ground temperature varies with depth, the thermal gradient in the pile and, accordingly, the thermal deformation of the pile is not uniform with depth.

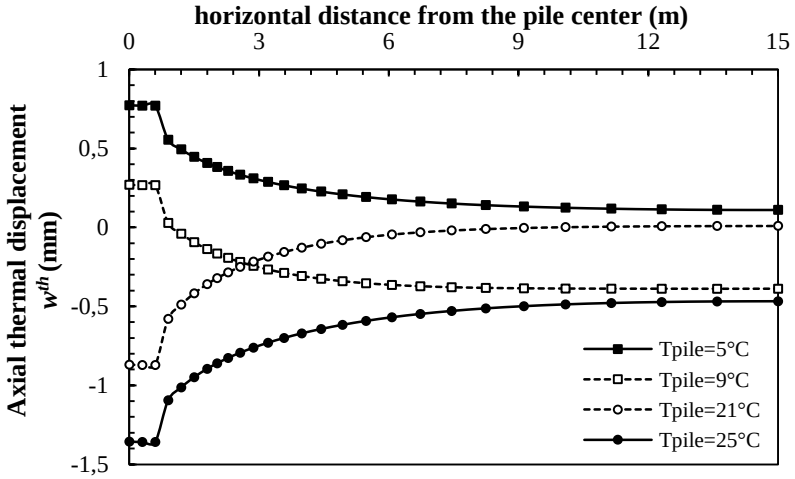

(a) at the soil surface at the end of each season of loading

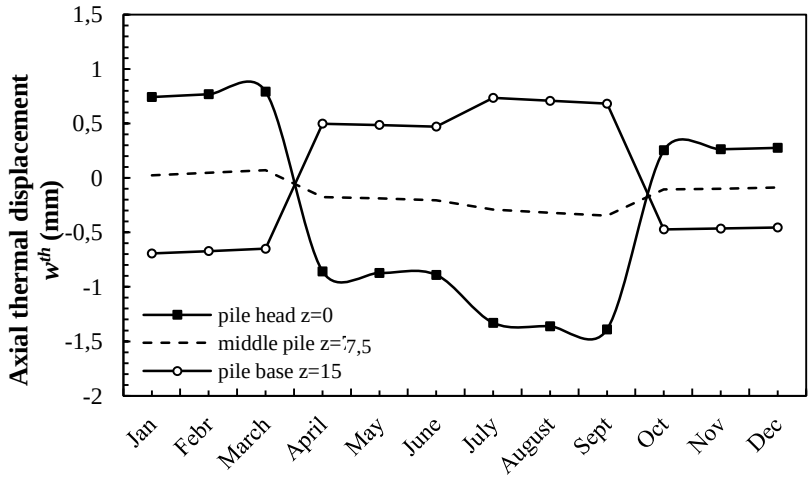

(b) at different depths of the pile over 1 year of thermal loading

Figure 2.17 – Axial thermal displacement

2.5 Conclusion

This chapter deals with the thermal diffusion analysis in a thermo-active pile aiming to adequately understand the diffusion process within the system and thus identify the temperature effect on the mechanical response of such pile. The study is limited in the case of a thermo-active pile located in a fully-saturated sandy soil subjected to a single

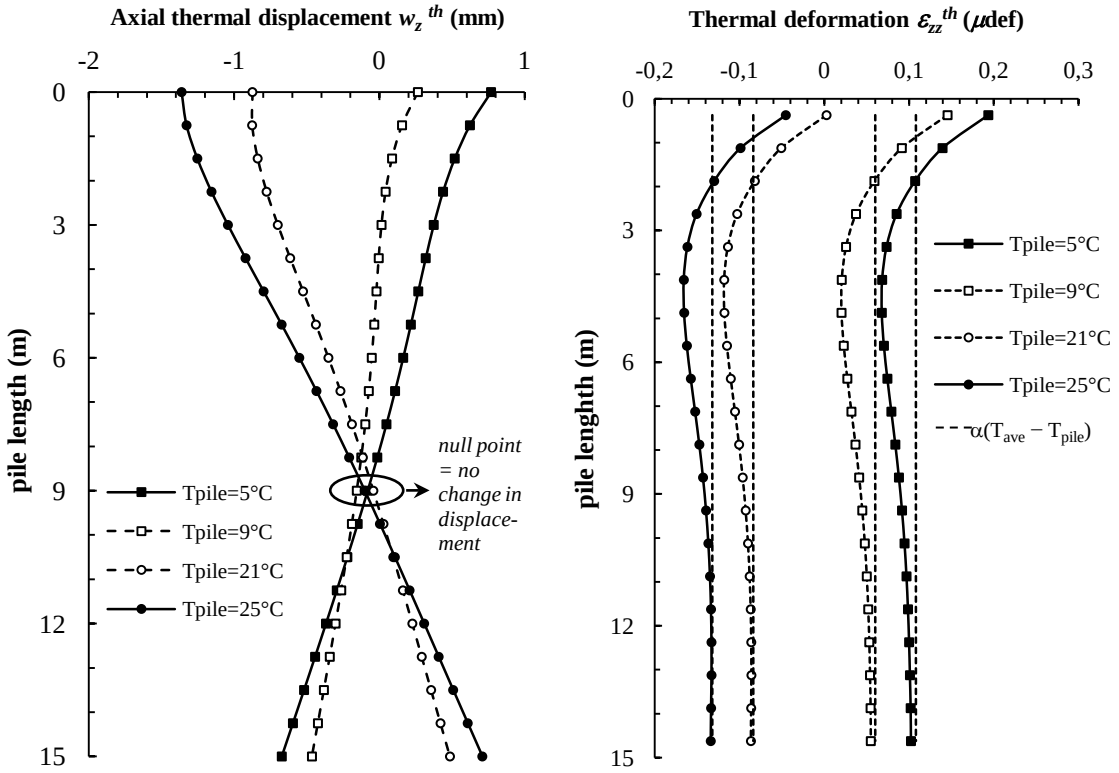

(a) Axial thermal displacement *(b) Axial thermal deformation*

Figure 2.18 – Mechanical response of the pile induced by temperature

thermal loading without any consideration of mechanical loading caused by the weight of the upper structure is given.

In the first part of study, a two-dimensional analysis of the heat diffusion inside the pile is conducted. This study is capable of determining the temperature produced in the pile and at the soil–pile interface due to the fluid injected in the absorber pipes. The results show that the pile temperature over the entire section is homogeneous close to the average temperature of the absorber pipes, with respect to only heat conductive transfer is taken into account. The influence of various types and configurations of the absorber pipe is also analyzed. The W-shaped type delivers higher heat energy than the U-shaped type. However, the study chooses the reference model with 4 U-shaped in anti-symmetric configuration because it produces the most uniform and homogenous temperature and heat flux density inside the pile.

The variation in the ground temperature with time and depth is taken into account in the three-dimensional analysis conducted in the second part of study. The 3D model intends to observe the change in ground temperature profile and thus quantify the additional thermal stress carried in the pile. Analysis is carried out in uncoupled thermo-mechanical model with a continuous seasonal thermal loading. The thermal loads are applied uniformly over the entire pile section with the values equal to the average temperature of the absorber pipes respecting the results of the preceding 2D modeling. After the installation of the thermo-active pile, the ground temperature profile is severely disturbed in time and depth. As a result, the steady annual mean ground temperature T_{ave} moves deeper down beneath 15 m. The heat build-up is produced around the pile and brings up the concentration of the additional thermal stress in the pile and at the soil–pile contact zone.

The change in mechanical response of the pile over 1 year of thermal operation confirms the cyclic variation in the pile behavior. This cyclic response needs to be considered in the geotechnical capacity design of the thermo-active piles foundation. Moreover, during a long-term thermal operation cycles, cyclic degradation in load–settlement capacity in the pile and mobilized shaft resistance at the soil–pile interface could develop. Therefore, modeling the interface elements at the zone of contact between the pile and the soil is necessary to provide a better analysis of the thermo-active piles behavior under cyclic thermal loading.

CHAPTER 3
SOIL–PILE INTERACTION ANALYSIS OF A SINGLE THERMO-ACTIVE PILE*

3.1 Introduction

In the case of thermo-active piles, the concrete pile foundations are used not only as bearing elements but also as heat exchanger elements. For such piles that are located in a fully-saturated sandy soil, the high permeability of the sand makes the heat mass is mostly accumulated around the soil–pile contact surface and thus no temperature change occurs in the sand grains. Accordingly, only the concrete piles undergo additional thermal stress which varies over the season, i.e. contraction during the winter and dilatation during the summer. Since the ratio between the pile diameter and the pile length is very small, the change in mechanical behavior of the pile induced by thermal stress takes place mainly in axial direction. The surrounding soil also restrains the movement of the pile and thus mobilizes the reaction forces along the pile shaft and at the pile base. Hence, the response of thermo-active piles under axial mechanical and thermal loads depends strongly on the friction at the soil–pile interface. In-situ experiences conducted in EPFL and Lambeth College have remarked a variation in pile axial stress of 100–200 kPa and in mobilized shaft friction of –2,1 to +2,5 kPa with a temperature change of 1°C (Amatya *et al.* 2012; Bourne-Webb *et al.* 2009; Laloui *et al.* 2006). It is worth mentioning that the thermal contraction–dilatation in the piles is repeated during the operation cycles, and, therefore, the soil–pile interaction in such piles becomes more complicated. Despite many studies have been conducted in analyzing the thermo-active piles behavior under thermo-mechanical loading, not much

* Some of the materials presented in this chapter have been published in [SUR 14], [SUR 13a], [SUR 13b], [SUR 13d], [SUR 12b], and [SUR 12c] as listed in Appendix C

attention is paid to the impact of cyclic thermal loading on the soil–pile interface over the long-term operation. Indeed, the cyclic fatigue effects can cause degradation in the soil–pile capacity (Poulos 1982).

A remaining issue in the thermo-active pile system is how to optimize the design method and to ensure the safety of the foundation in taking into consideration the thermal interaction and the cyclic effects within the foundation. Despite many installation projects of thermo-active piles have been realized in European countries, the knowledge about the long-term behavior of such piles is still limited. In addition, the conception of thermo-active piles installed in those projects has used a conservative method by multiplying the safety factor, which in fact causes a pile over sizing (Boënnec 2009; Knellwolf *et al.* 2011). This chapter addresses to analyze the soil–pile interaction of an isolated thermo-active pile under combined axial mechanical and cyclic thermal loads. The temperature variations in the circulating fluid are transformed into cyclic thermal deformation, and accordingly, the analysis is conducted in pure mechanical model. The need of correctly modeling the soil–pile interaction is provided by modeling the interface elements at the soil–pile contact zone. Cyclic plasticity in the soil–pile interface is taken into account using the constitutive Modjoin law (Shahrour and Rezaie 1997). With the help of finite difference code, the impact of cyclic thermal loading on the thermo-active pile behavior is analyzed in integrating the cyclic degradation effects.

3.2 Numerical model

For the sake of simplicity in modeling the interface elements, hereafter the thermo-active pile is modeled in rectangular section of width B = 60 cm and length H = 15 m. The pile is located in the center of fully-saturated homogeneous cohesionless soil mass. The surrounding sandy soil is considered very loose. Due to the symmetric condition, only one-fourth of the complete domain is modeled, with the soil lateral extension is set at 15 m (25B) and the height of soil mass at 30 m (2H). Figure 3.1 shows the domain of the model conducted in this present study.

The pile is modeled in linear elastic behavior but the soil behaves in nonlinear elastic. Interface elements using Modjoin law are introduced at the vertical zone of contact between the soil and the pile. The interfaces are pure sliding with no detachment is allowed. No interface element is modeled at the pile base thus the pile base is perfectly bonded to the soil. The interface normal stiffness k_n and shear stiffness k_t are chosen in accordance with the interfaces theory and background of FLAC^{3D} code (ITASCA 2005): 22 MN/m for the normal stiffness and 8,33 MN/m for the shear stiffness. According to the type of soil, the interface strength properties are fixed at 30° of friction angle and 1° of dilation angle and the Modjoin parameters *DR* and *ADR* are set in negative values of −0,05. With regard to the parameters used in the Modjoin interfaces, the behavior of interface has a softening tendency. Tables 3.1–3.2 summarize the properties of the materials used in this present model.

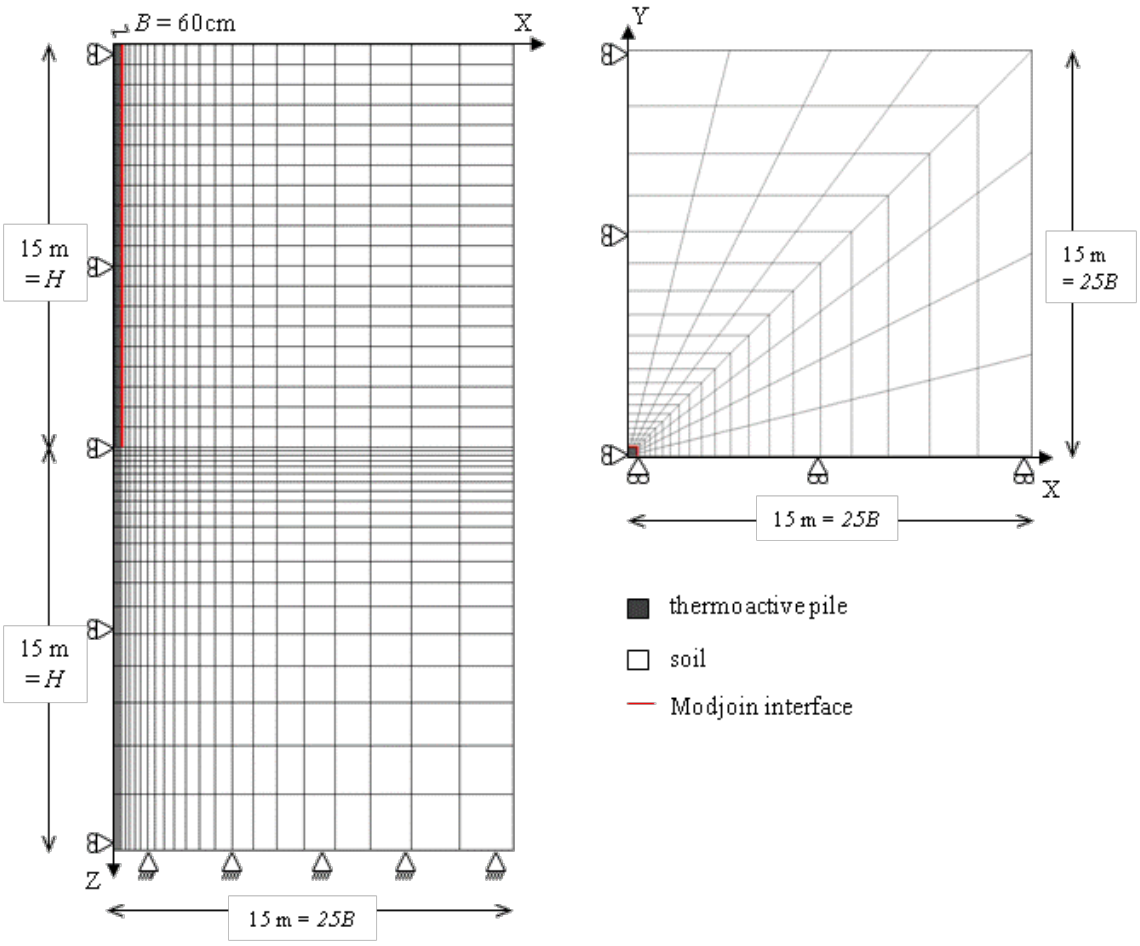

Figure 3.1 – Domain of the numerical model

Table 3.1 – Elastic properties of materials

Material	*Density*	*Young's modulus*	*Poisson's ratio*	*Bulk modulus*	*Shear modulus*	*Thermal expansion coefficient*
	ρ_c	E	v	K	G	α_T
Soil	1950 kN/m^3	10 MPa	0,33	10 MPa	3,75 MPa	5×10^{-6} °C^{-1}
Pile	2500 kN/m^3	20 GPa	0,33	20 GPa	7,5 GPa	$1{,}25\times10^{-5}$ °C^{-1}

Table 3.2 – Characteristic of Modjoin interface

Elastoplastic parameters			***Hardening parameters***	
Normal stiffness	k_n	22 MN/m	*DR*	−0,05
Shear stiffness	k_t	8,33 MN/m	*ADR*	−0,05
Friction angle	φ	30°	γ_c	10 kPa/m
Dilation angle	Ψ	1°	β_c	+1,00
			a_c	−0,03

Modeling the nonlinearity behavior in soil can be done by varying the soil Young's modulus with either stress or strain level (Poulos 1989). In this study, the initial soil Young's modulus E_0 is set to vary with the second deviatoric stress invariant J_2 in a hyperbolic relationship given by:

$$E^* = \left(E_0 + \Delta E\ \bar{z}\right)\left(1 - R_f\sqrt{\frac{J_2}{J_{2\max}}}\right) \qquad [3.1]$$

where ΔE is the increment of Young's modulus per unit depth, $\bar{z}$ is the depth of gravity center of the soil zone, and J_{2max} indicates the second invariant of the maximum deviatoric stress. R_f is the hyperbolic curve-fitting constant equal to 0,9 which corresponds to a compression state in the soil.

The maximum deviatoric stress is defined by the modified Mohr-Coulomb failure criterion, which is based on the fundamental relationship between the soil principal stresses and the Mohr-Coulomb shear strength parameters formulated in *p-q* space (Parry 2004; Schofield and Wroth 1968) as illustrated in Figure 3.2. The failure surface relationship is given as below:

$$f = q - Mp - c^* = 0 \qquad [3.2]$$

where p and q indicate the mean stress in compression and the deviatoric stress related to the soil principal stresses according to equations 3.3–3.4. M and c^* are the Mohr-Coulomb strength parameters given in equations 3.5–3.6 (Schofield and Wroth 1968).

$$p = \bar{\sigma} = -\frac{1}{3}(\sigma_1 + \sigma_2 + \sigma_3) \quad [3.3]$$

$$q = (\sigma_1 - \sigma_3) \quad [3.4]$$

$$M = \frac{6\sin\varphi}{3 - \sin\varphi} \quad [3.5]$$

$$c^* = \frac{6c\cos\varphi}{3 - \sin\varphi} \quad [3.6]$$

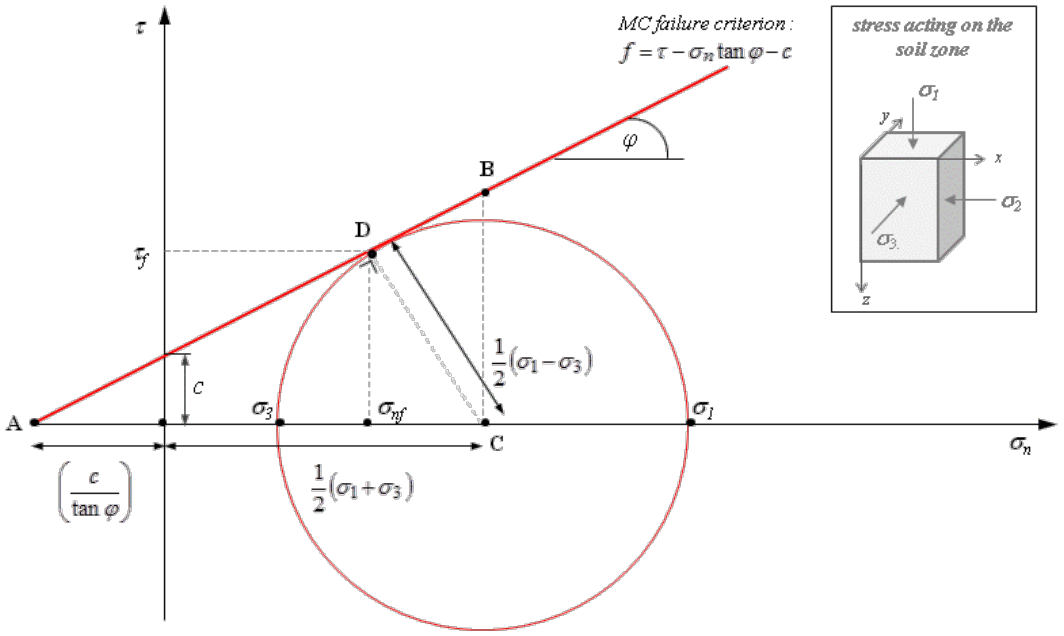

Figure 3.2 – Modified Mohr-Coulomb diagram in p-q space (Schofield and Wroth 1968)

In order to solve equation 3.1, the calculation of the second deviatoric stress invariant is provided by equations 3.7 and 3.8 (Fung and Tong 2001; Malvern 1969) as below:

$$J_2 = \frac{1}{2} s_{ij} s_{ji} = \frac{1}{6}\left\{(\sigma_1 - \sigma_2)^2 + (\sigma_2 - \sigma_1)^2 + (\sigma_3 - \sigma_1)^2\right\} \quad [3.7]$$

$$J_{2\max} = \frac{1}{2} s_{ij\max} s_{ji\max} = \frac{1}{3}(Mp + c^*)^2 \quad [3.8]$$

3.3 Load sequences

When an external axial force P is applied at the pile head, the equilibrium of external forces in the pile is given by the following relation:

$$P = Q_b + \sum Q_s \qquad [3.9]$$

where Q_b denotes the reaction mobilized at the pile base and ΣQ_s denotes the total reaction mobilized at the pile shaft. In the first stage, the pile is subjected to incremental monotonic loading up to the point of failure. According to the French design standard, the ultimate load Q_{ULT} is defined by the applied load causing a pile head settlement of 10% of the pile diameter (AFNOR 2012; Borel 2001). Considering the dead load of the building, the mechanical working load P_W acting at the pile head is fixed at 33% of the ultimate load. Figure 3.3 shows the load–settlement curve of the pile in this case study.

In addition to the mechanical working load $P_W = 792\ kN$, the pile is also subjected to the temperature variations during the seasonal energy extraction with a gradient value of ±10°C from the annual mean ground temperature. The temperature gradient in the pile is assumed to be uniform over the entire pile with respect to the results from the thermal analysis conducted in Chapter 2. Accordingly, the addition of thermal loading is applied in terms of a uniform thermal deformation by multiplying the temperature gradient with the concrete thermal expansion coefficient. Thermal loadings are performed during 12 cycles comprising of 12 cooling phases and 12 heating phases where the schematic of loading cycles is shown in Figure 3.4. The numerical simulations do not depend on time, i.e. steady state condition. However, one cycle of loading corresponds to 1 year of thermal operation, for each thermal phase corresponds to one peak temperature gradient at winter mode or summer mode. For each cycle of loading, the additional thermal loading induces change in total deformation of the pile as follows:

$$\varepsilon^n = \varepsilon^{mec} \pm \varepsilon^{th} = \varepsilon^{mec} \pm \left(\alpha_T \Delta T\right) \qquad [3.10]$$

For the sake of clarity, the positive sign indicates a contraction, compressive stress and downward movement while the negative sign indicates a dilatation, tensile stress and

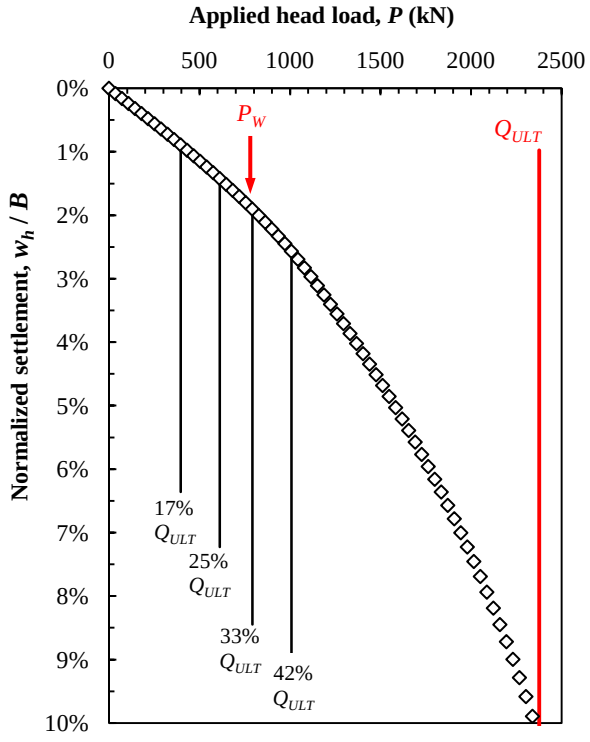

Figure 3.3 – Load–settlement relationship under monotonic loading

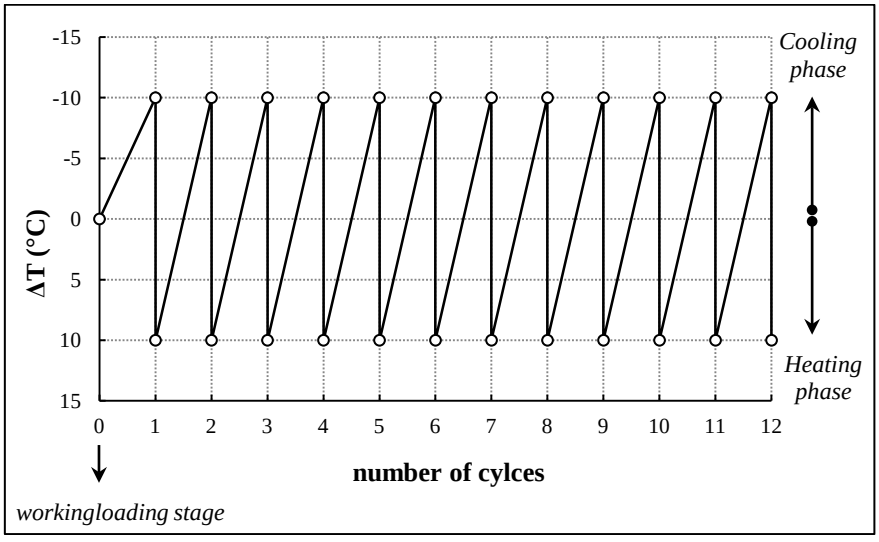

Figure 3.4 – Schema of loading cycles

upward movement. The letter *P* and *Q* are used for the external forces acting on the pile, *P* stands for the load applied at the pile head and *Q* for the reaction forces mobilized in the pile. The indexes "*mec*", "*th*", and "*n*" are used to indicate the stage of loading: "*mec*" for mechanical loading caused by the weight of building, "*th*" for thermal loading induced by temperature variations and "*n*" for cyclic loading comprising of mechanical

and thermal loading over the cycles. Another set of indexes is used to specify where a reaction acts: *"h"* is for the pile head, *"b"* is for the pile base, and *"s"* is for the pile shaft.

In order to properly understand the response of the thermo-active pile, two extreme end-connections representing the pile head axial fixity K_h are modeled: (i) the free head pile with a flexible connection (K_h = 0) and (ii) the restrained head pile with a rigid connection (K_h = ∞). Figure 3.5 shows the load–settlement relationship during cyclic thermal loading. In the free head condition, the pile head is subjected to the constant working load over the thermal cycles thus leads to the increase in head settlement. On the contrary, in the restrained head condition, the head settlement at the mechanical loading stage is maintained constant thus the head load decreases over the cycles.

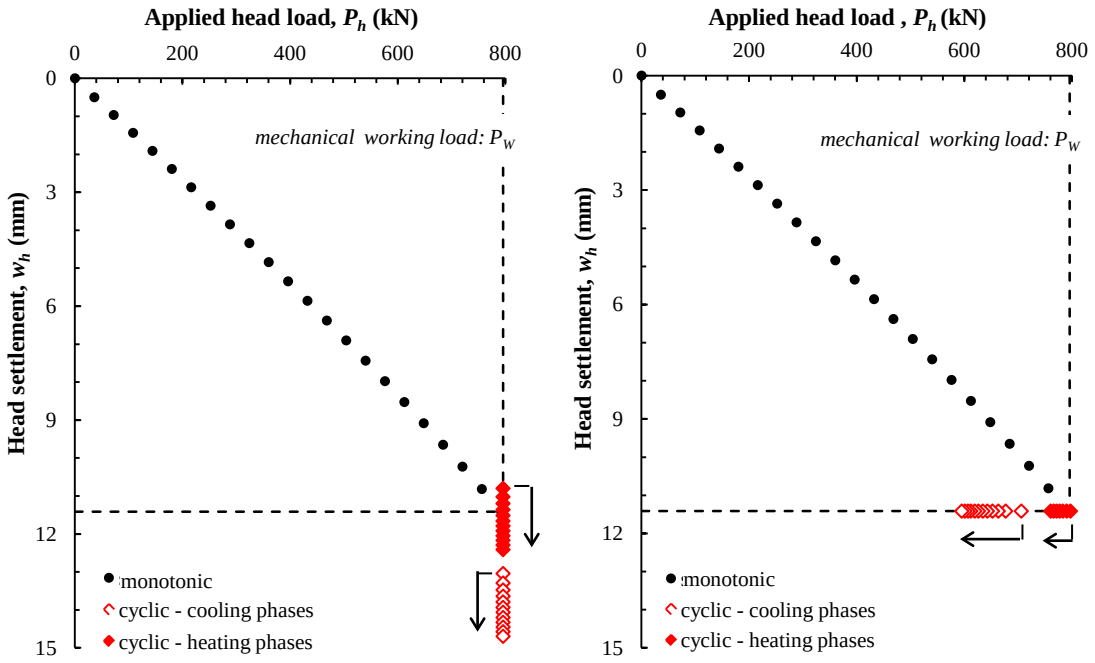

(a) Free head pile ***(b) Restrained head pile***

Figure 3.5 – Load–settlement relationship under cyclic loading

The global response of the pile is shown in Figures 3.6a and 3.7a in terms of the force mobilized along the pile shaft and at the pile base. At the mechanical loading stage, the pile shaft mobilizes the force of 77,5 % and, thus, 22,5 % of the remaining force is mobilized at the pile base. With regard to the mobilization of force, the pile in this study

can be classified as a floating pile. Along the cycles, the forces mobilized vary relative to the restraint condition at the pile head. In general, the forces mobilized along the pile shaft become lower during the cycles while the force mobilized at the pile base increases. This condition is possibly due to the degradation in interface capacity during the cyclic loading. Figures 3.6b–c and 3.7b–c show in more detail the friction mobilized at the Modjoin interface in different depths. It is clearly shown that the interface shear stress decreases progressively over the cycles. The different response of the free head and restrained head pile during the cyclic thermal loading will be explained in details in the next section 3.4.

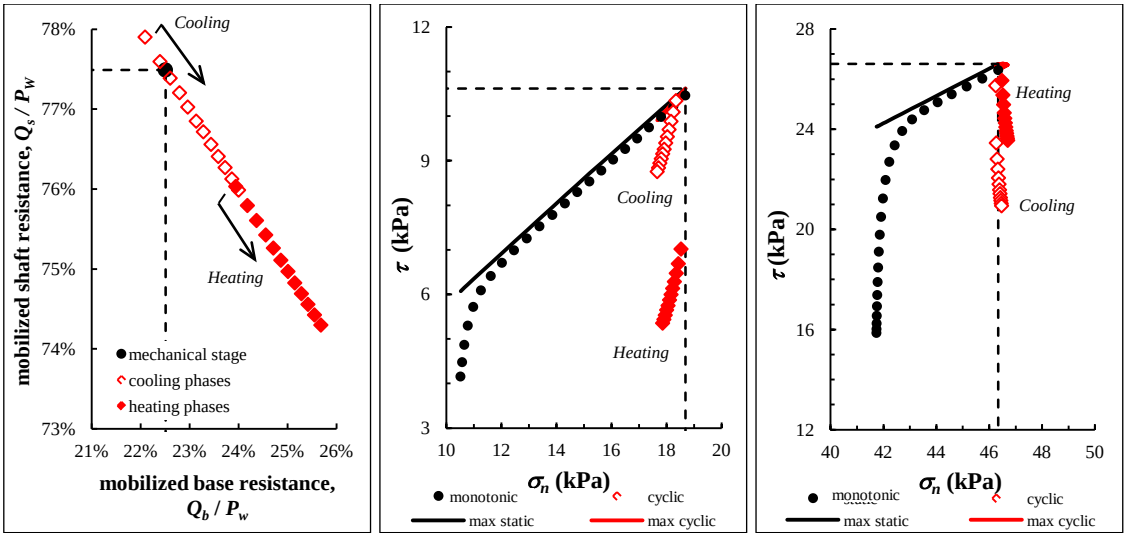

(a) Mobilized resistance ***(b) Mobilized friction at z = 0,2H*** ***(c) Mobilized friction at z = 0,8H***

Figure 3.6 – Mobilized resistance and mobilized friction in the free head pile

3.4 Temperature-induced change in pile behavior

During two-way cyclic thermal loading, the variations of temperature induce change in pile axial stress and in shaft friction at the soil–pile interface. In order to properly understand the effect of temperature on the pile behavior, it is important to compare the pile response during cyclic thermal loading to the initial responses at the mechanical loading stage. Three critical responses are of interest: (i) the change in reaction of the pile head, (ii) the change in normal forces distribution in the pile, and (iii) the change in shaft friction and tangential displacement at the soil–pile interface.

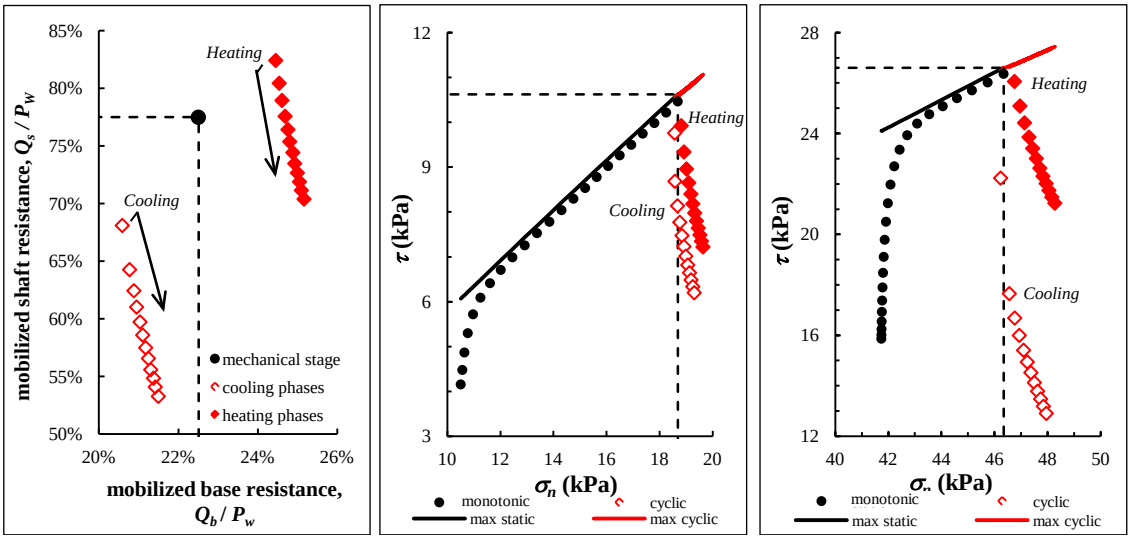

(a) Mobilized resistance *(b) Mobilized friction at z = 0,2H* *(c) Mobilized friction at z = 0,8H*

Figure 3.7 – Mobilized resistance and mobilized friction in the restrained head pile

3.4.1 Change in pile head reaction

In the free head pile, the temperature variations generate change in head displacement on the order of –5% (heave) to +30% (settlement) from its mechanical settlement (Figure 3.8a). Owing to the pile expansion during heating, a pile head heave occurs only in the first five heating cycles and then the pile head becomes to settle due to the cyclic degradation of the soil–pile resistance. At the final thermal cycles, the settlement of the pile is about 3 mm deeper than the mechanical settlement.

Figure 3.8b shows that in the restrained head pile, the head force decreases progressively in the cooling phase from –10% to –25% of its value at the mechanical stage. During heating phases, the first expansion of the pile leads to an additional head reaction force of approximately +7% from its mechanical value and then diminishes during the cycles up to –4% because of the degradation of the soil–pile resistance. Along the 24 thermal cycles, the head force decreases of approximately 200 kN for a temperature change of 10°C.

3.4.2 Change in normal force distribution

Figure 3.9 shows the thermally induced normal force over the length of the pile in the

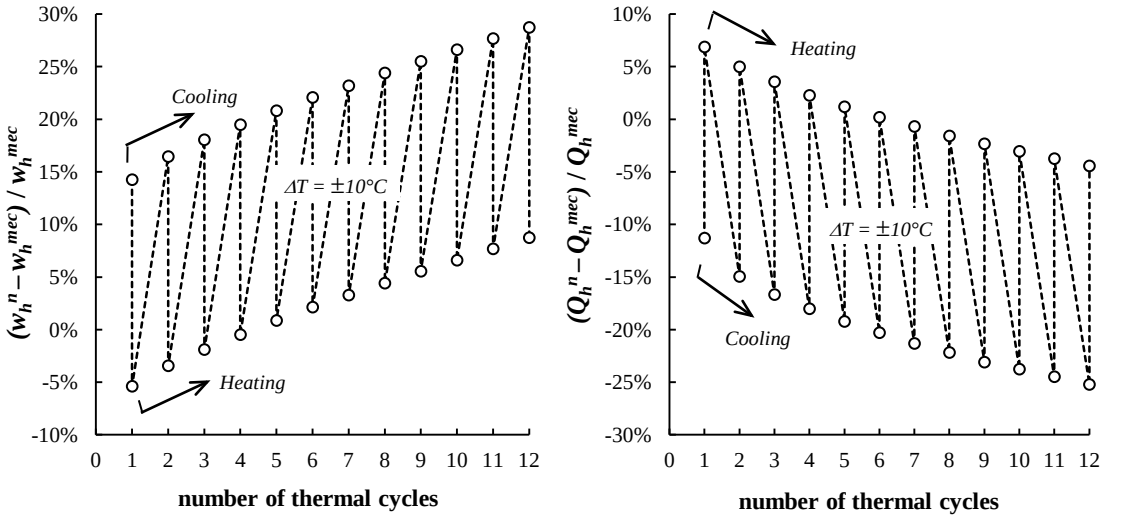

(a) Increase in settlement in free head pile ***(b) Decrease in head force in restrained head pile***

Figure 3.8 – Temperature-induced change in pile head reaction

beginning and in the end of the thermal cycles. In the free head pile, a reduction in normal force is found at the first cooling cycle. This is due to the pile shortening so that the forces are more mobilized to the shear stress at the soil–pile interface. During the cycles, the change in normal force increases with respect to the degradation of the interface resistance. However, the highest value of normal force variation at the final cycle is about 16% of its value at the mechanical stage (Figure 3.9a).

In the restrained head pile, the variation of temperature-induced normal force during the cycles decreases greatly at the pile head and followed by a stiffer bearing resistance due to a bonded interface at the base of the pile with the soil. Figure 3.9b shows that the head force decreases of approximately –25% in the cooling phase and –5% in the heating phase at the end of loading cycles. The decrease in normal forces is more significant during the cooling cycles than during the heating cycles and can lead to the appearance of tensile force in the pile.

3.4.3 Change in shaft friction and tangential displacement at the soil–pile interface

Since the head is free to move, the mobilized shaft friction shows an opposite response at the upper part and the lower part of the pile. In the cooling phase, the pile shortening

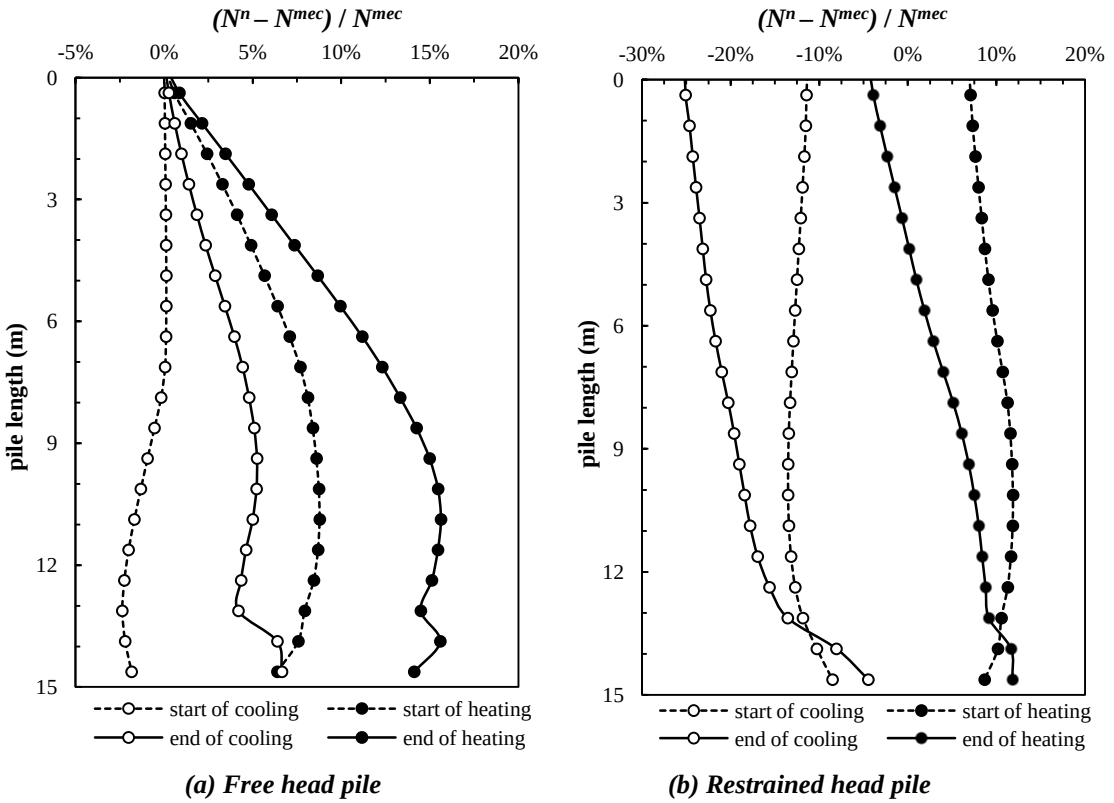

Figure 3.9 – Temperature-induced change in normal force

results in reducing the tip friction while increasing the mobilized shaft friction. In contrast, the heating phase produces an increase in tip friction and a higher reduction in mobilized friction at the upper part of the pile. In this study, the soil–pile interfaces employing the Modjoin law are set to undergo cyclic degradation while the surrounding soil remains elastic with no cyclic degradation. Hence, the forces induced by cyclic thermal loading are accumulated at the soil-pile interface causing a progressive increase in tangential displacement, thus a strain ratcheting phenomenon appears (Figure 3.10a). At the lower part of the pile, a lower degradation of the interface resistance is observed due to the presence of the soil underneath the pile that resists the stress mobilized as well.

For the pile with a rigid connection, the mobilized friction gradually decreases along the entire length of the pile. The deeper the pile shaft is located, the greater the degradation of mobilized friction becomes. Nevertheless, the change in tangential displacement becomes smaller along the pile length. The degradation of temperature-induced

mobilized friction is greater in the cooling phases than in the heating phases due to the reduction in end-bearing resistance when the pile base lifts during contraction. Figure 3.10b illustrates the response of the soil–pile interface during the cycles which shows a relaxation phenomenon.

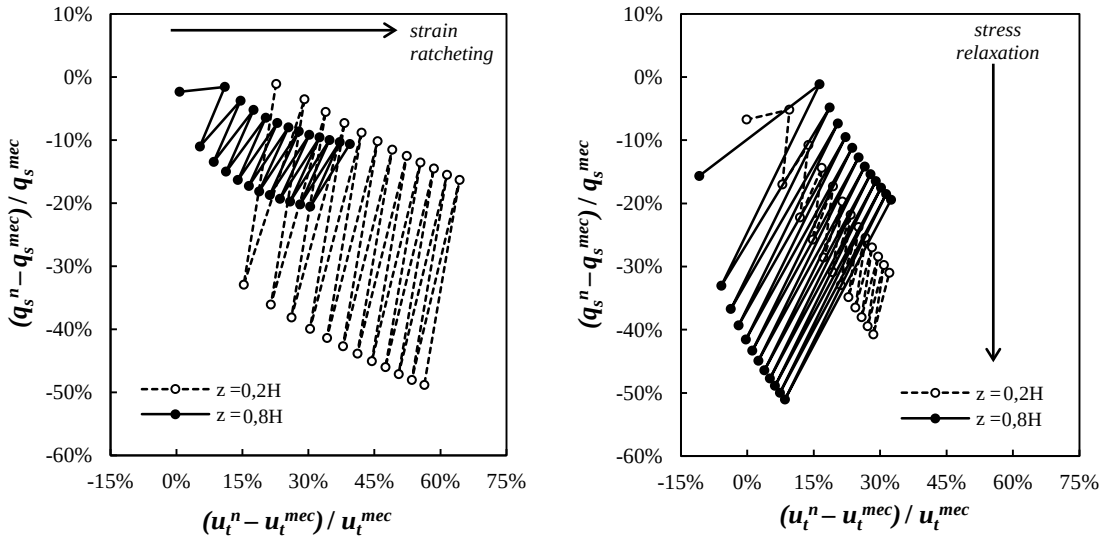

(a) Free head pile *(b) Restrained head pile*

Figure 3.10 – Temperature-induced change in shaft friction and tangential displacement

3.5 Effect of the amount of mechanical working load

According to Eurocode 7, the design of pile foundation can be performed using the ultimate limit state (ULS) and the serviceability limit state (SLS). Depending on the approach, the allowable working load applied at the pile head varies and thus influences the pile dimensioning. The case study analyzed in the preceding section has considered a working load of 33% of the ultimate load. This section is devoted to observe the effect of the amount of mechanical working load on the thermo-active pile response. In reality, the working load applied on the pile head can represent the stage of the building construction.

Figure 3.11 shows the temperature-induced head settlement for several stages of applied mechanical working load. In other way, Figure 3.12 shows the increase in settlement relative to the settlement at the first thermal cycle which represents the cyclic

degradation over the thermal cycles. A small loading rate (i.e. <33% of its ultimate load) leads to a greater amplitude of variations in head settlement during cooling–heating phase but the cyclic degradation over the thermal cycles is relatively small (i.e. low cyclic softening). In contrast, the higher the loading rate is, the smaller the amplitude of settlement–heave variations becomes but the rate of cyclic softening increases rapidly due to the plasticity of the soil–pile interfaces. For example, in the end of 12 years of thermal operation, the increase in head settlement reaches 75% of its mechanical settlement if the pile is loaded at 42% of its ultimate load.

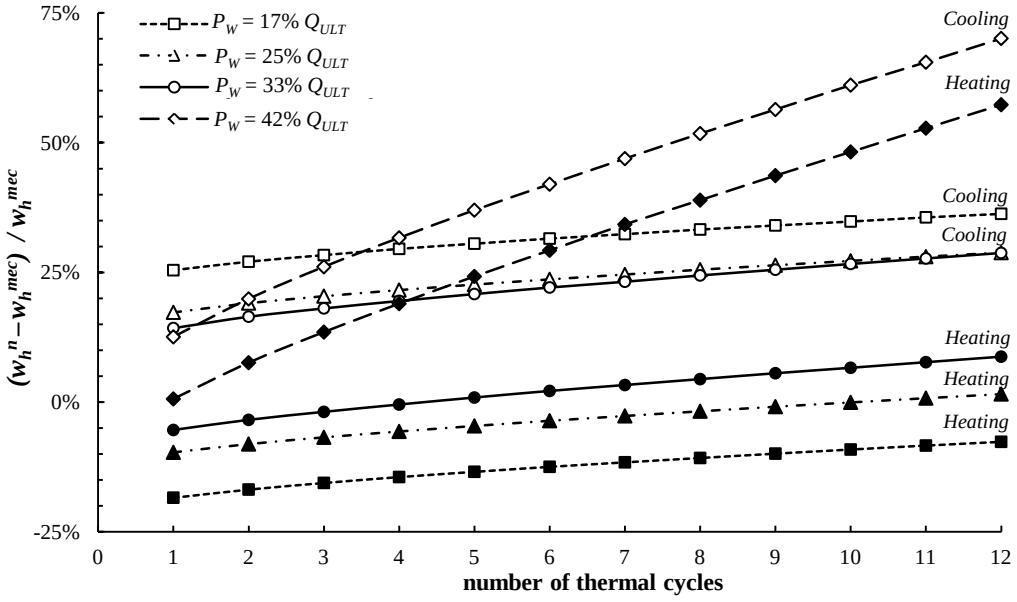

Figure 3.11 – Temperature-induced head settlement for different working loads

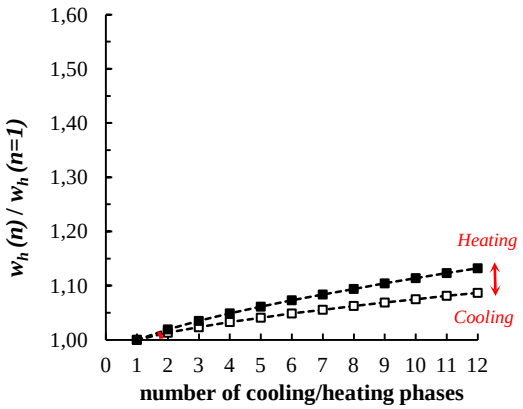

(a) P_W = 17% Q_{ULT}

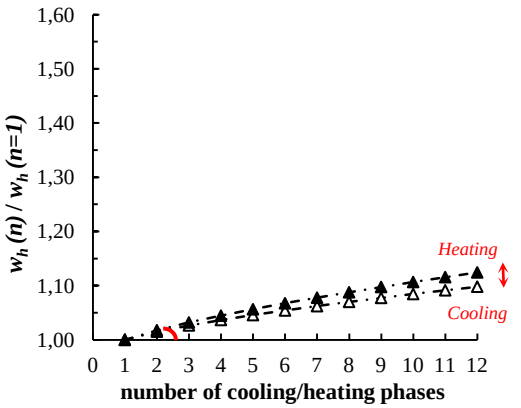

(b) P_W = 25% Q_{ULT}

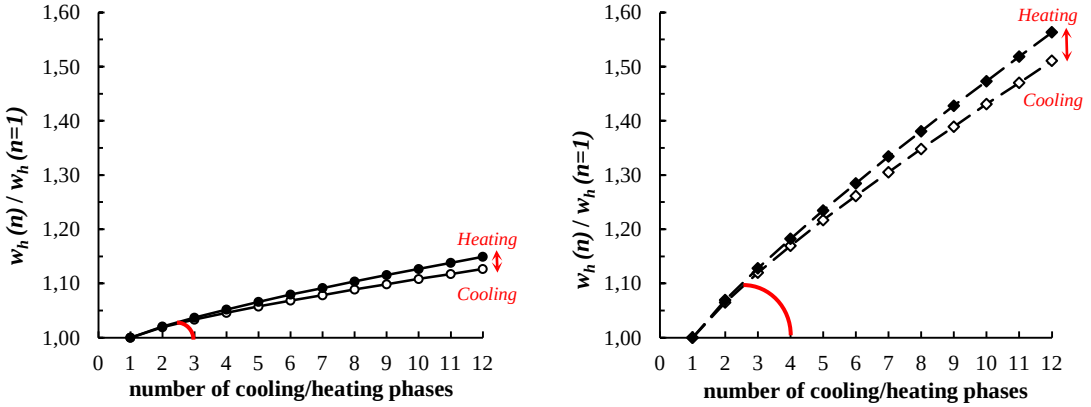

(c) $P_W = 33\%\ Q_{ULT}$ *(d)* $P_W = 42\%\ Q_{ULT}$

Figure 3.12 – Cyclic hardening in head settlement related to different working loads

In the restrained head pile, the effect of the mechanical working load on the change in head force is clearly shown in Figure 3.13. The mechanical working load plays a role in producing the amplitude of variation during the cooling–heating phase. The more the pile is loaded in the mechanical stage, the smaller the amplitude of change is produced. However, in terms of cyclic degradation over the thermal cycles as shown in Figure 3.14, the influence of mechanical working load on the restrained head pile is not as significant as in the free head pile.

With regard to the thermo-active pile responses under different mechanical working loads, the change induced by temperature variations depends absolutely to the initial condition at the mechanical stage of loading. Attention should be paid to the long-term design of the thermo-active piles by considering the effects of working loading rate on the additional thermal stress produced.

3.6 Spread of plasticity

In the reference numerical model described in Section 3.2, the model of soil is limited to nonlinear elastic condition. This section is devoted to observe the influence of the cyclic thermal loading applied in the thermo-active pile on the spread of plasticity in the soil. According to that, an addition of soil plasticity condition is carried by applying the Mohr-Coulomb strength parameters. The soil condition is taken according to the data of

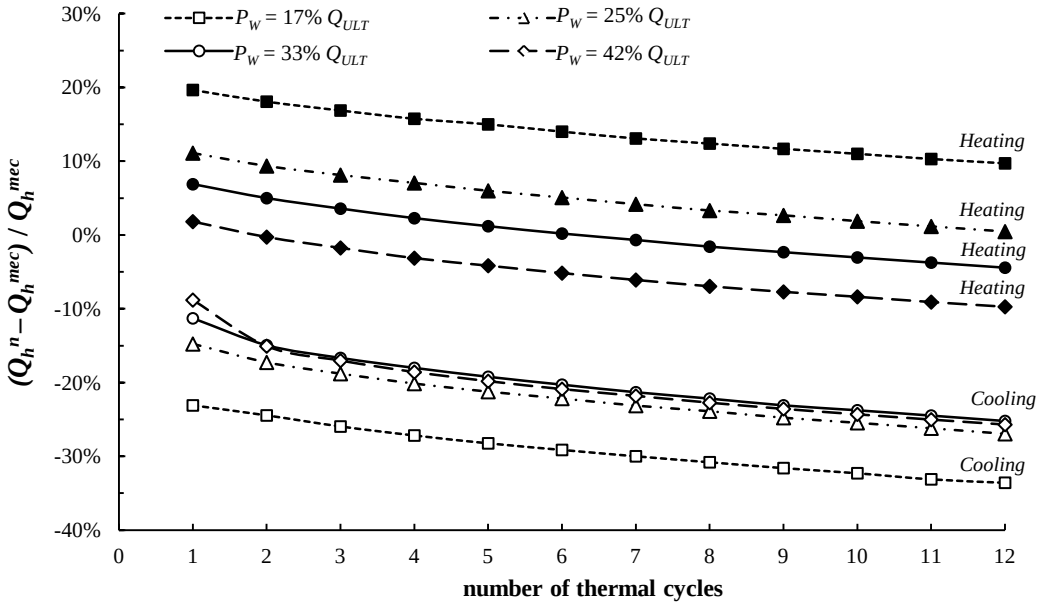

Figure 3.13 – Temperature-induced head axial force in different working loads

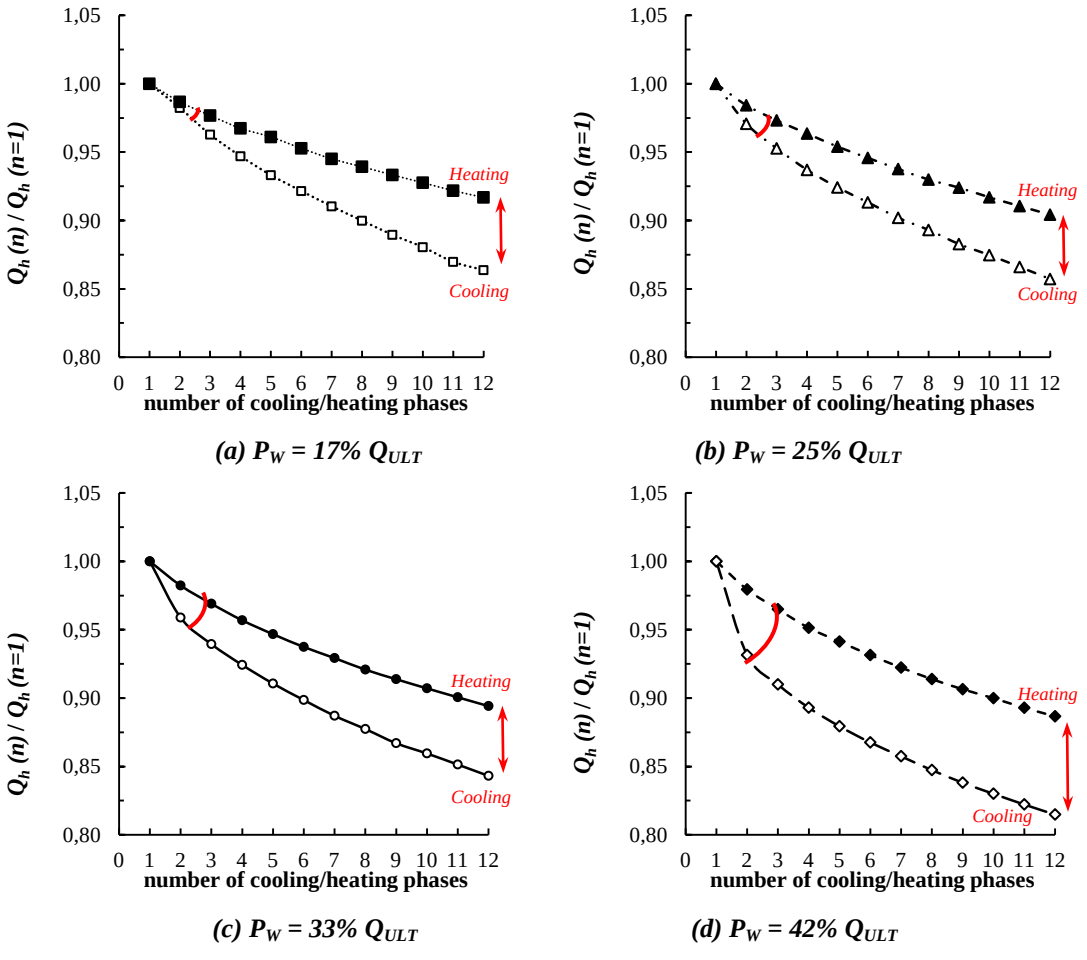

(a) P_W = 17% Q_{ULT}

(b) P_W = 25% Q_{ULT}

(c) P_W = 33% Q_{ULT}

(d) P_W = 42% Q_{ULT}

Figure 3.14 – Cyclic hardening in head force related to different working loads

the Flandres sand with 38° of friction angle, 1 kPa of cohesion, and 0° of dilation angle. Other properties of model (i.e. elastic properties and Modjoin parameters) remain the same as listed in Tables 3.1 and 3.2.

Figure 3.15 shows the evolution of soil plastic zone in the case of 33% of the ultimate load was applied in the mechanical stage. The plasticity in the soil spreads mainly around the contact zone between soil and pile. Over the cycles, there is no variation in the soil plastic zone. This is because the interface elements are employed using the nonlinear cyclic plasticity law, the Modjoin law. Thus, the spread of plasticity is concentrated in the Modjoin interfaces.

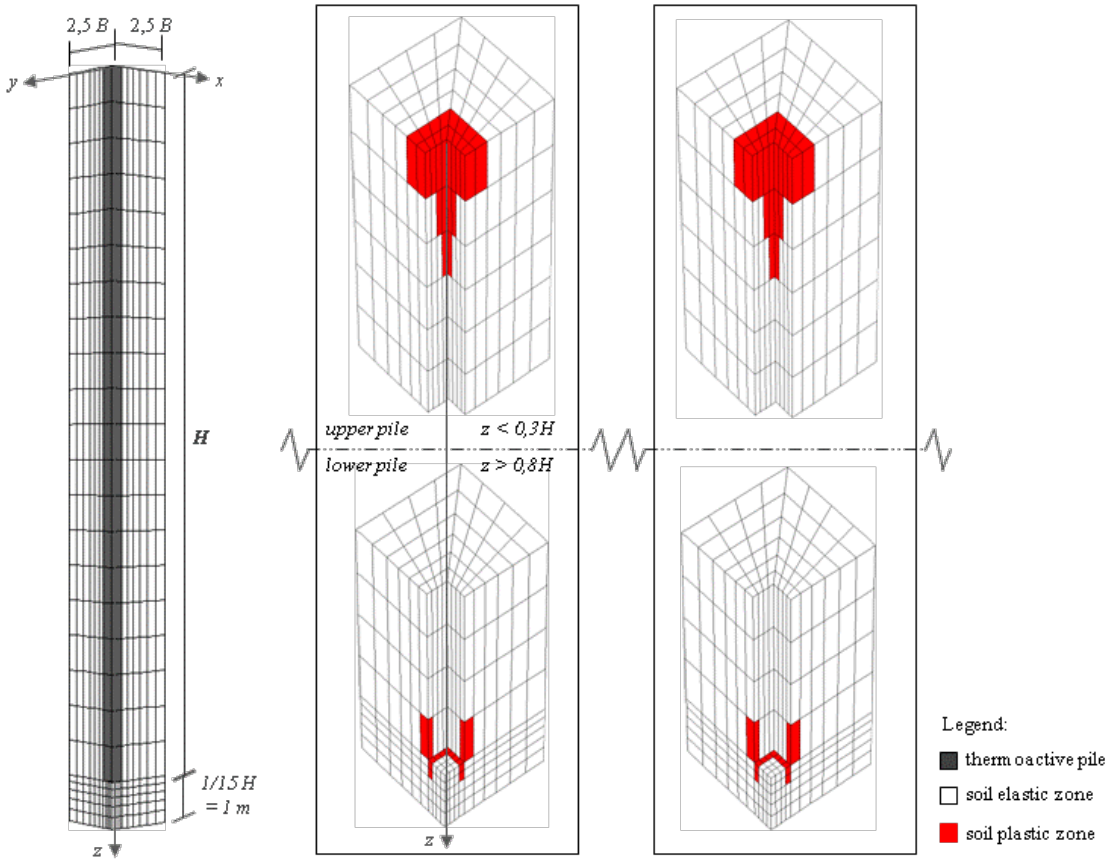

(a) Domain of observation *(b) Initial condition – Mechanical loading* *(c) No change in plastic zone over cycles*

Figure 3.15 – Evolution of plastic zone in soil over the cycles at P_W = 33% Q_{ULT}

But, if the mechanical working load applied to the pile is equal to 42% of the ultimate load, two additional plastic zones are found near the pile base (Figure 3.16). This result

is in accordance with the study conducted in the Section 3.5 about the effect of the amount of mechanical working load. When the pile is loaded initially at 42% of the ultimate load, the Modjoin interfaces undergo high degradation in their capacity. In this state, the spread of plasticity is also distributed to the soil zone to prevent failure in interface elements.

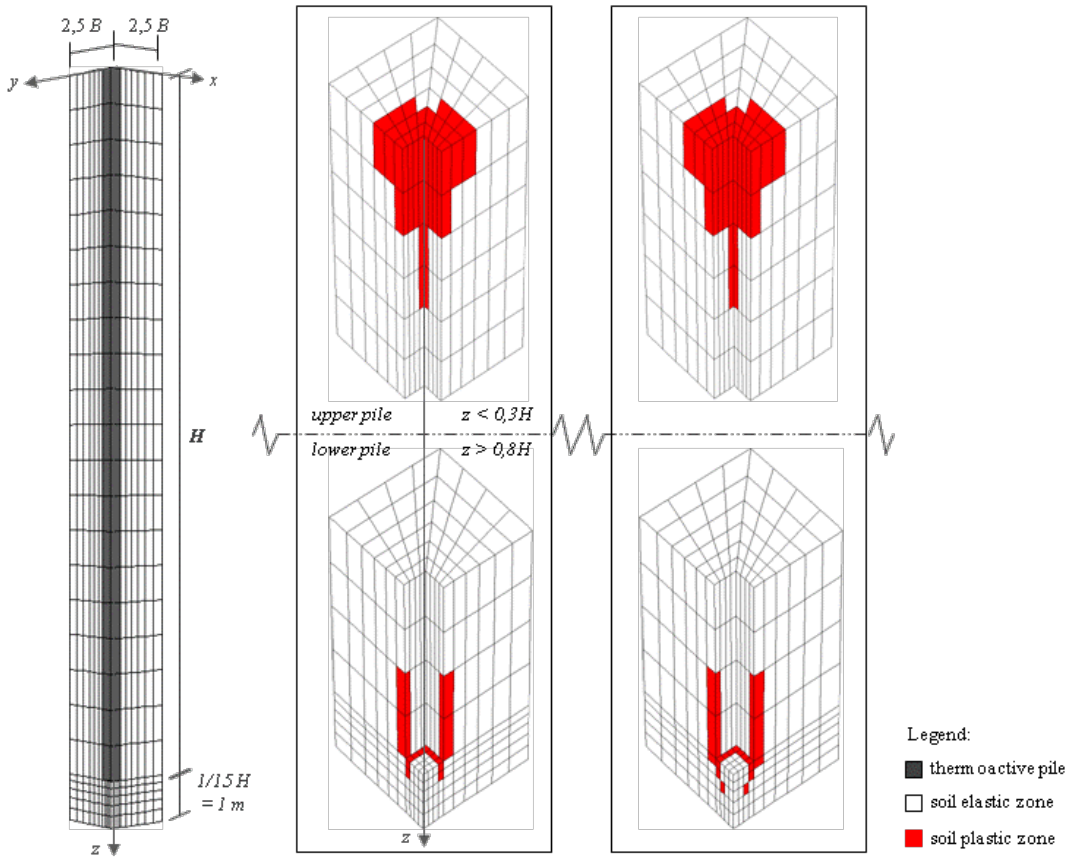

(a) Domain of observation *(b) Initial condition – Mechanical loading* *(c) Increase in plastic zone at cycle n = 22*

Figure 3.16 – Evolution of plastic zone in soil over the cycles at P_W = 42% Q_{ULT}

3.7 Conclusion

This chapter presents a numerical study of a single thermo-active pile behavior in taking soil–pile interaction into account. The case study concerns a single pile which is subjected to axial mechanical load coming from the permanent loads of the building and also to cyclic thermal load induced by temperature variations. The temperature

variations in the pile are modeled as thermal deformation by multiplying the temperature gradient with the concrete thermal expansion coefficient. Accordingly, the analysis is conducted in pure mechanical model at steady state condition. Interface elements are introduced at the soil–pile contact zone in attempting to properly model the soil–pile interaction under axial loading. With regard to the repeated thermal contraction–dilatation in the thermo-active pile, a consideration of cyclic plasticity behavior is required. Therefore, the sophisticated Modjoin law developed in the laboratory LGCgE is implemented in the interface elements, which allows the interfaces to have a kinematic hardening under cyclic loading.

The numerical study conducted allows observing the influence of cyclic temperature variations in thermo-active piles on the long-term geotechnical capacity, in terms of the change in head force and head settlement at the pile–upper structure interface and the change in mobilized shaft friction and bearing capacity at the soil–pile interface. The values of change resulting from the numerical study are still permissible below the failure limit. These results give a perspective that the thermo-active pile can still resist the additional cyclic thermal stress when the pile is correctly modeled using the actual design code.

However, the values of change in head settlement, normal stress, and mobilized shaft friction which are induced by temperature variations can be useful to verify three following aspects for both the SLS and ULS design methods:

(i) the load–settlement capacity,
(ii) the concrete tensile limit state, and
(iii) the ultimate bearing capacity.

Thus, a more refined geotechnical design for the thermo-active piles foundation can be achieved instead of doubling the safety factor. In addition, the magnitude of the additional stress produced is strongly related to the working load applied at the mechanical loading stage. A greater working load is advantageous in the first thermal cycle but becomes unfavorable in the long-term thermal operation due to the yielding of soil and the greater cyclic degradation in soil–pile interface. At last, the parameters

chosen for the Modjoin interface in this study lead to the emergence of cyclic degradation effects: strain ratcheting and stress relaxation. An ongoing project of loading tests on full-scale thermo-active piles will provide the real data to calibrate the cyclic parameters used in numerical model.

CHAPTER 4
ANALYSIS OF THE THERMO-ACTIVE PILES LOCATED IN A GROUP OF PILES*

4.1 Introduction

When piles are arranged in a closed-spaced group, the piles and the soil contained within the group act together as a single unit structure (Ng *et al.* 2004). With respect to the number of piles, a group of piles can obviously support a greater load than a single pile foundation. However, the group capacity is strongly influenced by the piles–soil interaction which is dependent on the group configuration, the size of the group and the spacing between piles. In practice, a pile cap is laid in direct contact with the subsoil to connect the head of piles, which is known as piled raft system. This system will achieve a higher bearing capacity due to the presence of the cap. Nevertheless, the position of cap in direct contact with soil will lead to a complex piles–soil–cap interaction problem.

As a consequence of interaction in the group, the center pile suffers greater settlements than the peripheral piles under a flexible cap or carries the smallest load distribution among the other piles under a rigid cap (Chow and Thevendran 1987; Fleming *et al.* 2008; Poulos and Davis 1980). This condition is generally obtained for uniformly loaded pile groups with identical size and properties for all piles. The interaction effects on the overall group capacity can be analyzed by determining the ratio of the average settlement of pile groups to that of a single pile at a comparable mean load per pile (Poulos and Davis 1980). On the other hand, the interaction between piles has a much greater effect on the group stiffness efficiency, which is defined as the ratio of the group stiffness to the sum of individual pile stiffness in the group. The group stiffness

* Some of the material presented in this chapter has been submitted to *Acta Geotechnica* as listed in Appendix C

efficiency is generally reduced by the proximity of other piles due to a closer interaction among the piles, and, accordingly, the settlement ratio increases (Comodromos *et al.* 2003; Fleming *et al.* 2008; Randolph 2003b).

In the case of using the thermo-active piles to provide heating/cooling of the building, not all of the piles in the foundation system is necessarily needed to be activated as thermo-active element. The number of piles required as thermo-active element is related to the energy demand of the building and the energy source capacity of the ground. Since the thermo-active piles undergo cyclic contraction–dilatation over the thermal operation and the other neighboring piles have only a compressive load caused by permanent load of the building, it becomes a great interest to study the interaction between the thermo-active and classic bearing piles. This chapter is addressed to study the behavior of the thermo-active piles within a group of piles by numerical modeling method with the help of finite difference code FLAC^{3D}. Consideration of cyclic degradation effects is taken into account by modeling interface elements along the vertical soil–pile contact zone, employing the Modjoin law in nonlinear cyclic plasticity behavior. In the first time, a pile group without cap representing a very flexible cap not in contact with the ground is modeled in order to fully understand the group effect on the thermo-active piles behavior. Afterwards, a pile cap is modeled in direct contact with the ground to create a piled raft foundation system. Several values of cap rigidity are taken into account in attempts to represent the end-restraint connection between the foundation and the upper structure. This second case intends to study the effect of pile–soil–structure interaction on the thermo-active piles behavior in a group.

4.2 Pile group model

A group of 3×3 piles is embedded on very loose sandy soil. Among the piles, there are 4 thermo-active piles located in the corner of the group. All piles are identical in size: $B \times B \times H$ equals 60 cm × 60 cm × 15 m. Based on economic and practical viewpoint, Prakash and Sharma (Prakash and Sharma 1990) suggested an optimal pile spacing equals 3,0–3,5 times of the pile diameter, while Frank (Frank 1995) stated that a minimal centre to centre spacing between two piles should be 2,5 of the pile diameter. If

a cap is laid on the head of piles, a distance of minimum 250 mm should be provided beyond the outside face of the corner piles (Bowles 1997). Otherwise, to achieve a rigid connection between the foundation elements and the upper structure, a cap thickness of 2*B* is required (Fleming *et al.* 2008).

Accordingly, the pile group model in this study has a pile spacing of 3*B* equals 1,8 m, an edge clearance in the cap of 1*B* (60 cm), and a cap thickness of 1*B* (60 cm). The geometry detail of the model is shown in Figure 4.1. The abbreviations "P1", "P2", and "P3" indicate the pile in the centre, the piles at the side, and the piles in the corner of the group, respectively.

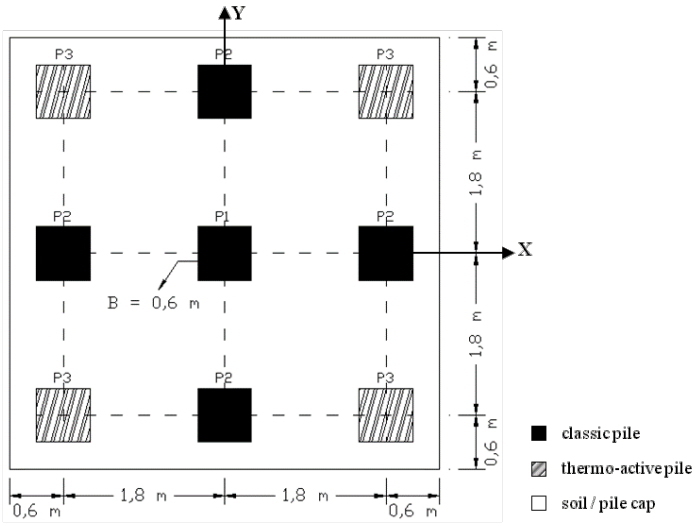

Figure 4.1 – A 3×3 group configuration

All piles are in sliding contact with the surrounding soils employing the Modjoin law. The surrounding soil is modeled in nonlinear elastic condition by varying the initial soil Young's modulus according to equation 3.1. The properties of soil, piles, and Modjoin interfaces as well as the loading stages applied in the pile group remain the same with the previous study of a single thermo-active pile (see Sections 3.2–3.3 and Tables 3.1–3.2). The axial mechanical load is applied in the form of uniform compressive stress distributed equally to the head of all piles (for the group without cap) or to the pile cap (for the group with cap). In order to correctly compare the response of a pile group to that of a single pile, the group is loaded with the same mean load per pile. Thus, the mechanical load applied in the group is equal to the sum of the mechanical load applied on a single pile multiplied with the number of piles in the group:

$$P_{Group} = \sum_{i=1}^{9} P_{SP} = 9 \times \overline{P} \qquad [3.1]$$

where i = number of piles in the group, P_{SP} = load applied on a single pile, and $\overline{P}$ = mean load applied in the group per pile.

Under axial loads, the group interaction can be related to the relative stiffness between the pile and the soil, which is defined as the ratio of the Young's modulus of the pile to that of the soil (Frank 1995; Poulos and Davis 1980). The model in this study has a soil–pile relative stiffness K_{ps} equals to 2000 that represents a high interaction factor ($K_{ps} = E_{pile} / E_{soil} = 20\,\text{GPa}/10\,\text{MPa} = 2000$).

Analysis of the thermo-active piles under axial mechanical and cyclic thermal loads in a group of 3×3 piles will be detailed in the next section as proposed earlier: the case of pile group without cap and the case of piled raft foundation.

4.3 Case I – Pile group without cap

This case is addressed to fully understand the group effect on the thermo-active pile response and the piles–soil interaction effect between the thermo-active piles and the other classic bearing piles. For the sake of symmetrical condition, only a quarter of the complete domain is modeled as shown in Figure 4.2. In the first stage of loading, the group is loaded up to a comparable working load to that of single pile, P_W = 33% of the ultimate load of the singe pile. Since no cap is modeled and all piles are identical in size, all piles have an equally distributed load $\overline{P} = P_W$. The comparative response of the pile group and single pile in terms of load–settlement curve and force mobilized along in the piles is shown in Figure 4.3. Hereafter, the abbreviation "SP" and "GP" will be used to refer to the case of single thermo-active pile and pile group without cap.

Since the design of pile groups in sand is usually controlled by settlement considerations, it is important to determine the ratio of settlement of pile groups to that of single pile at the same working load. Vesic (1997) proposed a theoretical relationship

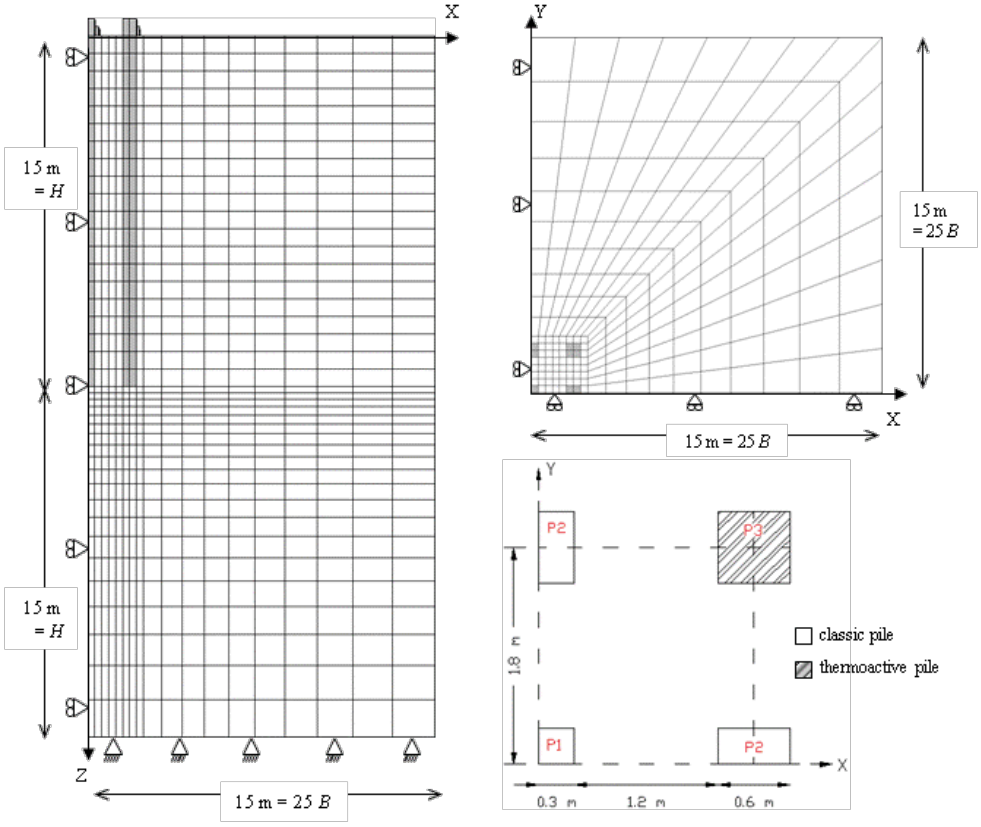

Figure 4.2 – Domain of numerical model for the GP case

to determine the settlement ratio R_a as below:

$$R_a = \frac{\text{average group settlement}}{\text{settlement of a single pile for the same mean load}} = \sqrt{\frac{B_{group}}{B}} \qquad [3.2]$$

where B_{group} = the width of the pile group and B = the pile width. Based on this relationship, the pile group in this study has a theoretical settlement ratio equals to 2,82.

However, according to Figure 4.3a, for the same P_W applied to the pile group, the group settlement equals 5% of the pile diameter while the settlement of a single pile equals 2% of the pile diameter. A settlement ratio resulting from the numerical analysis is equal to:

$$R_a = \frac{\text{average group settlement}}{\text{settlement of a single pile for the same mean load}} = \frac{3\,\text{cm}}{1{,}2\,\text{cm}} = 2{,}5$$

The group stiffness efficiency factor, which is defined by the ratio of the stiffness of the overall group to the sum of individual pile stiffness in the group, is calculated as below:

$$R_G = \frac{\text{stiffness of the group}}{\text{sum of individual pile stiffness}} = \frac{P_W / w_{Group}}{\sum_{i=1}^{9} (P_W / w_{SP})} = \frac{1}{R_a} = 0{,}4$$

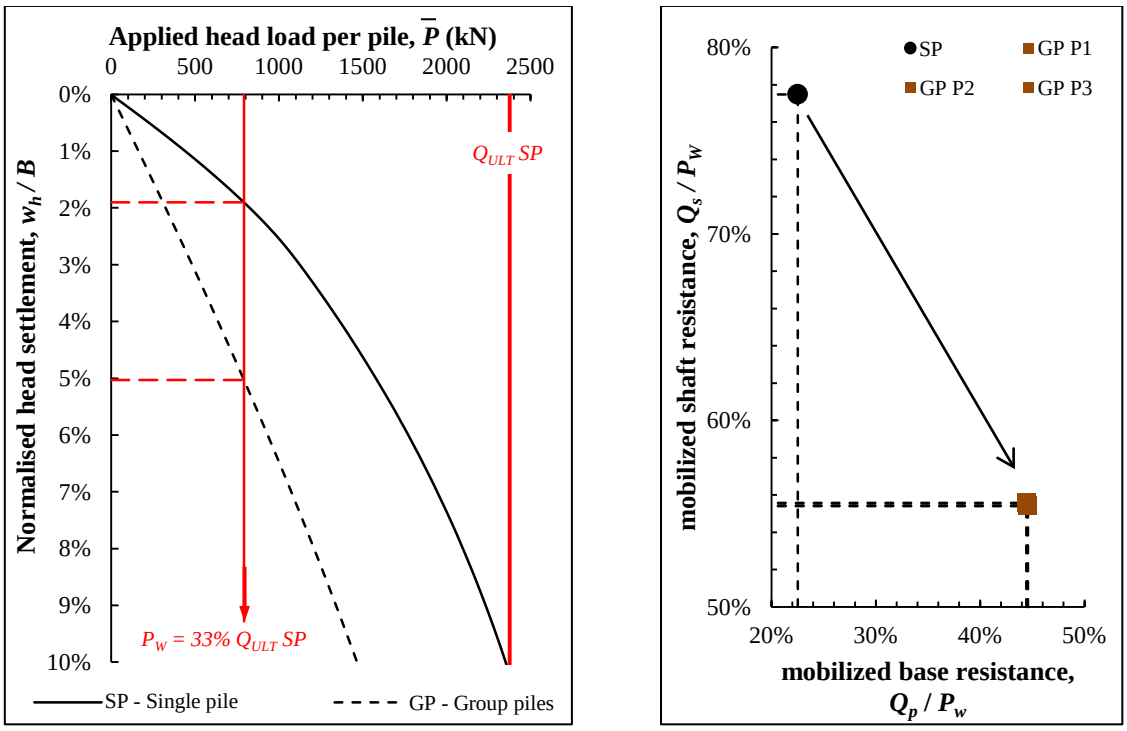

(a) Load–settlement curve *(b) Force mobilized at the working load*

Figure 4.3 – Response of pile group and single pile under monotonic loading

The great value of settlement ratio and the low value of stiffness efficiency factor are obtained due to the close proximity between the piles (i.e. 3*B* of centre to centre spacing) which produces a high piles–soil interaction in the group. As a consequence, the force mobilized at the pile base increases 22% of that of single pile while the force mobilized along the pile shaft decreases 22% of that of single pile. The comparison result of mobilized force for the GP and SP cases is best described in Figure 4.3b.

In the second stage of loading, 4 thermo-active piles in the corner of the group (P3) are activated as thermo-active elements. These 4 piles are subjected to 12 cycles of axial thermal deformation with temperature gradient of ±10°C from the ground temperature. The schematic of thermal loading cycles in the thermo-active piles was previously presented in Figure 3.4. No additional load is applied on the other neighboring piles (P1

and P2) during this second stage of loading. Since all the pile heads in the group are free to move, the GP case is intended to be compared with the SP case in the free head condition.

4.3.1 Comparison with the single pile case in free head condition

4.3.1.1 Change in pile head settlement

Under the same working load, the piles–soil interaction in the group results in a smaller thermal stress in the thermo-active piles. Figure 4.4a shows that the percentage of additional thermal settlement in the thermo-active piles in the group is smaller than that of a single pile. Moreover, the increase in pile head settlement over the cycles has a tendency to stabilize, which means that the thermo-active piles in the GP case has a lower cyclic hardening (Figure 4.4b). This is possibly due to the group effect which increases the overall rigidity of the foundation system and distributes the thermal variations effect to other piles. As a result, the neighboring piles undergo increase in pile head settlement during the thermal cycles even though the values of variation are very small.

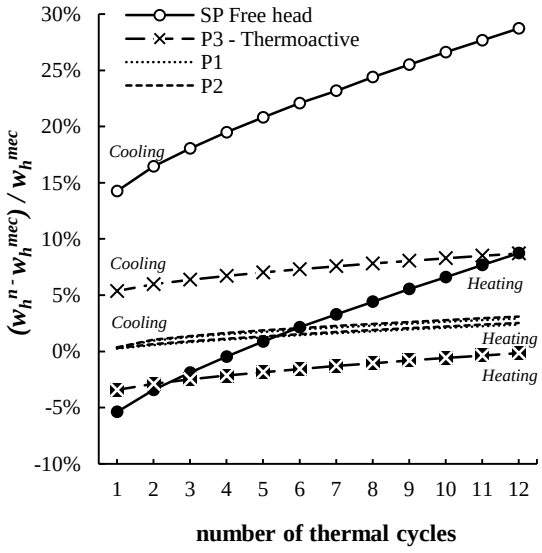

(a) Increase in head settlement relative to mechanical stage

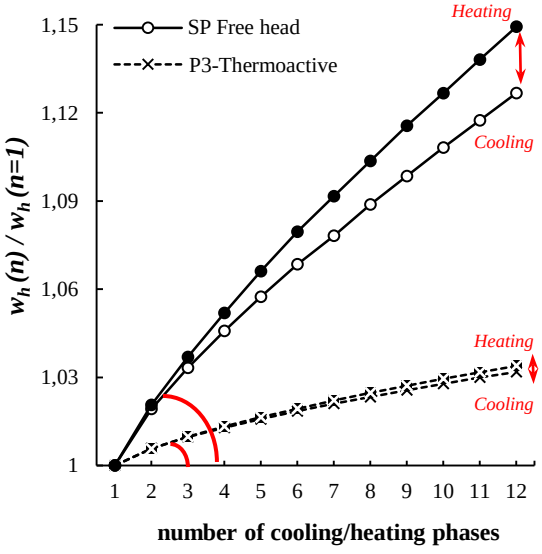

(b) Cyclic hardening in the thermo-active pile relative to the first cooling/heating phase

Figure 4.4 – Comparison of the pile head response for the SP and GP cases

4.3.1.2 Distribution of axial displacement and normal force

To have a better understanding, Figures 4.5 and 4.6 show the distribution of thermal axial displacement over the entire pile length in the beginning and in the end of thermal cycles. Figure 4.5 concerns the thermo-active piles for the SP case in free head condition and the GP case (P3) while Figure 4.6 concerns the neighboring piles in the group (P1 and P2). Thermo-active piles have a reverse response in displacement at the upper-half and at the lower-half of the pile. A null point is found representing a node in the pile which does not undergo change in displacement due to temperature variations. The influence of thermo-active piles (P3) on the other neighboring classic piles (P1 and P2) is better shown in Figure 4.6. The presence of thermo-active piles in a pile group does not influence a change in other classic piles behavior at the beginning of the thermal cycles. However, due to the interaction effect with the thermo-active piles, the displacement of the classic piles increases with the number of cycles. Nevertheless, the distribution of displacement over the pile length is uniform in the classic piles because the piles do not have contraction–dilatation phenomena unlike the thermo-active piles.

In terms of normal force distribution over the pile length, as previously stated, the additional thermal stress produced in the thermo-active piles in the group is smaller than that of single pile since the group effect plays a role to also distribute the thermal variations effect to the other piles. Accordingly, the neighboring piles receive indirect influences of thermal variations. While the thermo-active piles P3 undergo a contraction phenomenon during cooling phases (i.e. a decrease in normal force), the piles P1 and P2 undergo tension and get an increase in normal force. Similar response occurs during heating phases, while the thermo-active piles P3 expand and have an increase in normal force, the normal forces in P1 and P2 decrease. Figures 4.7 and 4.8 illustrate the response of the group in distributing the normal force under temperature variations.

4.3.1.3 Soil movement around the piles in the group

The group effect does not only change the state of force–displacement on the other neighboring piles but also change the state of force–displacement in the soil contained within the group. The change in soil movement is best described in Figure 4.9 which

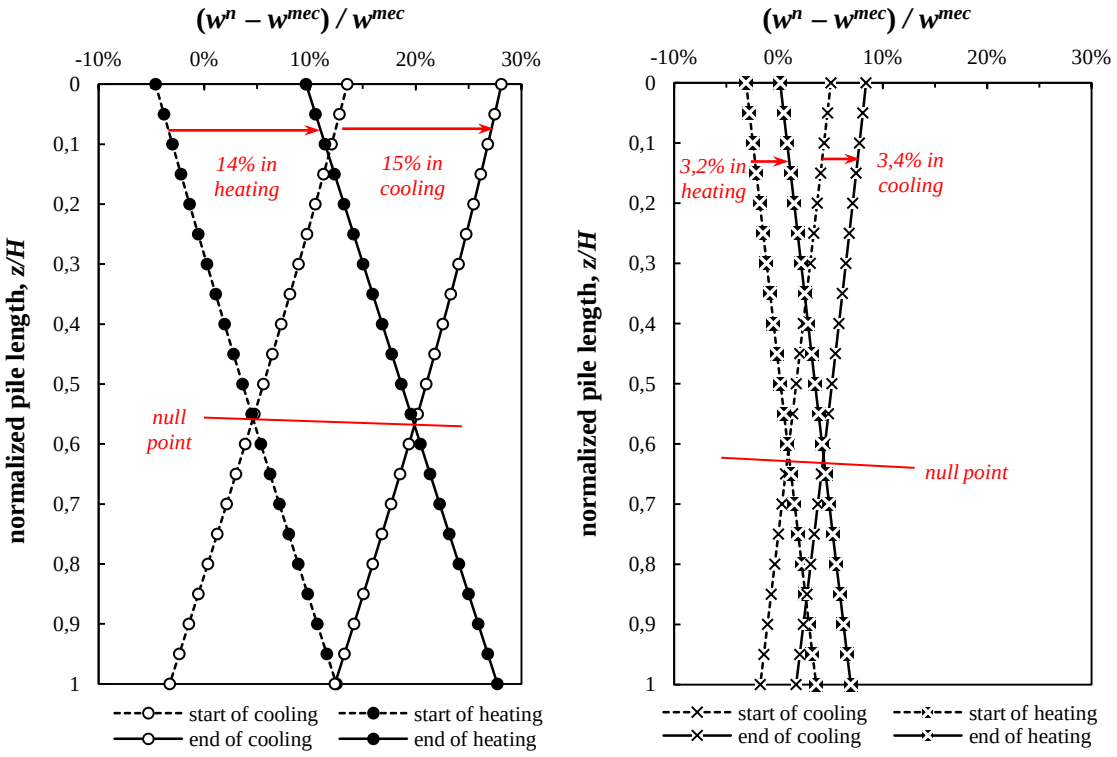

(a) SP – Free head pile *(b) GP – P3 Corner*

Figure 4.5 – Comparison of the temperature-induced axial displacement in the thermo-active piles

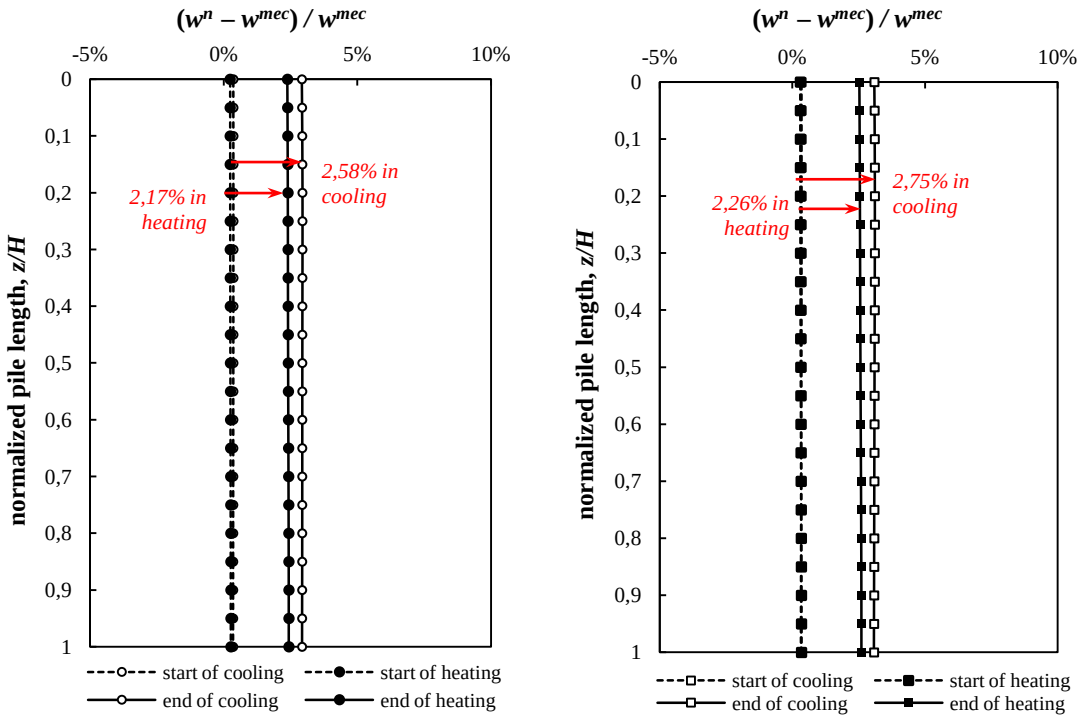

(a) GP – P1 Centre *(b) GP – P2 Side*

Figure 4.6 – Response of other piles in the group induced by thermo-active piles

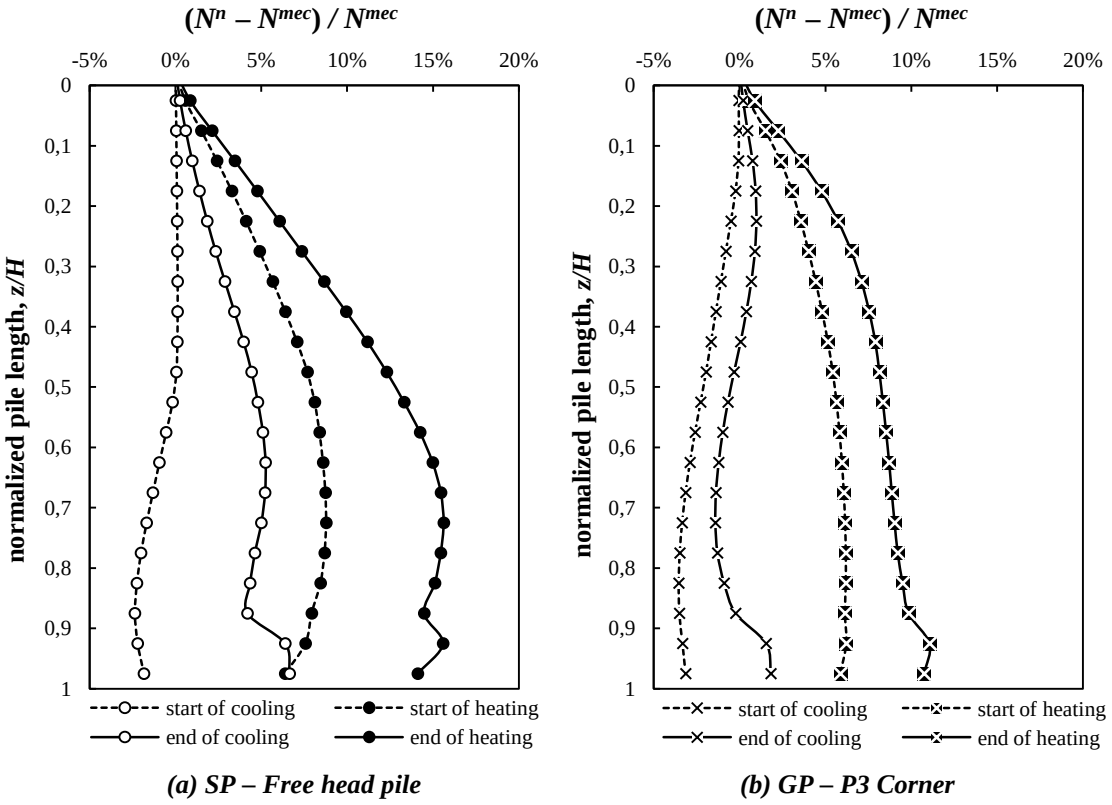

Figure 4.7 – Comparison of the temperature-induced normal force in the thermo-active piles

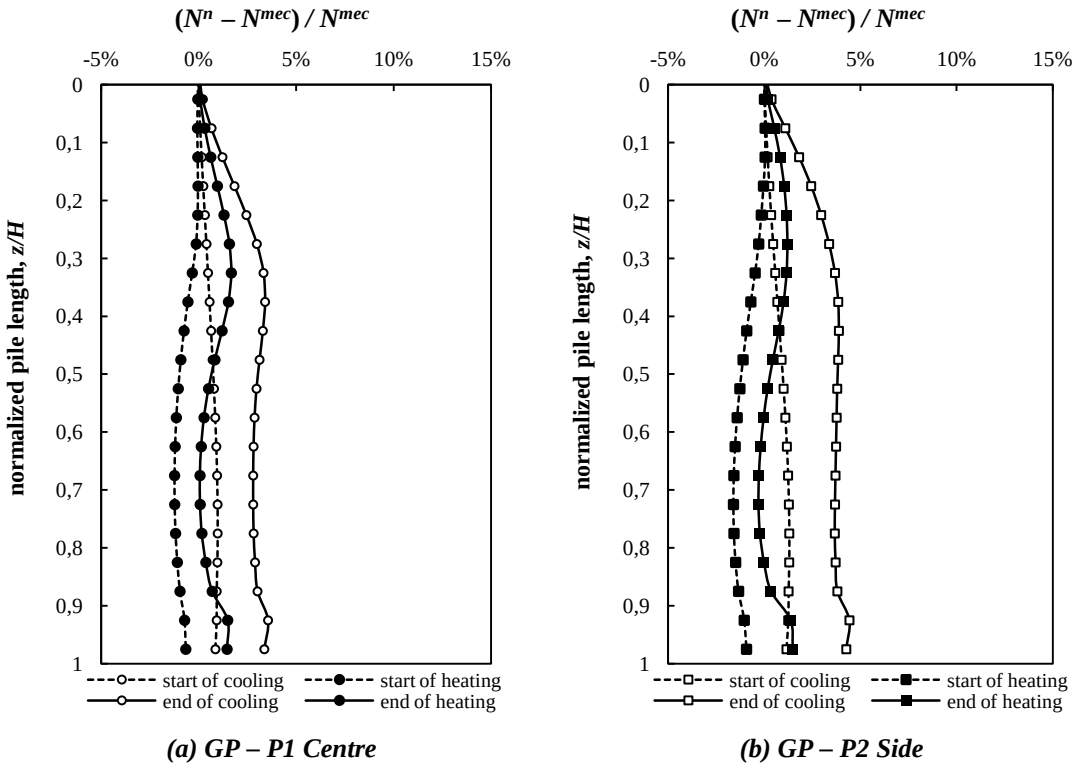

Figure 4.8 – Force repartition to other piles in the group induced by thermo-active piles

shows the contour of thermal displacement in the end of thermal cycles. At the surface level, a ground heave occurs since the first heating phase until the end of thermal cycles of approximately 3 mm from the initial condition at working load stage. However, in reality, a pile cap laid in the ground will restraint the ground heave at the surface. At the lower level around the pile base, an increase in settlement occurs during the thermal cycles. As a result, the soil zone around the piles is affected by cyclic thermal variations. High concentration of differential displacement around the piles–soil zone in the group and cyclic variation in displacement are clearly shown in Figure 4.9. It means that analysis of cyclic variation in the soil mass should be taken into consideration in the design of thermo-active piles in the pile groups.

4.3.1.4 Change in shaft friction and tangential displacement at the soil–pile interface

In this study, the interface elements at the soil–pile contact zone are provided using the Modjoin law of nonlinear cyclic plasticity behavior. Due to the group effects, the effect of thermal variations in the thermo-active piles is distributed to all piles and to the soil around the piles thus makes the pile group foundation system varies with the cycles. Without a cap is modeled at the head of all piles, there is no axial restraint at the surface level during cyclic movements. However, the soil confinement around the piles in the group increases the lateral restraint of the piles and makes the system foundation having a smaller differential displacement between the piles and the soil. This restraint condition is then translated to a higher degradation in shaft friction along the interface elements, which represents a higher relaxation phenomenon. The analysis of group effect is best described in terms of the comparison of the thermo-active piles in the group to the single thermo-active pile in free head condition as shown in Figure 4.10.

Figure 4.10 shows also the response of the neighboring piles (P1 and P2) induced by the presence of thermo-active piles P3 in the group. As the classic piles P1 and P2 do not subjected to direct contraction–dilatation loading, the response of the classic piles is differently in contrast to that of thermo-active piles. Under contraction of the thermo-active piles, shaft friction in such piles becomes greater at the upper-half part and goes

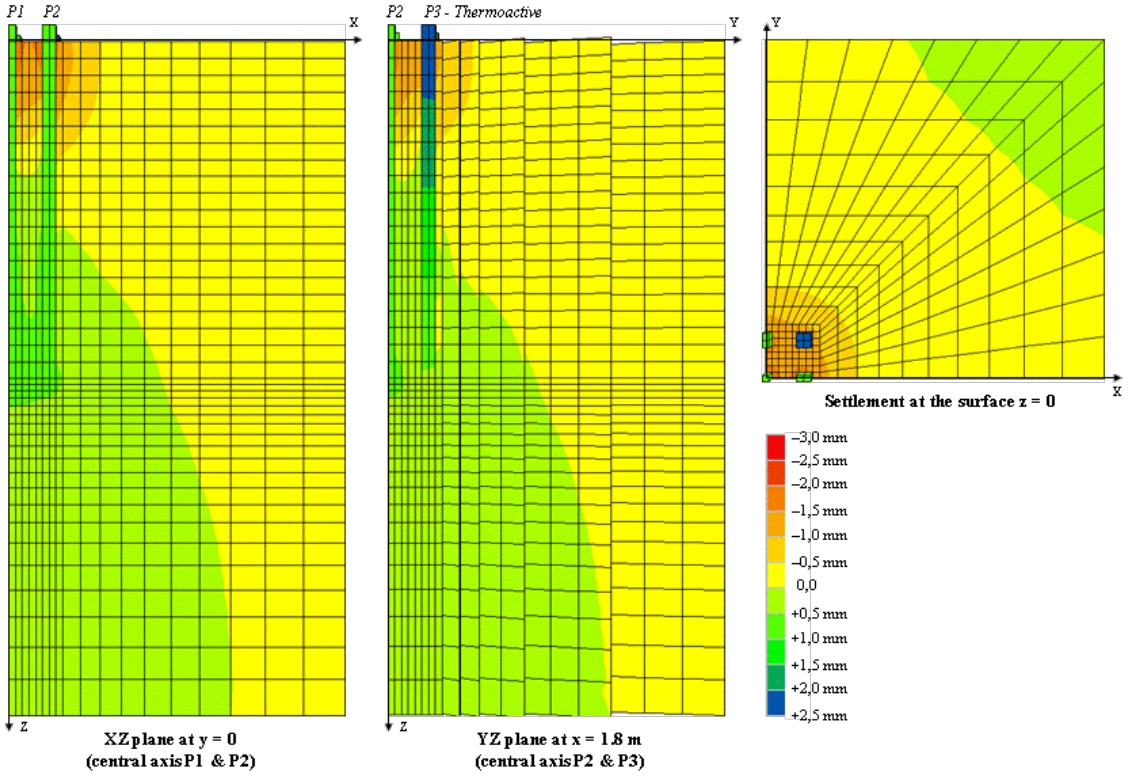

(a) in the end of cooling phases

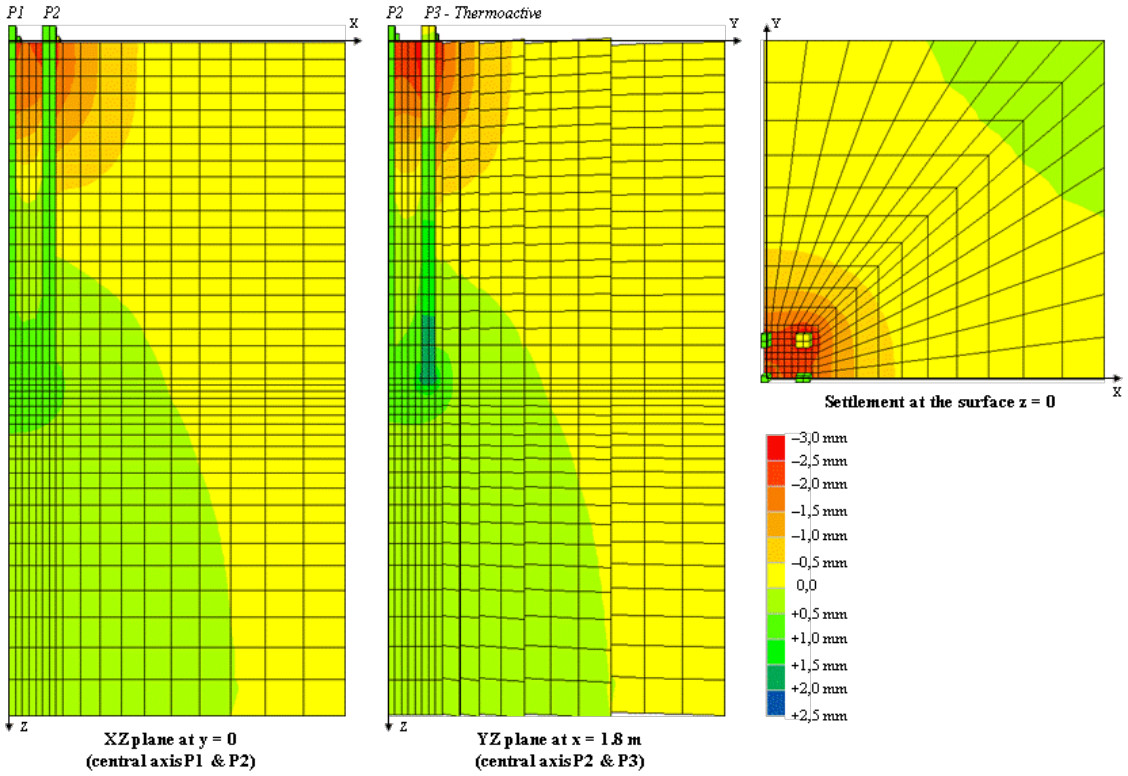

(b) in the end of heating phases

Figure 4.9 – Contour of axial displacement in a pile group without cap

lower at the lower-half part of the pile. However, the neighboring piles have a decrease in shaft friction at the upper-half part and an increase in shaft friction at the lower-half part of the pile. Opposite condition is obtained when the thermo-active piles expand in heating phases. The opposite responses of mobilized shaft friction in thermo-active piles and neighboring piles are equivalent to the opposite variation in normal force distribution (see Section 4.3.1.2), which is notably due to the free restraint at the head of piles. As a result, the group effects change the response of each pile in the group.

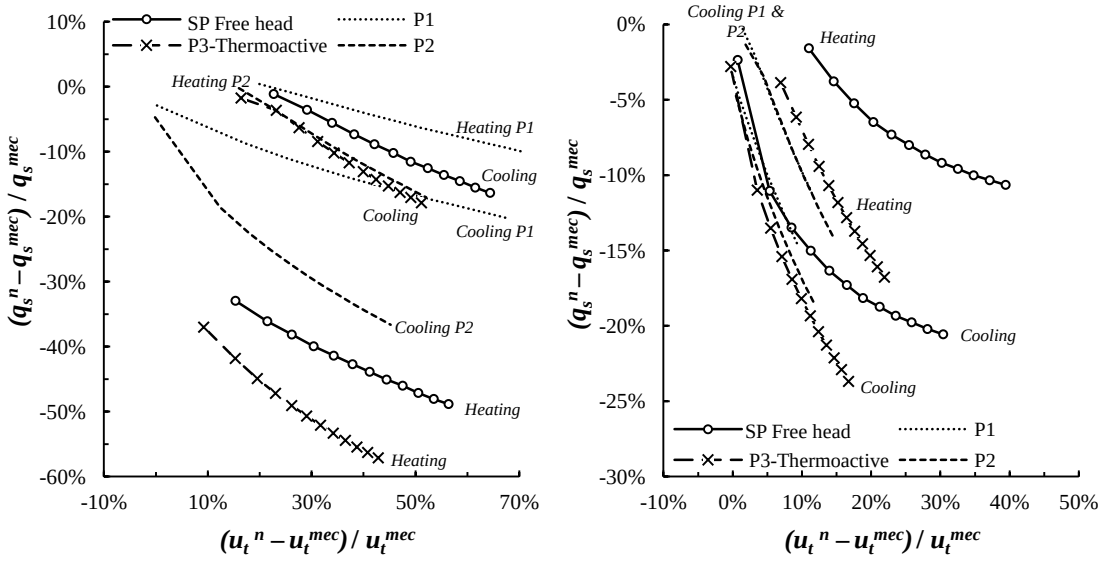

Figure 4.10 – Change in shaft friction and tangential displacement at different depths

4.3.2 Influence of thermo-active piles position in the group

The behavior of a pile in a group may differ greatly depending on the position due to the interaction effect with the neighboring piles (Chow and Thevendran 1987; Fleming *et al.* 2008; Poulos and Davis 1980). According to that, it is of major interest to model different configurations of the thermo-active piles in the group to achieve a better understanding of the group effects on the thermo-active piles behavior. This subsection presents a comparison study of three possible positions of the thermo-active piles in a 3×3 pile group as shown in Figure 4.11. The position of the thermo-active piles in the group are moved to the side of the group (for Model GP B) and to the centre of the group (for Model GP C).

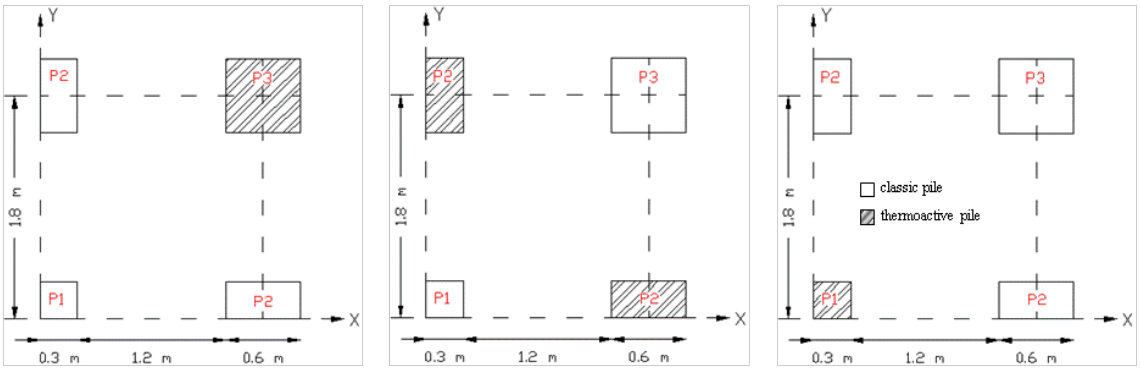

(a) Model GP A – Reference model *(b) Model GP B* *(c) Model GP C*

Figure 4.11 – Position of thermo-active piles in a 3×3 pile group

By moving the position of the thermo-active piles to the side or to the centre of the group, a slight difference of temperature-induced axial displacement is found. Table 4.1 summarizes the response of the group with different thermo-active piles position in terms of increase in axial displacement from the beginning to the end of thermal cycles. This increase can be equated as cyclic hardening during cyclic thermal loading. Concerning the values of increase in the thermo-active piles, the different values between the three possible positions are below 0,5 %. Thus, there is no significant effect of moving the thermo-active piles position in the group on the local response of such piles.

Table 4.1 – Increase in axial displacement along the pile length relative to the first thermal cycles

Model	***Thermo-active pile position***	***over the cooling phases***			***over the heating phases***		
		P1 Centre	P2 Side	P3 Corner	P1 Centre	P2 Side	P3 Corner
GP 1	Corner	2,58 %	2,75 %	**3,4 %**	2,71 %	2,26 %	**3,3 %**
GP 2	Side	3,67 %	**3,2 %**	2,48 %	2,87 %	**3,15 %**	2,08 %
GP 3	Center	**2,95 %**	1,09 %	0,68 %	**2,85 %**	0,98 %	0,65 %

However, due to the group effect, moving the position of thermo-active piles affects the global response of the group, such as the force repartition within the group and the differential displacement around the piles–soil zone. Figures 4.12–4.13 show the change in pile head settlement and interface response in the pile group induced by temperature variations for three different model configurations. When P1 functions as thermo-active pile (i.e. Model GP C, see Figures 4.12c and 4.13c), the detrimental effects induced by

thermal variations are concentrated in P1 itself and the distribution of thermal effects to the other piles is very small. Thus, P2 and P3 do not undergo significant changes in pile head settlement, shaft friction mobilized, and tangential displacement during cyclic thermal loading. By observing the other model configurations (Model GP A and GP B), the influence of thermo-active piles on the other neighboring piles is more remarkable; the other piles have a clear contraction–dilatation behavior (Figure 4.12a-b) and undergo cyclic degradation phenomenon in their interfaces such as relaxation or ratcheting (Figure 4.13a-b).

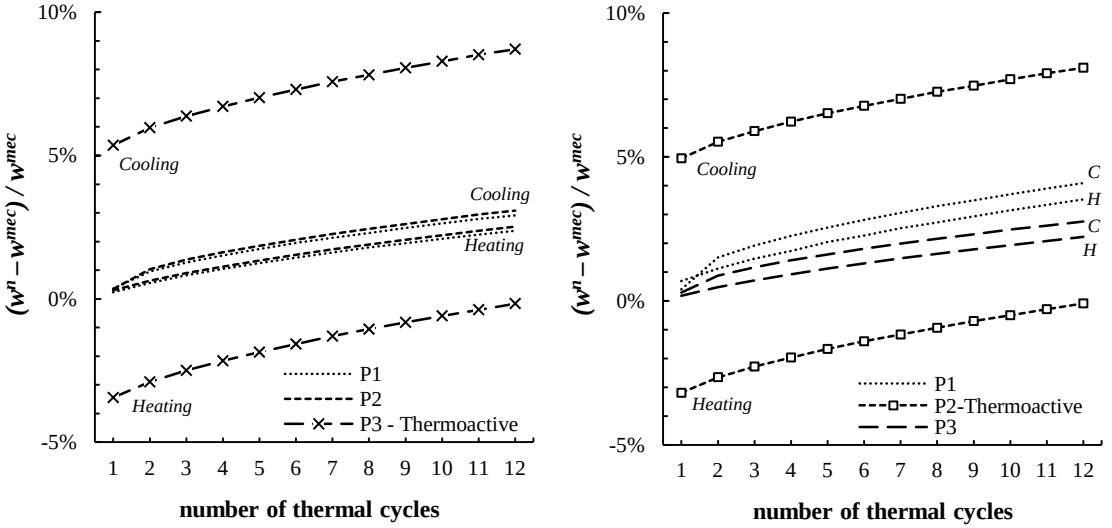

(a) Model GP A *(b) Model GP B*

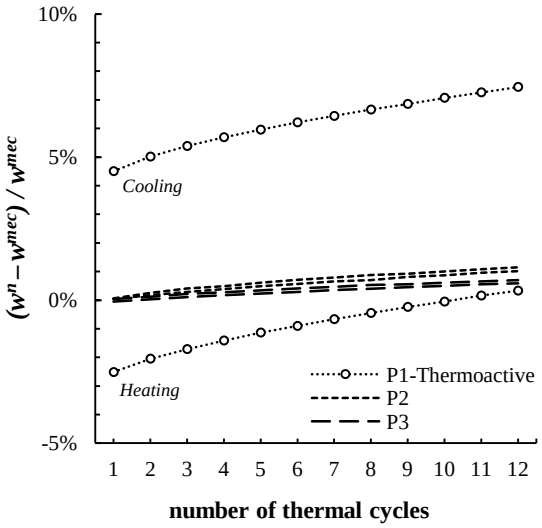

(c) Model GP C

Figure 4.12 – Temperature-induced head settlement in a 3×3 pile group

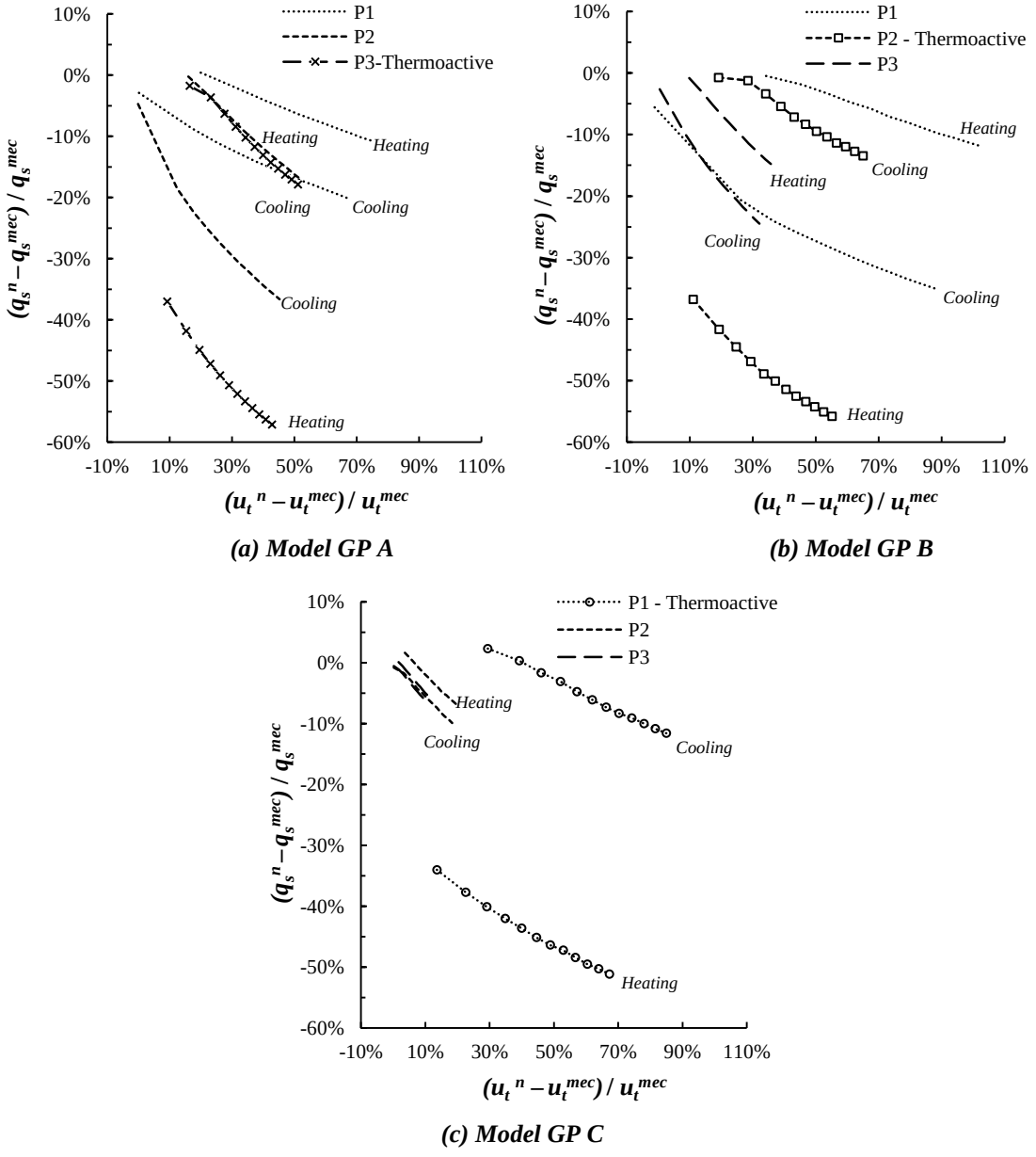

(a) Model GP A

(b) Model GP B

(c) Model GP C

Figure 4.13 – Temperature-induced mobilized friction at z = 0,2 H in a 3×3 pile group

It is worth analyzing the effect of moving the thermo-active piles on the overall group behavior by regarding the surface settlement profile line. Figure 4.14 shows the settlement profile between the piles in the group: on the left side is the settlement profile line between P1 and P2 (horizontal/vertical interaction) while on the right side is the settlement profile line between P1 and P3 (diagonal interaction). As mentioned earlier, model GP C has a concentration of thermal effects in P1, which leads to a high differential settlement that exists only around the soil–P1 interface (see Figures 4.13c

and 4.14c). Since the concentration takes place in the centre of the group, the differential settlement to the other piles forms a symmetrical profile (Figure 4.14c). Other models (GP A and GP B) have asymmetric settlement profile with a greater ground heave in the soil zone between the piles. The effect of thermo-active piles position in a pile group can be related also to the relative stiffness between thermo-active piles and other classic bearing piles. In a 3×3 group pile, the relative stiffness of the thermo-active piles placed in the centre is obviously smaller than that of thermo-active piles placed in the corner of the group.

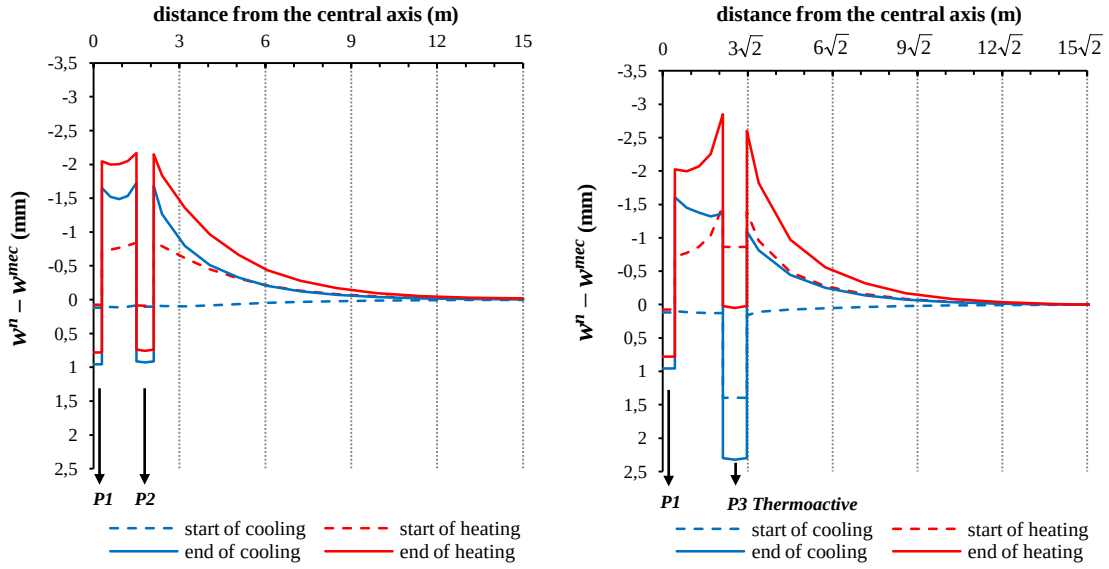

(a) Model GP A – Thermo-active piles in the corner of the group

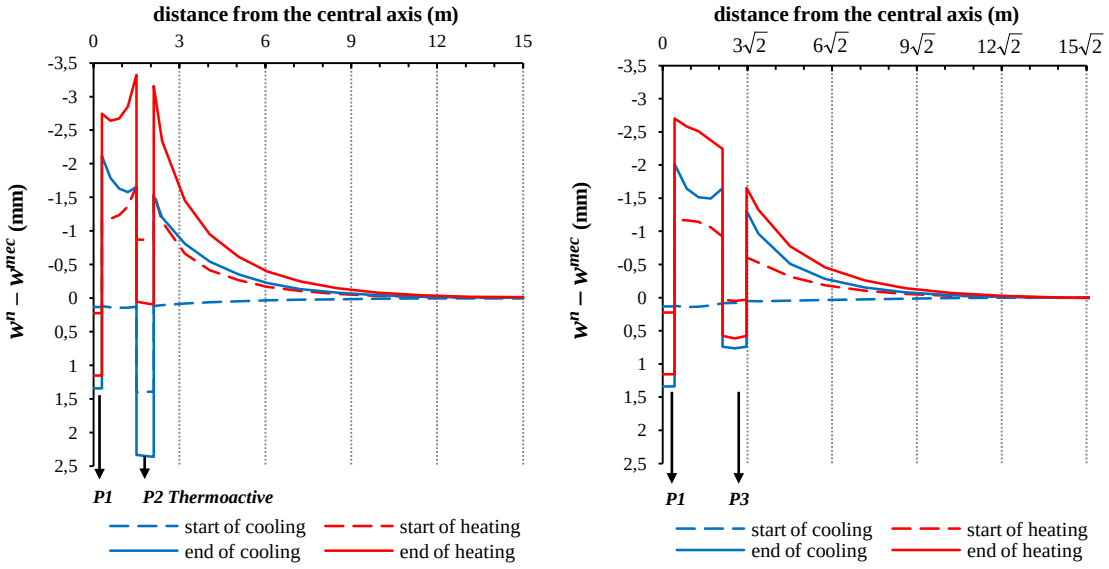

(b) Model GP B – Thermo-active piles at the side of the group

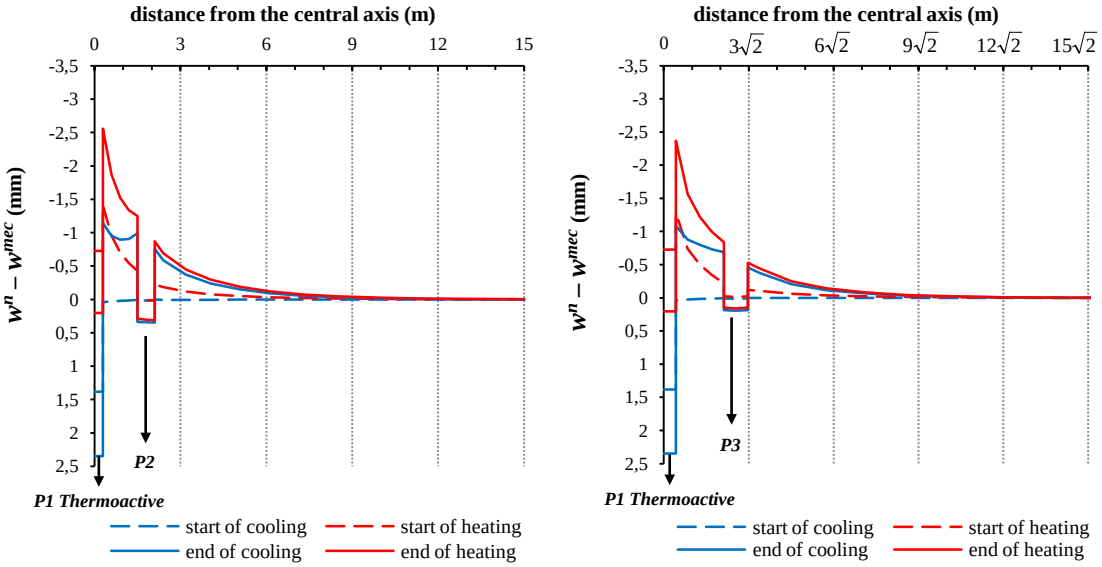

(c) Model GP C – Thermo-active pile in the centre of the group

Figure 4.14 – Surface settlement profile in the group over the thermal cycles

4.4 Case II – Piled raft foundation

In practice, a pile group that is connected to a pile cap laid in contact with the ground forms a piled raft foundation system. Compared to the more conventional pile group foundations where the bearing effect of the pile cap is ignored, the piled raft system can effectively reduce the number of piles required (Clancy and Randolph 1993). However, the bearing effects of pile cap cannot be simply estimated by adding the bearing capacity of the cap to that of the pile group, since the behavior of such system is affected by piles–soil–cap interaction.

In piled raft system, the interaction behavior is dependent on relative stiffness between the raft (i.e. cap) stiffness and the soil stiffness. For a rectangular pile cap under axial loads, Brown (1975) defined that the relative raft–soil stiffness as follows (Borel 2001; Brown 1975; Brown and Yu 1986):

$$K_{rs} = \frac{16}{\pi}\frac{K_r}{K_s} = \frac{4}{3\pi}\frac{E_r\left(1-\nu_s{}^2\right)}{E_s}\frac{B_r}{L_r}\left(\frac{t_r}{L_r}\right)^3 \qquad [4.3]$$

where K_r and K_s indicate the absolute stiffness of the raft and the soil, respectively. E_r, I_r, B_r, L_r, and t_r denote the Young's modulus, the moment of inertia, the width, the length, and the thickness of the raft. E_s and υ_s stands for the Young's modulus and the Poisson's ration of the soil.

The case study was previously described in Section 4.2, a group of 3×3 piles with a cap thickness of 1*B*, an edge clearance of 1*B*, and a pile spacing of 3*B*. Geometry detail of the piled raft was presented in Figure 4.1. The contact between pile cap, pile head and soil surface is perfectly bonded without any interface element modeled. Due to symmetry, the complete numerical domain is cut to ¼, shown in Figure 4.15. The properties of soil, piles, and Modjoin interfaces remain the same with the preceding numerical model. In addition, the properties of the raft are set to 20 *GPa* of the Young's modulus and 0,33 of the Poisson's ratio. The raft properties are taken similar to the properties of the piles.

In the first stage of loading, a uniform load is applied on the raft, with an equivalent value of the sum of load of 3×3 piles. The working load is set at 33% of the ultimate load of single pile. Since the load is transferred uniformly through a pile cap, the cap takes a part in the load distribution, and thus each pile does not receive an equal average load. In general, the corner piles will take a higher proportion of the applied load than the central piles due to the interaction effects(Fleming *et al.* 2008; Poulos and Davis 1980). The load proportion for each pile in the raft is usually described as the ratio of the load per pile to the load of single pile at the comparable mean working load. In this case study, the load proportion per pile can be described as follows:

$$P_{Group} = \sum_{i=1}^{9} P_{SP} = 9 \times \overline{P} = \left(1 \times \frac{P_{P1}}{\overline{P}}\right) + \left(4 \times \frac{P_{P2}}{\overline{P}}\right) + \left(4 \times \frac{P_{P3}}{\overline{P}}\right) + \frac{P_{RAFT}}{\overline{P}} \qquad [4.4]$$

Figure 4.16 shows the load distribution in the raft for each pile under axial mechanical loading. At the comparable mean working load P_W = 33% of Q_{ULT} SP, as predicted, the corner piles P3 have a higher load proportion than other piles of approximately 104% of the applied working load. The side piles P2 and central pile P1 support 85% and 60%, of the applied working load, respectively.

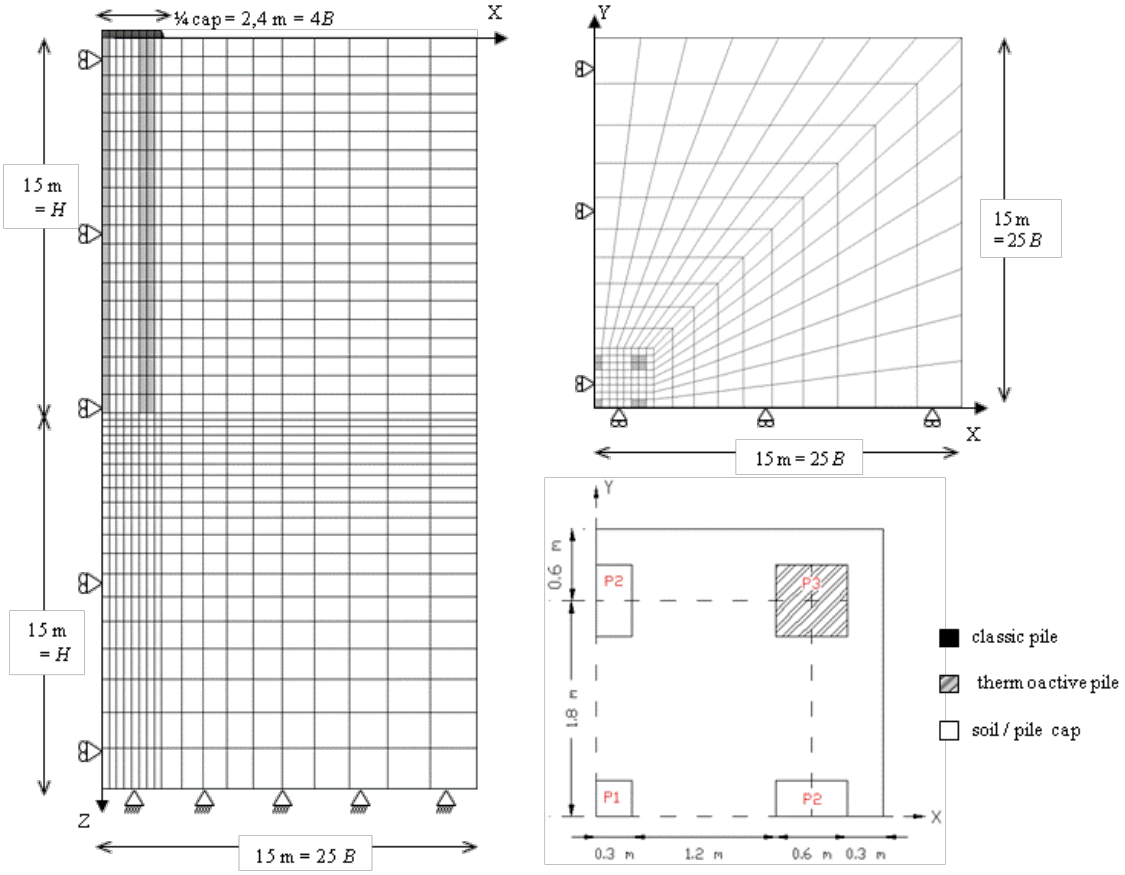

Figure 4.15 – Numerical domain of a 3×3 piled raft foundation

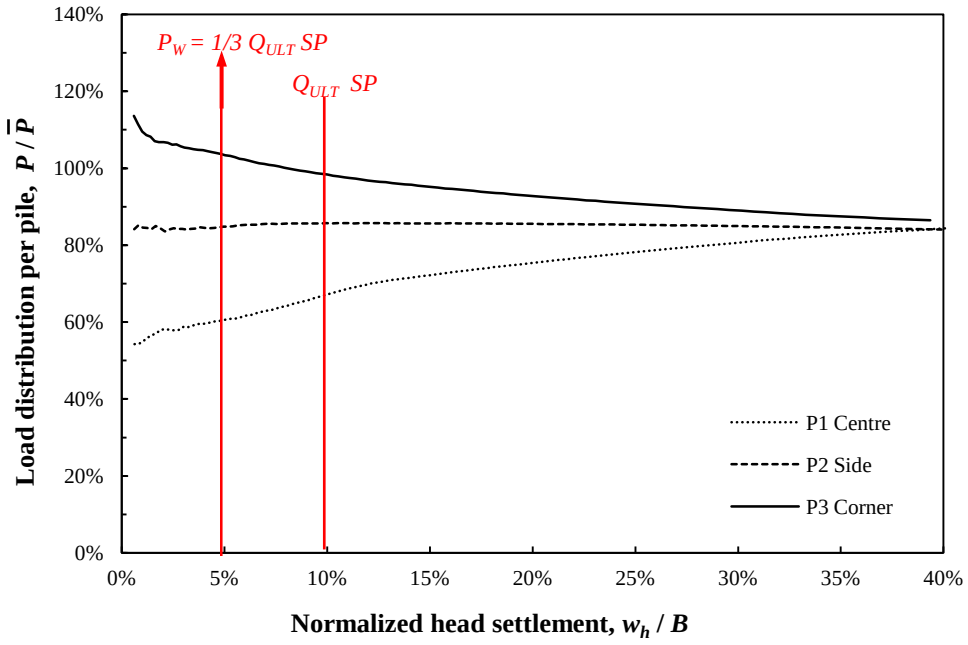

Figure 4.16 – Load distribution in the raft under axial mechanical loading

In the second stage of loading, the corner piles P3 are activated as thermo-active elements. A uniform thermal axial deformation is applied ($\varepsilon^{th} = \alpha_T \Delta T$) with temperature gradient ±10°C from the ground temperature during 12 cycles. The schematic of loading cycles in the thermo-active piles was previously presented in Figure 3.4. The global response of the raft under cyclic thermal loading is illustrated in Figure 4.17, in terms of the variation in load distribution ratio per pile relative to the comparable mean working load. The thermo-active piles P3 have tendency to decrease the proportion of load during thermal cycles while the other piles (P1 and P2) have an increase in load proportion during thermal cycles. Detail analysis of the thermo-active piles behavior in the raft and their influence on the other neighboring piles will be presented in the next subsection.

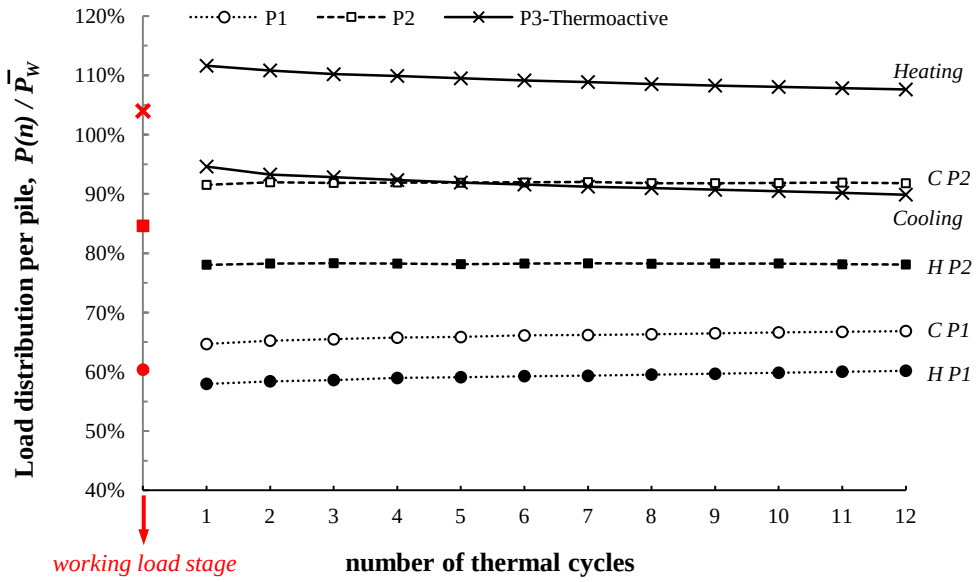

Figure 4.17 – Load distribution under cyclic loading

4.4.1 Thermo-active piles behavior in a piled raft

4.4.1.1 Change in pile head reaction

Since the cap restraints the movement of the head of piles in the raft, the variation in head settlement of thermo-active piles in a piled raft is largely smaller compared to the single thermo-active pile or to the thermo-active piles in a pile group without cap (Figure 4.18a). The cap laid on the head of piles allow the piles to have an intermediate

value of axial fixity in the range of $0 < K_h < \infty$, where $K_h = 0$ represents the single thermo-active in free head condition and $K_h = \infty$ represents the single thermo-active pile in restrained head condition. The thermo-active piles in a piled raft do not only have axial restraint by the cap but also lateral restraint caused by the group effect. Group effect makes the piles undergo a lower decrease in pile head reaction compared with the single pile in restrained head condition (Figure 4.18b). Taking the cyclic degradation effects into account, Figure 4.18 shows clearly that a piled raft system has a very low cyclic hardening which makes insignificant change in pile reaction over the thermal cycles.

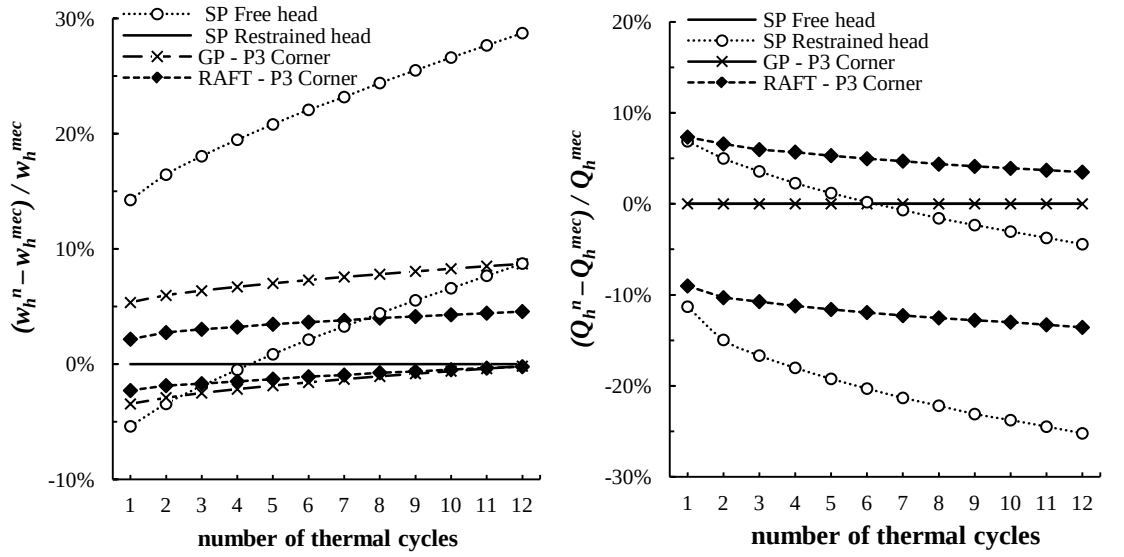

(a) Variation in pile head settlement ***(b) Variation in head reaction force***

Figure 4.18 – Change in pile head reaction of the thermo-active piles

A pile cap laid in contact with the ground will change the response of the group, particularly in the load distribution and differential settlement between piles and soil. Figure 4.19 shows the change in pile head settlement for each pile relative to the initial settlement at working load stage between the pile group without cap system (Case I) and the piled raft system (Case II). It is clear that the variation in pile head settlement for the thermo-active piles in the piled raft system is smaller than that of the thermo-active piles in the pile group without cap system due the presence of the cap (see Figures 4.18a and 4.19). However, the influence of thermo-active piles on the other neighboring piles is clearly remarkable in the piled raft system. Figure 4.19b shows that

the side and central piles in the raft have relatively the same range of variation values with the corner thermo-active piles. Since the thermo-active piles are located in the corner of the raft, the additional thermal stress is subjected to the piles with the greatest initial mechanical load. Therefore, the influence on the other neighboring piles is important.

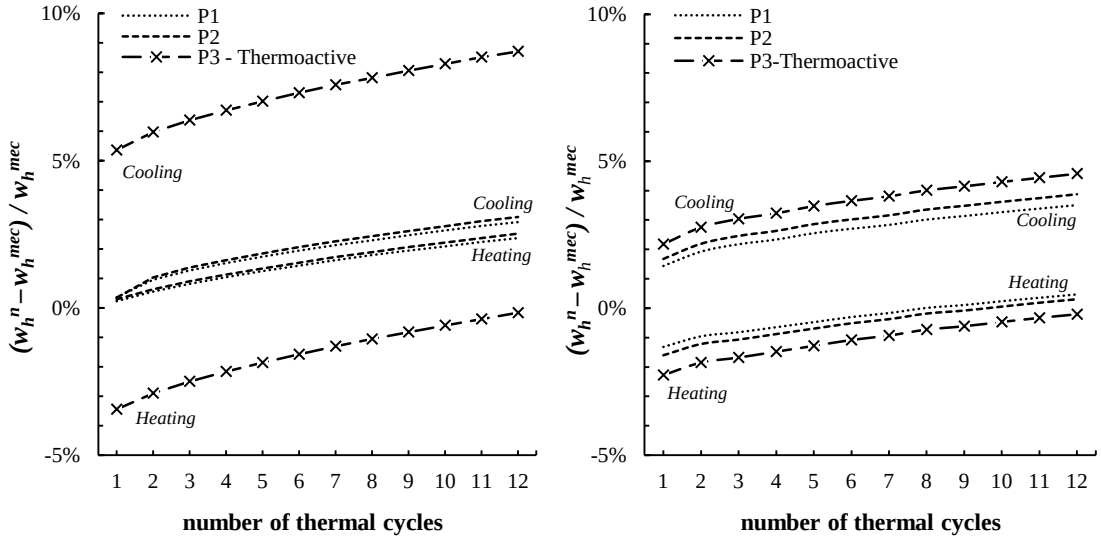

(a) Case I – Pile group without cap system ***(b) Case II – Piled raft system***

Figure 4.19 – Variation in pile head settlement during thermal cycles

4.4.1.2 Distribution of normal force and axial displacement

To better comprehend the influence of thermo-active piles in a raft on the other neighboring piles, Figures 4.20–4.21 show the distribution of change in normal force and axial displacement per pile in the raft. The variations of values presented in Figures 4.20–4.21 are related to the initial state of each pile under axial mechanical working load. Based on the group effects, the neighboring classic piles share opposite behavior towards the thermo-active piles. For example, in the cooling phase, the neighboring piles undergo an increase in normal force when the thermo-active piles undergo a decrease in normal force caused by the pile contraction. Opposite phenomenon occurs in the heating phase. Distribution of axial displacement in the neighboring piles remains uniform along the pile length, contrary to the thermo-active piles, but the values of cyclic hardening from the beginning and the end of thermal cycles are in the same margin of approximately 2% – 2,5%.

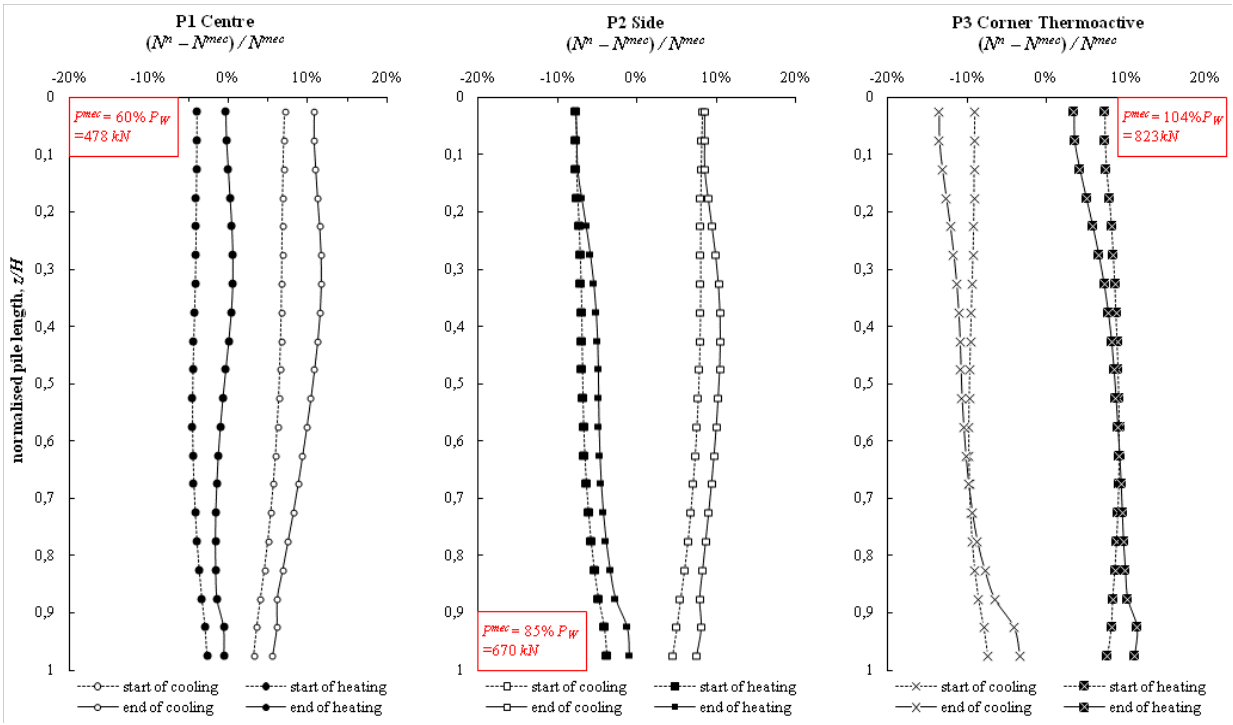

Figure 4.20 – Change in normal force per pile over thermal cycles

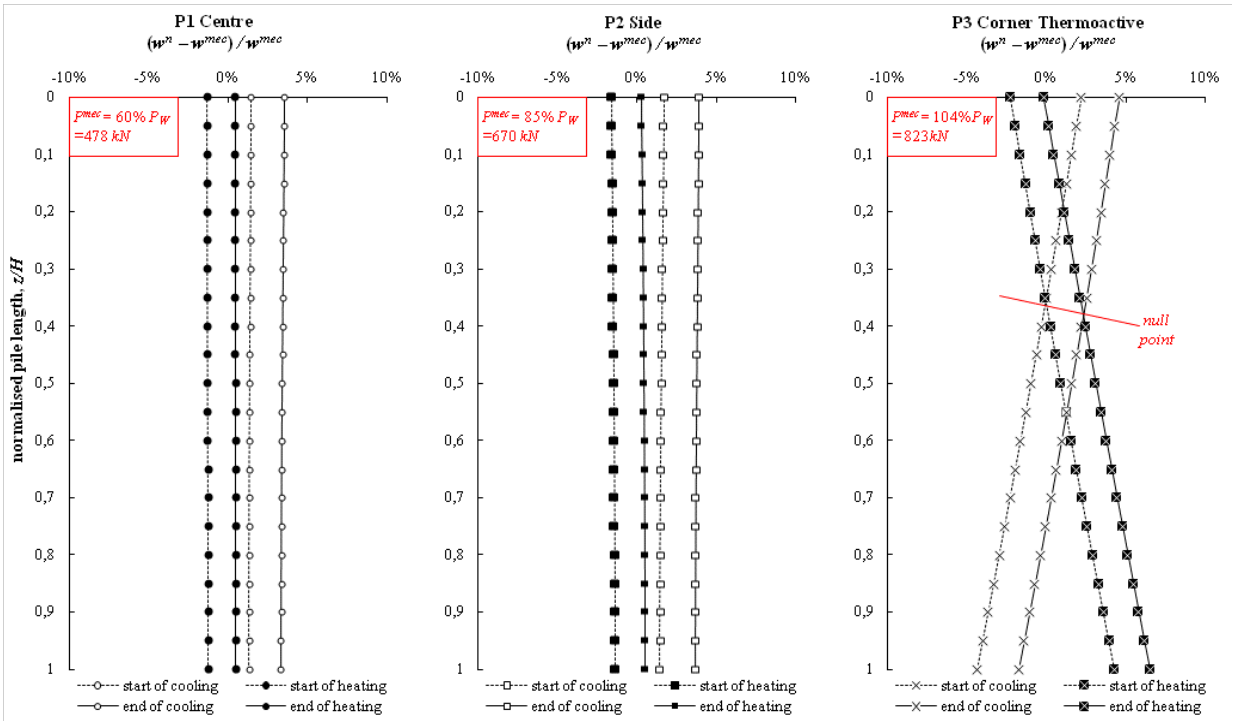

Figure 4.21 – Change in axial displacement per pile over thermal cycles

Although the presence of the cap restrains the axial movement at the head, the cap is not rigid enough to completely block the head movement. Thus, the responses of displacement at the pile head and pile base are opposed. The distribution of change in axial displacement over the pile length shows the presence of null point in the thermo-active piles at the upper-half of the pile (of approximately $0{,}3H < z < 0{,}4H$). Through a logical comparison from the other model cases, the null point is located close to the end-restraint fixity.

4.4.1.3 Soil movement around the piles in the group

The presence of thermo-active piles in a 3×3 pile group induces change in the behavior of other neighboring piles. For a group with very flexible cap or without cap (i.e. Case I presented in Section 4.3), the soil mass within the piles and the piles themselves can freely shrink and expand under thermal contraction–dilatation. The zone where less restraint condition is found has the greatest effects induced by thermal contraction–dilatation. In the case of pile group without cap, the detrimental effects are therefore concentrated at the surface level.

In the case of piled raft foundation, as the cap is perfectly in contact with the ground and with the head of piles, no differential settlement is allowed at the surface level. Accordingly, the settlement profile line at the surface level is continuous though varies in upward–downward movement during thermal cycles. The variation in settlement of the cap is due to the low rigidity of the raft, since the Young's modulus of the raft equals to that of the piles. Down to the pile length, differential settlements in the soil zone between the piles are much smaller in comparison with the pile group without cap system (Figure 4.22). However, the contour of axial displacements in the end of thermal cycles shows a concentration of ground heave and a high differential settlement in the upper-half part of the pile (in a depth of approximately $0{,}1H < z < 0{,}6H$). This condition indicates also the phenomenon of cyclic variation in the soil mass due to temperature variations, such as ground compaction and swelling.

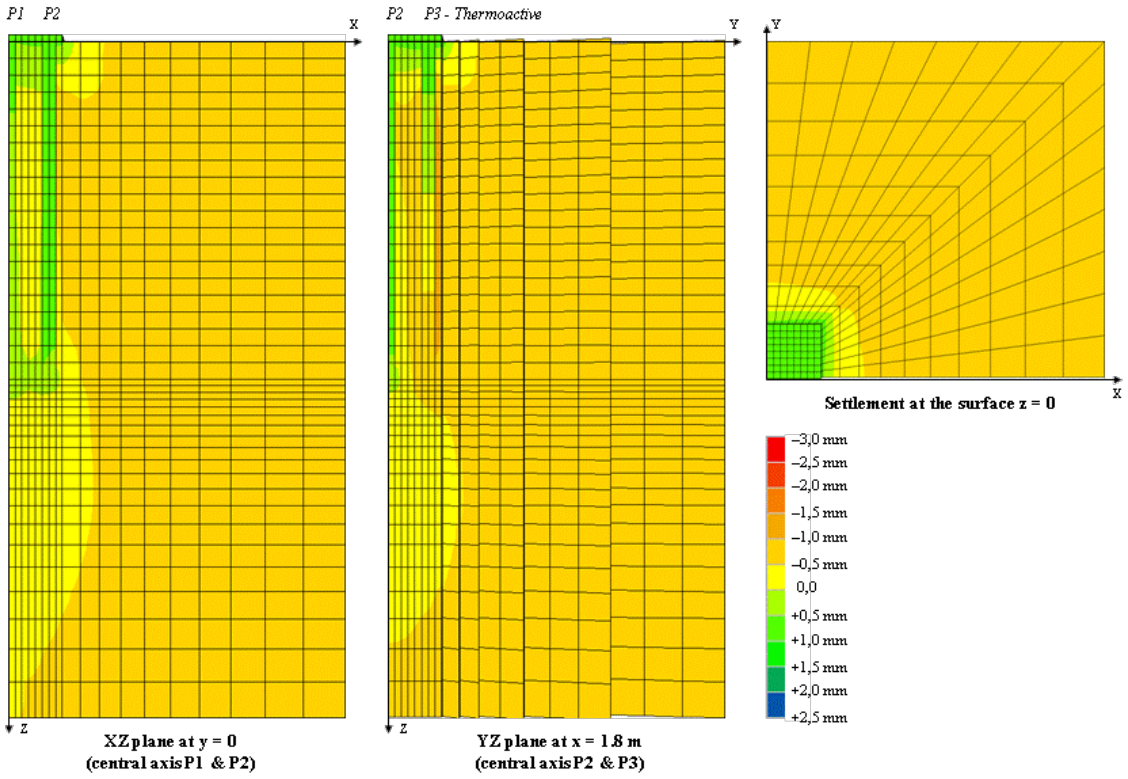

(a) in the end of cooling phases

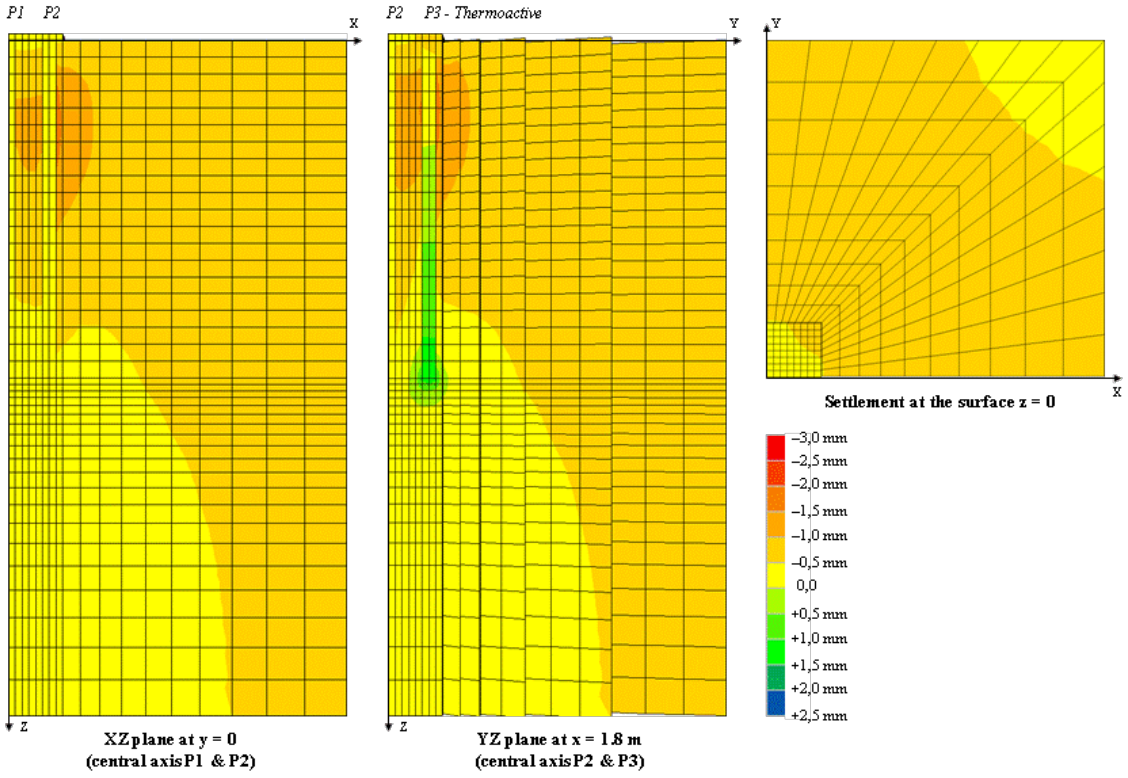

(b) in the end of heating phases

Figure 4.22 – Contour of axial displacement in a piled raft system

4.4.1.4 Change in shaft friction and tangential displacement at the soil–pile interface

The group effect also induces degradation in interface resistance of the neighboring piles. Figure 4.23 shows the variation in interface response over thermal cycles and indicates clearly the degradation phenomenon in interface, particularly at the upper-half of the pile. Refer to Figure 4.22; a high differential settlement between piles–soil occurs at the upper-half of the pile due to the effect of contraction–dilatation in the thermo-active piles and compaction–swelling in the soil zone between piles. Therefore, at this zone, the neighboring piles undergo a progressive increase in tangential displacement showing a ratcheting phenomenon.

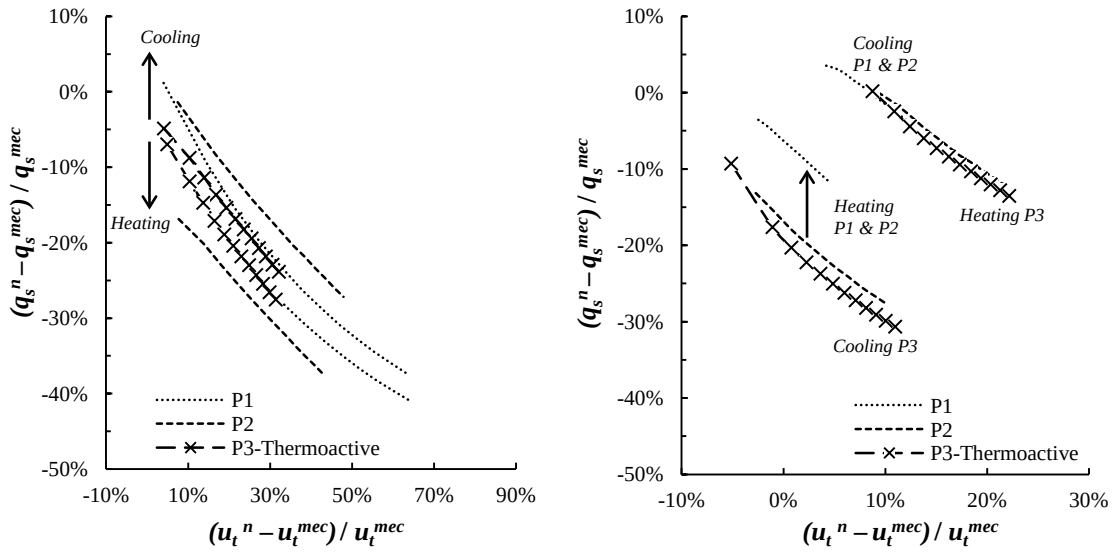

Figure 4.23 – Change in shaft friction and tangential displacement at different depths

4.4.2 Influence of raft stiffness on the thermo-active piles response

From the analysis of the preceding model described in Section 4.4.1, the end-restraint condition at the head of the piles is not sufficiently rigid. In order to better understand the behavior of the thermo-active piles in a piled raft, it is worth modeling different rigidities of the raft since the response of such piles depends strongly on the end-restraint condition at the pile head and pile base (Amatya *et al.* 2012; Bourne-Webb *et*

al. 2009). Modeling the rigidity of the raft can be related to the ratio of raft–soil stiffness proposed by Brown (1975) which is previously expressed in equation 4.3. According to Brown (1975), a value of raft–soil stiffness should be above 10 to have a rigid raft system.

In the previous reference model, the value of Young's modulus of the raft was set at the same value with that of the piles. Thus, according to equation 4.3, the raft-soil stiffness of the reference model is 1,47. Table 4.2 summarizes the different values of raft property to model a more flexible raft and more rigid raft than the reference model.

Table 4.2 – Model parameters

Model	*Property*	*Raft stiffness, K_r*	*Raft-soil stiffness, K_{rs}*	*Thermo-active piles position*
A – Raft Reference	$E_{raft} = E_{pile}$	3,26 MPa	1,47	Corner
B – Raft Flexible	$E_{raft} = 0{,}1\ E_{pile}$	0,326 MPa	0,147	Corner
C – Raft Rigid	$E_{raft} = 100\ E_{pile}$	0,326 GPa	147	Corner

In the first stage of loading, the raft is subjected to a mechanical working load in a comparable value with that of single pile $\overline{P}_W = 792kN$. Table 4.3 recaps the load distribution in each pile under the working load stage. Under a flexible raft, the load distribution is almost equal in each pile in the range of approximately 83%–92% of the mean working load. In accordance with the in-situ experiences conducted by Poulos (1980), Chow (1987), and Fleming et al. (2008); the results in this numerical model show that the more rigid the raft is, the greater proportion is taken to the corner piles.

Table 4.3 – Load distribution in working load stage $\overline{P}_W = 792kN$

	Raft A - Reference	*Raft B - Flexible*	*Raft C - Rigid*
P1 Centre	60% $\overline{P}_W$	83% $\overline{P}_W$	48% $\overline{P}_W$
P2 Side	85% $\overline{P}_W$	90% $\overline{P}_W$	82% $\overline{P}_W$
P3 Corner	104% $\overline{P}_W$	92% $\overline{P}_W$	109% $\overline{P}_W$

When the second loading stage is applied (i.e. cyclic thermal loading in the corner thermo-active piles), the initial condition of the thermo-active piles is different. The

corner piles are subjected to 104% of $\overline{P_W}$ under the reference raft, 92% of $\overline{P_W}$ under the flexible raft, and 109% of $\overline{P_W}$ under the rigid raft. The initial state of the thermo-active piles under different raft rigidities can be equated to the various working load in the single pile case (presented in Chapter 3.5). Under a greater working load in the thermo-active piles, the amplitude of change in pile behavior induced by thermal variation is smaller but the cyclic hardening due to cyclic degradation effects is more significant.

Figures 4.24–4.25 show the response of pile head over the thermal cycles under different raft rigidities. These figures clearly show that the thermo-active piles under a flexible raft undergo the highest amplitude of change with the lowest hardening. With the lowest hardening, the change in pile behavior under the flexible raft has a tendency to be stabilized over the cycles. Otherwise, the thermo-active piles under the rigid raft show a nonlinear variation in pile head settlement over the cycles. These piles have reached a yielding point under cyclic loading stage thus the degradation in pile behavior is very significant.

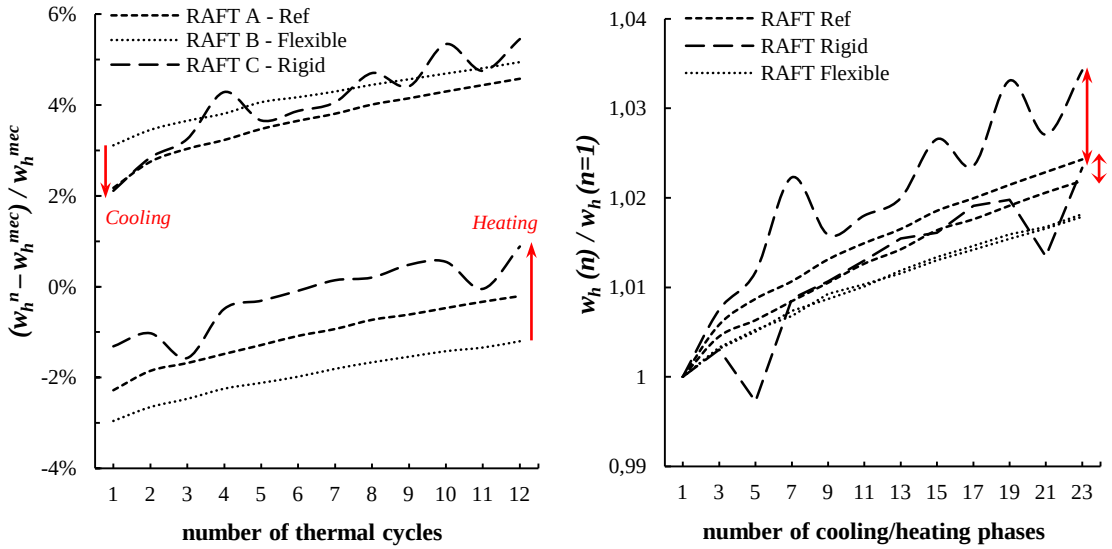

(a) Increase in head settlement relative to mechanical working load stage

(b) Cyclic hardening relative to the first cooling/heating phase

Figure 4.24 – Change in pile head settlement under different raft rigidities

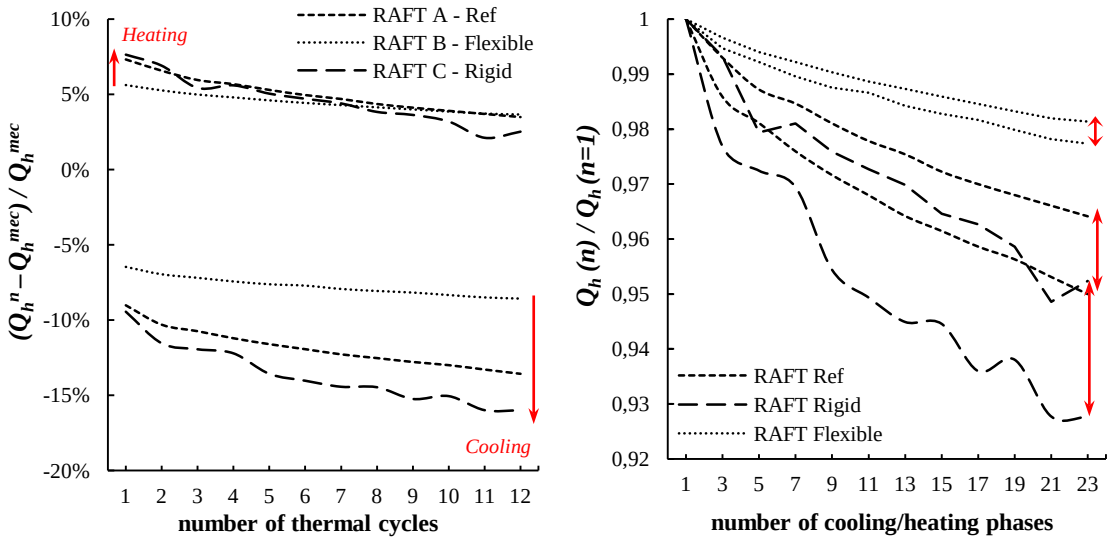

(a) Increase in head settlement relative to mechanical working load stage

(b) Cyclic hardening relative to the first cooling/heating phase

Figure 4.25 – Change in head force under different raft rigidities

4.5 Conclusion

This chapter presents a numerical study of the thermo-active piles behavior in a group of 3×3 piles under axial mechanical and cyclic thermal loads. In order to study the group effects on the piles behavior, several conditions are set to facilitate the understanding: (i) a symmetrical layout and geometry of the group, (ii) identical sizes and properties for all piles, and (iii) uniform loads applied on the group. Moreover, the group is loaded at the comparable load with that of single pile in order to correctly compare the behavior of thermo-active piles in a group and in isolated condition.

In the first part of study, the group is modeled without cap. This case study intends to analyze the group effect on the thermo-active piles behavior. Since the load distribution is equal in each pile and the heads of all piles are free of restraint, this case permits to study the influence of the position of the thermo-active piles. Moving the position of the thermo-active piles changes the global behavior of the group due to different interaction response between the thermo-active and other classic piles.

Approaching reality in practice, the second part of study presents a group with a cap in direct contact with the ground, usually known as piled raft foundation. The results of this study case are aimed to gain a better understanding of the behavior of thermo-active piles foundation in a group by taking the pile–soil–cap interaction into account. Different rigidities of the raft are modeled to represent different end-restraint connections between the foundation and the overlying structure.

At last, numerical results are presented in terms of change in pile responses relative to the initial condition of the piles at the working load stage. Four critical responses are analyzed as follows:

(i) response of the pile head, including pile head settlement and pile head force;
(ii) distribution of normal force and axial displacement along the pile length;
(iii) soil movement around the piles in the group; and
(iv) response of the soil–pile interface, including shaft friction mobilized and tangential displacement

From the study comparison of the single pile case, the pile group without cap case, and the piled raft foundation case; a chart of the margin of change in pile head response (ΔQ_h vs. Δw_h) induced by temperature variations is obtained and shown in Figure 4.26. It shows that the thermo-active piles which are formed in a group, which is the case in practice, undergo the smaller effect of temperature variations on the pile capacity. Because the single pile has the extreme value of head axial fixity, the change in pile behavior for the single pile case reaches a maximal value of change that could be induced by temperature change of ±10°C. This chart will help to enhance the design and dimensioning of the thermo-active piles under additional cyclic thermal loads.

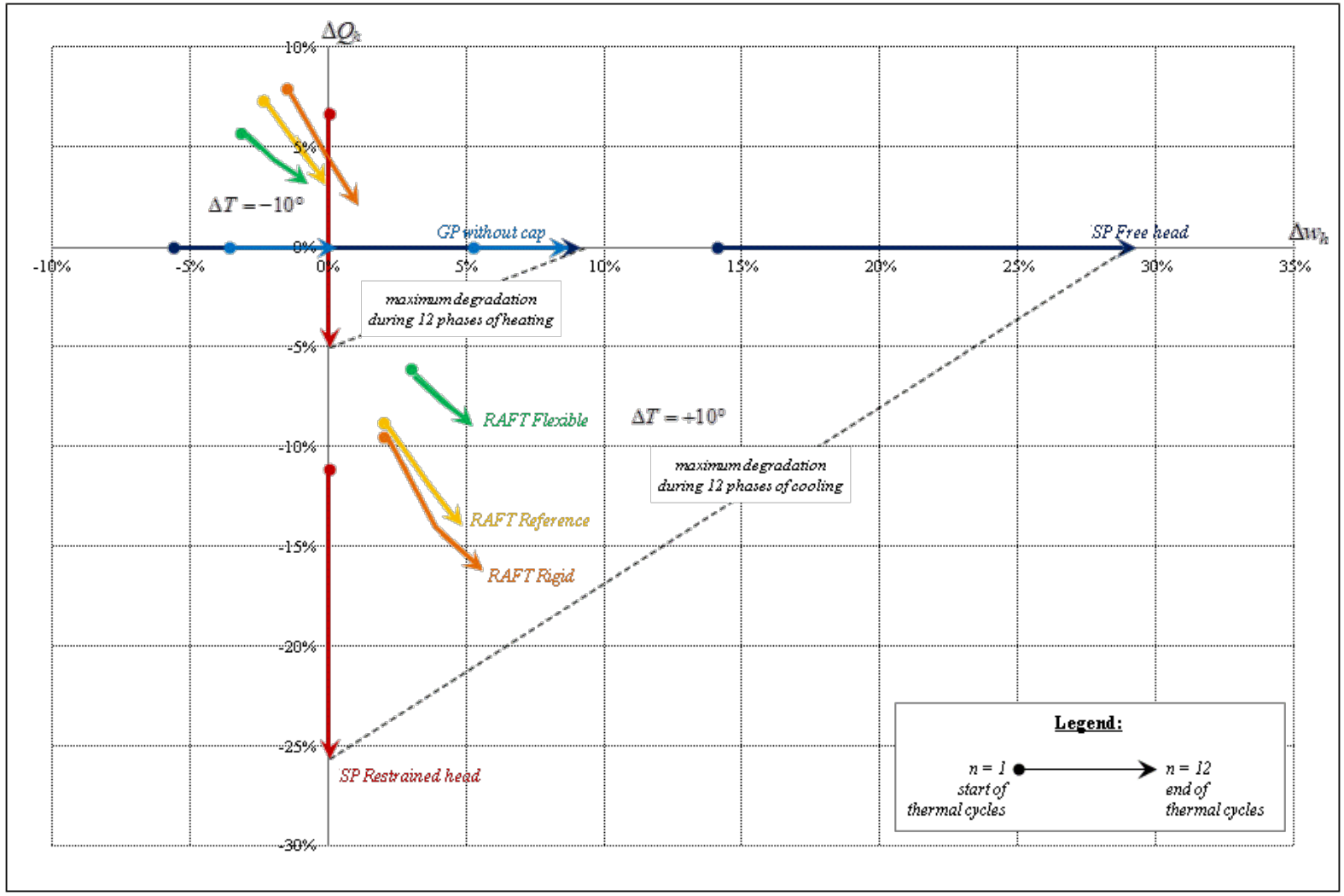

Figure 4.26 – Range of change in pile head response over 12 thermal cycles (ΔT=±10°C)

CHAPTER 5
LOAD TRANSFER ANALYSIS OF A SINGLE THERMO-ACTIVE PILE*

5.1 Introduction

In engineering practice, analysis of axially loaded pile can be conducted by load transfer method. This method requires a load transfer *t–z* function which defines the relations between the shaft friction and pile displacements as well as between the bearing stress and the pile displacement at the base. A number of *t–z* functions is available in the literature (Coyle and Reese 1966; Kraft *et al.* 1981; Randolph and Wroth 1978), in which the design of axially loaded pile in France refers to the *t–z* functions developed by Frank and Zhao (1982) or Monnet and Bernhardt (2000) based on the pressuremeter test.

Regarding the problem of the thermo-active pile, the pile is loaded axially by two-way cyclic thermal loading (i.e. contraction–dilatation). In the present time, there exist only two *t–z* functions which are able to model cyclic loading–unloading path: the one is developed by Randolph (1986; 2003a) and the other one is currently developed by Knellwolf *et al.* (2011) as an enhancement of the Frank and Zhao function. The Randolph function consists of a linear elastic part, a nonlinear parabolic shape function describing the strain hardening/softening mechanism, and also a function considering cyclic degradation effects (Randolph 1986; Randolph 2003a), but the implementation of the function in numerical program RATZ is limited to a single magnitude of the cyclic thermal strains for each analysis. In the other side, the function developed by Knellwolf *et al.* (2011) is implemented in Thermo-Pile program to analyze the behavior of a

* Some of the materials presented in this chapter have been published in [SUR 14], [SUR 12b], and [SUR 12c] as listed in Appendix C

thermo-active pile. However, the function is limited to two linear elastoplastic branches and a plateau corresponding to the ultimate stress value without having a kinematic hardening criterion (Knellwolf *et al.* 2011; Laboratory of Soil Mechanics 2011).

Aiming to analyze the behavior of a thermo-active in practical engineering approach with taking into account the two-way cyclic thermal strain, the softening/hardening mechanism, and the cyclic degradation effects; this chapter presents a new formulation of nonlinear *t–z* function. In the first part, the conceptual background, the workability, and the performance of the proposed *t–z* function are discussed. In the second part, the proposed *t–z* function is implemented to a computer program to offer a practical design tool of load transfer analysis for designing the thermo-active pile. At last, the response of such pile resulting from 1D load transfer analysis using the proposed *t–z* function is compared to that of resulting from 3D analysis using the Modjoin law.

5.2 Development of the proposed *t–z* cyclic function

The concept of the proposed *t–z* function in this study is based on hypotheses resulting from in-situ experiences conducted by many researchers. They stated that the relation between shaft friction and pile displacement under two-way cyclic loading should satisfy the following conditions:

- reduction in shaft friction with increasing the number of cycles (Bea *et al.* 1980; Holmquist and Matlok 1976; Poulos 1989),
- degradation in shaft resistance with the accumulation of absolute tangential displacement (Fakharian and Evgin 1997; Uesugi and Kishida 1991),
- reduction in normal stress by the volumetric strain with increasing the number of cycles (Fakharian and Evgin 1997; Poulos 1989; Uesugi and Kishida 1991),
- increase in shaft friction with increasing the rate of loading (Bea *et al.* 1980; Bjerrum 1973),
- increase in pile settlement with increasing the number of cycles (Bea *et al.* 1980),

- hardening and stiffening in interface with increasing the number of cycles (Desai *et al.* 1985),
- decrease in rate of stiffening with increasing the number of cycles (Desai *et al.* 1985).

With respect to the hypotheses above, a new formulation of nonlinear *t–z* function condition is developed. The proposed *t–z* function is divided into two stages of loading: the initial relation under monotonic loading and the extension under cyclic loading.

5.2.1 Behavior under monotonic loading

5.2.1.1 Basic principle

Under monotonic loading, the formulation of the proposed *t–z* function is based on the Frank & Zhao *t–z* function (Frank and Zhao 1982). The shaft friction mobilized at the soil–pile interface q_s related to the tangential displacement u_t is given by:

$$q_S = q_{S0}\left(1 - e^{-\frac{u_t}{\alpha}}\right) \qquad [5.1]$$

where q_{s0} (kPa) and α (m) denote the ultimate mobilized friction and the rate of mobilized friction under monotonic loading, respectively. A parametric study of the influence of parameter α on the evolution of shaft friction q_s is given in Figure 5.1. It shows that the smaller the value of α, the smaller displacement is needed for mobilizing friction at the pile shaft, which leads increasing the stiffness of interface.

The gradient of the function is given in equation 5.2. The value of the gradient represents the slope of the curve and can be equated to the slope k_s in the Frank & Zhao function (Frank and Zhao 1982).

$$\frac{\partial q_s}{\partial u_t}(u_t) = \frac{1}{\alpha} q_{s0}\, e^{-\frac{u_t}{\alpha}} = k_s \qquad [5.2]$$

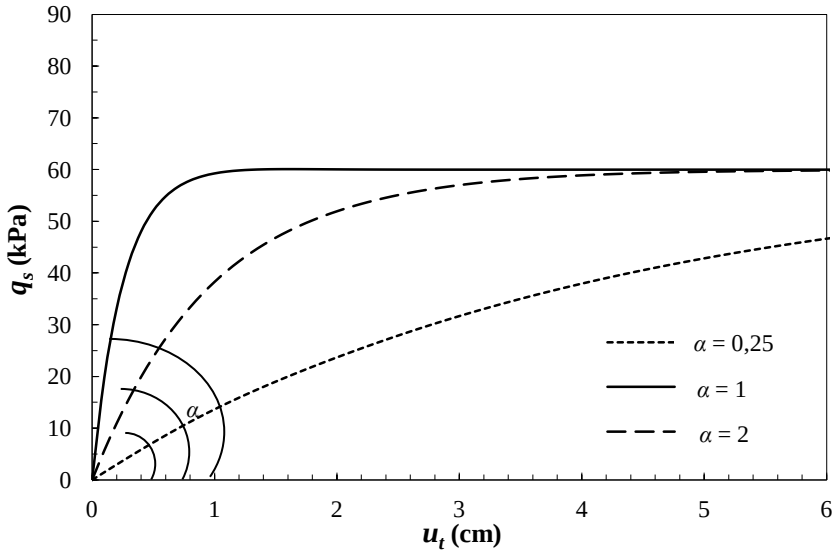

Figure 5.1 – Parametric study of α

Therefore, the choice of parameters q_{s0} and α is done by an approximation to the Frank & Zhao coefficient (Frank and Zhao 1982) or it can be taken from the Menard's pressuremeter modulus E_M and Menard's pressure limit p_{LM} (AFNOR 2012; Ménard 1975) according to the French national code for deep foundation (AFNOR 2012; Ménard 1975). For example, the adjustment relationship between α and k_s for granular soil is defined by the following equation:

$$\alpha_s = q_{s0}\left(\frac{B}{0{,}8E_M}\right)\times f \text{ and } \alpha_b = q_{b0}\left(\frac{B}{4{,}8E_M}\right)\times f \qquad [5.3]$$

where the indexes "s" and "b" indicate the pile shaft and pile base, respectively. f is a correlation factor and B is the pile diameter. The values within the parentheses denote the values of the coefficient k_s and k_b in the Frank & Zhao function.

Figure 5.2 shows the comparison of the proposed t–z function to that of Frank & Zhao for fine soils and granular soils. By setting the parameter α in accordance with k_s, the t–z curves resulting from the proposed function are very close to that of resulting from the Frank & Zhao function. When the value of α is equal to the tangential displacement u_t, the mobilized friction obtained using equation 5.1 is equal to 63% of the ultimate mobilized friction. At this state of displacement, the difference between the mobilized

frictions resulting from the proposed *t–z* function and the Frank & Zhao function is below 5 kPa.

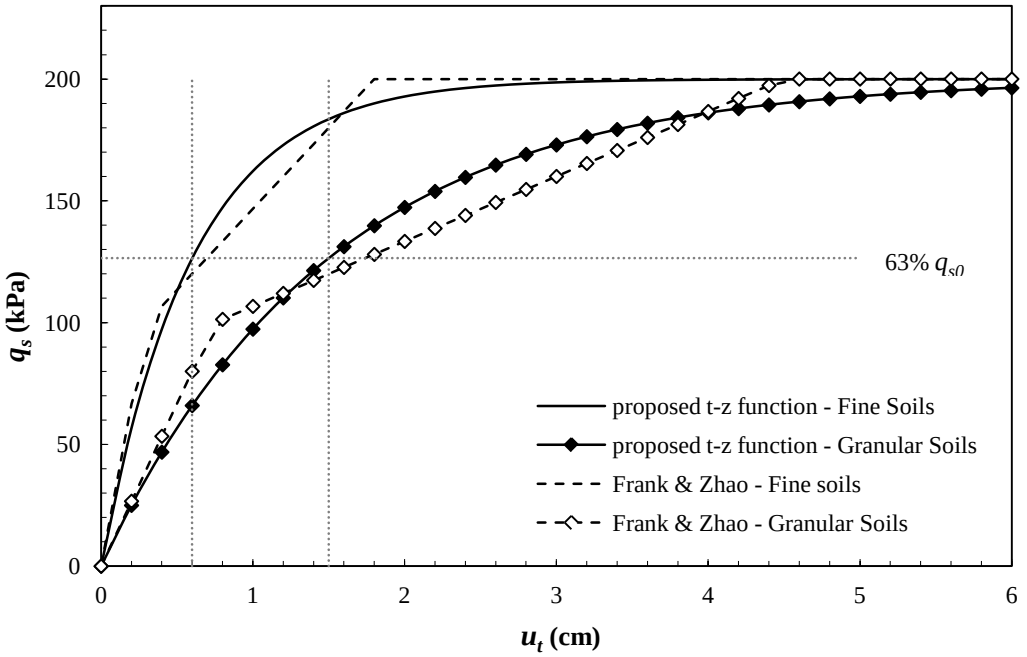

Figure 5.2 – Comparison of the proposed *t–z* function and the *t–z* function by Frank & Zhao

5.2.1.2 Strain hardening/softening parameters

Strain hardening/softening phenomenon in materials depends on the void ratio in granular soils and on the Atterberg limits in fine soils. In order to consider the nonlinear behavior of strain hardening/softening, the proposed *t–z* function introduces three other parameters β, δ, and γ in equation 5.4:

$$q_s = q_{s0}\left(1 - e^{-\frac{u_t}{\alpha}}\right) + \beta {u_t}^{\delta} e^{-\left(\frac{u_t}{\gamma}\right)^{\delta}} \qquad [5.4]$$

where β (kPa) and γ (m) indicate the amplitude of strain hardening/softening and the rate of strain hardening/softening under monotonic loading. δ is an unitless parameter which controls the time loading rate.

The first part of the equation defines the relation of shaft resistance and tangential dis-

placement with the control of ultimate shaft resistance, whereas the second part of the equation describes the peak of shaft resistance related to the loading rate that may be attained in parabolic function. The peak of shaft resistance may occur only in dense soil with a high loading rate, for example in over consolidated clay or in dense sand. The greater the parameter β is, the higher the peak of parabolic curve is obtained which corresponds effectively to the denser soil (Figure 5.3). For a same given value of β, parameter γ controls the radius of parabolic curve expressing the velocity of strain hardening/softening mechanism (Figure 5.4).

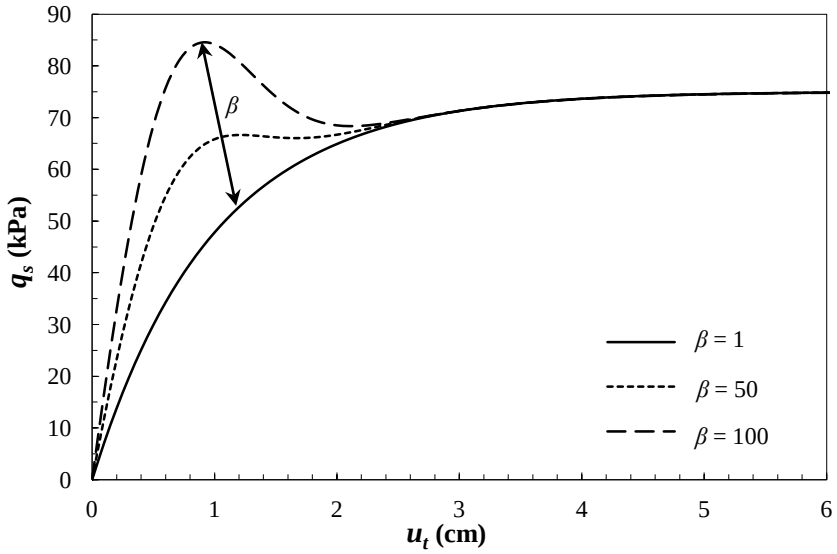

Figure 5.3 – Parametric study of β

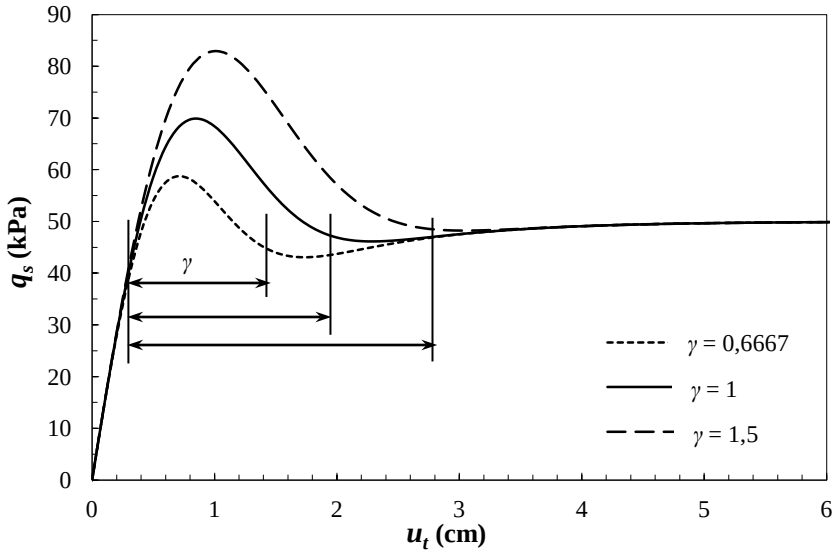

Figure 5.4 – Parametric study of γ

The parametric study of δ has successfully described the hypothesis of Bjerrum and Beat *et al.* (Bea *et al.* 1980; Bjerrum 1973) who showed that a more rapid loading rate contributes to an increase in pile capacity. Thus, a greater parameter δ reveals to a higher peak of shaft resistance (Figure 5.5).

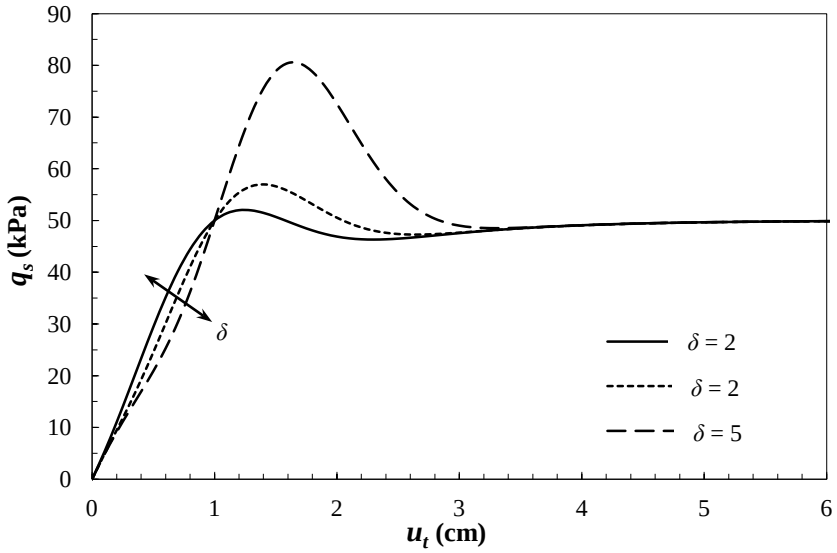

Figure 5.5 – Parametric study of δ

5.2.2 Behavior under two-way cyclic loading

In analyzing the behavior of piles subjected to cyclic loading, three aspects of soil response should be considered: the degradation of soil–pile resistance and/or soil modulus, the loading rate effects, and the accumulation of permanent displacements (Poulos 1989). The proposed *t–z* function under two-way cyclic loading comprising of those aspects is given in the following equation 5.5:

$$q_s = q_{si} + A(-1)^{n+1}\left[\begin{array}{c}\left(q_{s0} + \Delta q_s\left(1 - e^{-\frac{u_{ts}}{\varepsilon}}\right)\right)\left(1 - e^{-R\left|\frac{u_t - u_{ti}}{\alpha}\right|}\right) \\ + \beta e^{-\frac{u_{ts}}{\varepsilon}}\left|u_t - u_{ti}\right|^{\delta} e^{-\left(\frac{u_t - u_{ti}}{\gamma}\right)^2}\end{array}\right] \quad [5.5]$$

where n denotes the number of inversion loading during two-way cyclic loads. q_{si} (kPa) indicates the initial calculated friction at each inversion loading cycle (q_{si} = 0 for n = 1). u_{ti} (m) is the initial displacement obtained at each inversion loading cycle (u_{ti} = 0 for n = 1) and u_{ts} (m) is the cumulative displacements during cyclic loads ($u_{ts} = \sum |u_{ti}|$).

The degradation of interface resistance is controlled by the parameters Δq_s (kPa) and ε (m) which express the amplitude of cyclic strain hardening/softening and the rate of cyclic strain hardening/softening.

The function R in equation 5.6 controls the stiffness hardening of interface at each inversion loading cycle, ranging between 1 and ρ. Inside the function R, parameters ρ and ξ allow controlling cyclic degradation in interface behavior, such as stress relaxation or strain ratcheting, where ρ indicates the amplitude of cyclic degradation and ξ is the rate of degradation.

Factor A in equation 5.7 is the interface stiffness hardening factor which is dependent on the level of stress obtained. A takes into account the distance between the actual stress state q_{si} and the maximum cyclic stress state $q_{s0} + \Delta q_s$ which may vary with the cycles. If an inversion of loading cycle occurs at high level of stress, a higher value of A is produced and thus the interface becomes stiffer in the next cycle. This factor varies between 1,0 and 2,0.

$$R = e^{-(n-1)\xi} + \rho\left(1 - e^{-(n-1)\xi}\right) \qquad [5.6]$$

$$A = \left| \frac{q_{si} - (-1)^{n+1}\left(q_{s0} + \Delta q_s \left(1 - e^{-\frac{u_{ts}}{\varepsilon}} \right) \right)}{q_{s0} + \Delta q_s \left(1 - e^{-\frac{u_{ts}}{\varepsilon}} \right)} \right| \qquad [5.7]$$

5.2.3 Performance of the proposed *t–z* function

To study the performance of the proposed *t–z* function, several tests are conducted in two different modes: strain-controlled and stress-controlled. If the deformation is maintained constant with the increment of cycles, the stress will gradually decrease due to cyclic fatigue in interface. This phenomenon is known as stress relaxation (Ghali *et al.* 2002; Lemaitre *et al.* 2009; Xia *et al.* 1996). Otherwise, if the stress is sustained along the cycles, a progressive accumulation of plastic strain during cycles occurs, known as strain ratcheting phenomenon (Ghali *et al.* 2002; Lemaitre *et al.* 2009; Xia *et al.* 1996).

Figures 5.6–5.7 show the parametric study of cyclic degradation parameters ρ and ξ at strain-controlled and stress-controlled conditions. When the values of ρ and ξ are set at 1,0; the phenomena of stress relaxation and strain ratcheting are important. The higher the values of ρ and ξ are, the stiffer the interface behaves under cyclic loading. Accordingly, there is lower variation of the decrease in shaft resistance per cycle (Figure 5.6b) and the accumulation of plastic strain becomes slower and smaller (Figure 5.7b).

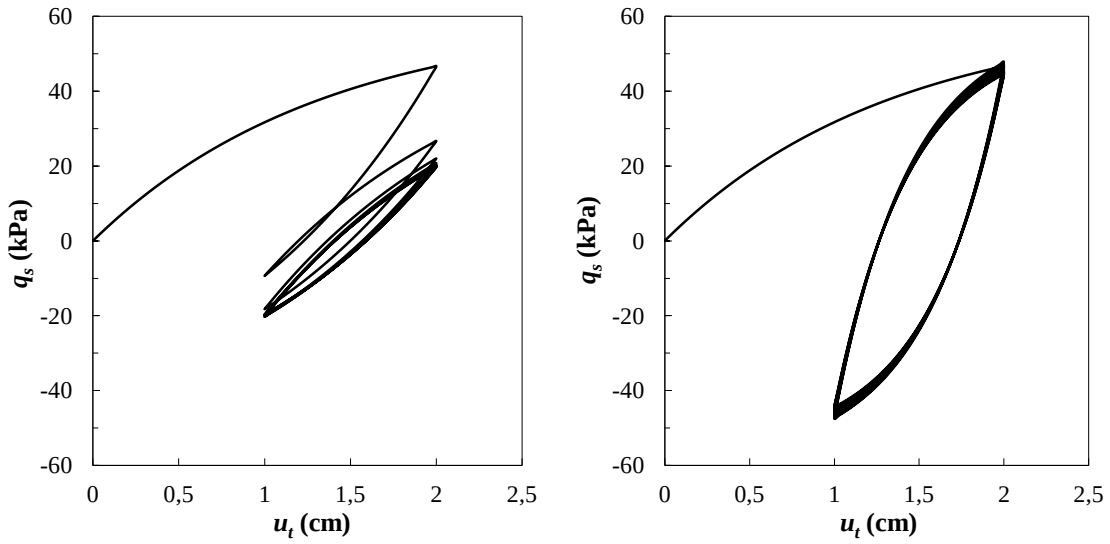

(a) stress relaxation when ρ and ξ = 1 *(b) no relaxation when ρ and ξ = 3*

Figure 5.6 – Parametric study of ρ and ξ at strain-controlled

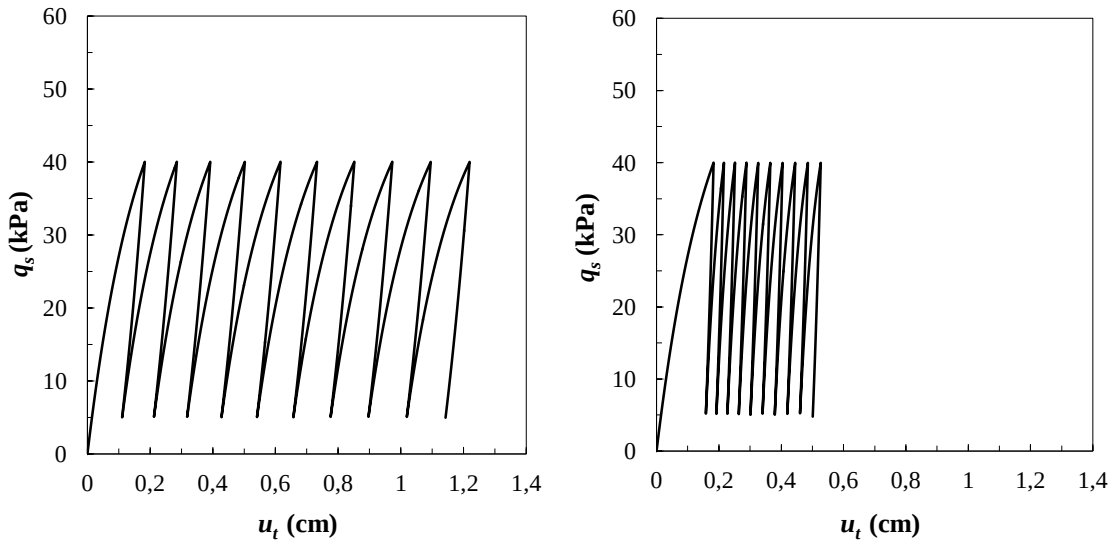

(a) strain ratcheting when ρ and ξ = 1 *(b) no ratcheting when ρ and ξ = 3*

Figure 5.7 – Parametric study of ρ and ξ at stress-controlled

5.2.3.1 Comparison to laboratory test

A direct shear test under cyclic loading in strain-controlled was conducted at *Centre d'Etudes et Techniques de l'Equipement* (CETE) Nord Picardie. Due to cyclic softening, the results showed that the friction mobilized became lower with increasing the number of cycles, but the interface stiffness increased at each load cycle. Figure 5.8 shows a comparison of the results from direct shear test and from modeling the interface behavior with the proposed *t–z* function. By setting the parameters in the proposed function in accordance with the material properties used in the direct shear test, the proposed *t–z* function can successfully describe similar phenomena in interface.

5.2.3.2 Comparison to Modjoin law

Laboratory of Civil and Geo-environmental Engineering (LGCgE) have developed a constitutive law of soil–pile interface under cyclic loading (Shahrour and Rezaie 1997). The law is called Modjoin law and is recently enhanced to control cyclic degradation phenomena, such as stress relaxation, strain ratcheting, and strain accommodation (Cao 2010). Figure 5.9 shows that the proposed *t–z* function can render similar response in interface behavior when compared to the Modjoin law by setting the parameters.

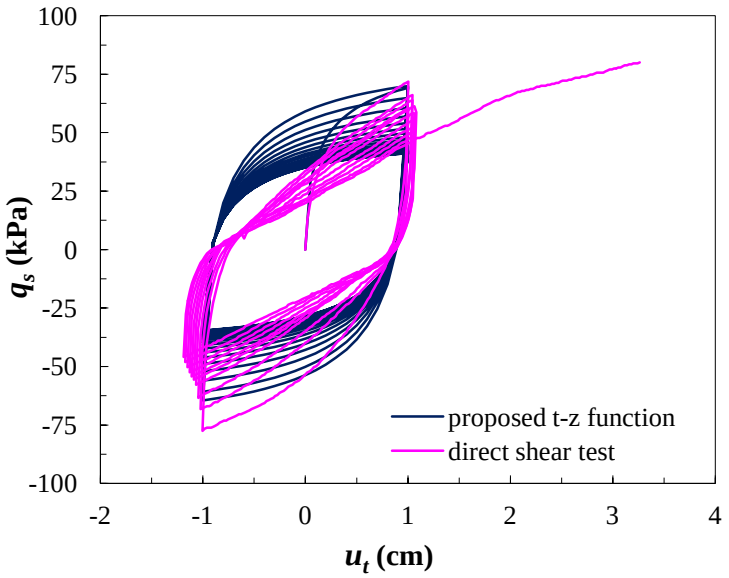

Figure 5.8 – Interface behavior with the proposed *t–z* function compared to direct shear test results

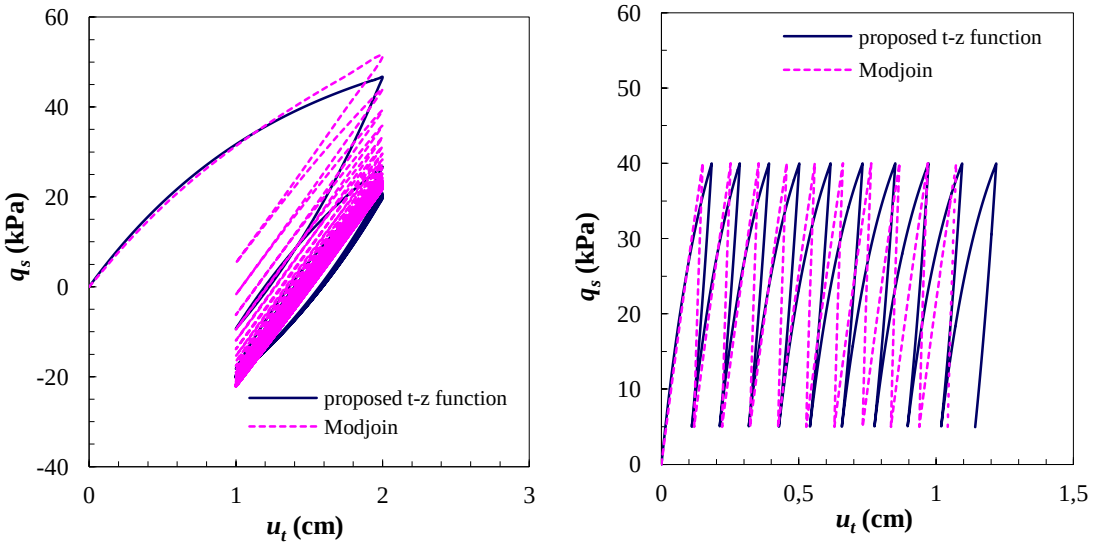

(a) stress relaxation phenomenon ***(b) strain ratcheting phenomenon***

Figure 5.9 – Comparison of the proposed *t–z* function and Modjoin law in modeling the interface behavior

5.3 Application of the proposed *t–z* function in analyzing the thermo-active pile behavior

In this section, the load transfer analysis using the proposed *t–z* function is performed to

analyze the behavior of a single thermo-active pile under combined axial mechanical and cyclic thermal loads. The analysis is conducted by implementing the proposed *t–z* function into a computer program. The program offers a practical tool in the design and analysis of a thermo-active pile. The behavior of such pile is compared to that of resulting from the 3D analysis using the Modjoin law, which is previously presented in Chapter 3.

5.3.1 Numerical model

A single thermo-active pile with a square section of width B = 60 cm and length H = 15 m is founded on homogeneous cohesionless soil mass. The pile is initially subjected to incremental monotonic loading corresponding to the permanent load of building during the construction phase. The mechanical working load applied to the pile P_W is fixed at 33% of the ultimate load Q_{ULT} when the pile head settlement is equal to 1/10 B (AFNOR 2012; Borel 2001). This stage of loading occurs at n = 0 with an index *"mec"*. The pile is then subjected to 12 thermal cycles with a uniform temperature gradient of ±10°C from the soil temperature. One cycle corresponds to one year of thermal operation, which comprises of cooling and heating phases. Thermal cycles start from cooling phase and followed by heating phase. The schematic of cyclic thermal loads remains the same with that of 3D analysis as shown in Figure 3.4.

Both pile and soil are assumed to behave in linear thermo-elastic conditions, with the Menard's pressure meter modulus of soil is equal to 10 MPa and the Young's modulus of the pile is equal to 20 GPa. The coefficients of thermal expansion α_T are taken as 5×10^{-6} °C^{-1} for soil and $1{,}25\times10^{-5}$ °C^{-1} for concrete pile. The soil properties are taken from CETE Nord Picardie data for loose sand. As a consequence, the value of parameter β in the proposed *t–z* function is set at zero and thus no intervention of this parameter takes place in the second part of equations 5.2–5.3. The parameters of soil and pile are summarized in Table 5.1.

The materials are considered to undergo cyclic fatigue effects with a cyclic softening tendency. Hence, the amplitude of cyclic degradation ρ_s for the shaft is set at 1,0 with

the rate of degradation ξ_s of 0,01. The pile base is set to have a higher stiffness of cyclic softening than that of pile shaft in order to limit the degradation in the base resistance. In addition, the bearing stress q_b is not allowed to have a negative value. Therefore the amplitude of cyclic degradation for the pile base ρ_b is set at 5,0 to avoid the cyclic fatigue effects with a very low rate of degradation ξ_b of 0,001. The ultimate bearing stress q_{b0} is calculated from the pressuremeter method according to French design standard: $q_{b0} = k^* p_{LM}$, where k^* denotes the bearing capacity factor and p_{LM} denotes the Menard's pressure limit (AFNOR 2012; Ménard 1975).

Other parameters in this proposed *t–z* function, such as α and ε, are set to render a comparable cyclic behavior with the single thermo-active pile resulting from 3D analysis using the Modjoin law. The parameters of the proposed *t–z* function used in this study are summarized in Table 5.2.

Table 5.1 – Properties of the materials used in the study

	Material density	***Menard's pressuremeter modulus***	***Young's modulus***	***Thermal expansion coefficient***
	ρ_c	E_M	E	α_T
Soil	1950 kN/m^3	10 MPa	–	5×10^{-6} °C^{-1}
Pile	2500 kN/m^3	–	20 GPa	$1{,}25\times10^{-5}$ °C^{-1}

Table 5.2 – Parameters of the proposed *t–z* function

	Pile shaft		***Pile base***	
Elasto-plastic parameters	q_{s0}	15 kPa	p_{LM}	3,5 MPa
			k^*	1
	α_s	0,10	α_b	0,02
Cyclic hardening/softening parameters	Δq_s	$-0{,}2\ q_{s0}$	Δq_b	$-0{,}01\ q_{b0}$
	ε_s	0,001	ε_b	0,001
	ρ_s	1	ρ_b	5
	ξ_s	0,01	ξ_b	0,001

Analysis is performed using load transfer method by applying the proposed *t–z* function described in Section 5.2. The pile is divided into a number of segments supported by discrete springs which represent the mobilized resistance along the shaft q_s and at the base of pile q_b. Schema of the pile division is shown in Figure 5.10. The load transfer

method consists of back-calculating the boundary condition at the pile head by imposing an assumed pile tip movement for each load cycle. Two cases are proposed representing the extreme cases of a single pile: the free head pile with constant thermal head load over the cycles (i.e. zero head axial fixity $K_h = 0$) and the restrained head pile with constant thermal head displacement over the cycles (i.e. infinite head axial fixity $K_h = \infty$). Each pile segment must satisfy the vertical equilibrium for each load cycle. A flowchart of iterative programming code is given in Figure 5.11 while the detail equations used to solve the equilibrium are presented in Appendices A and B.

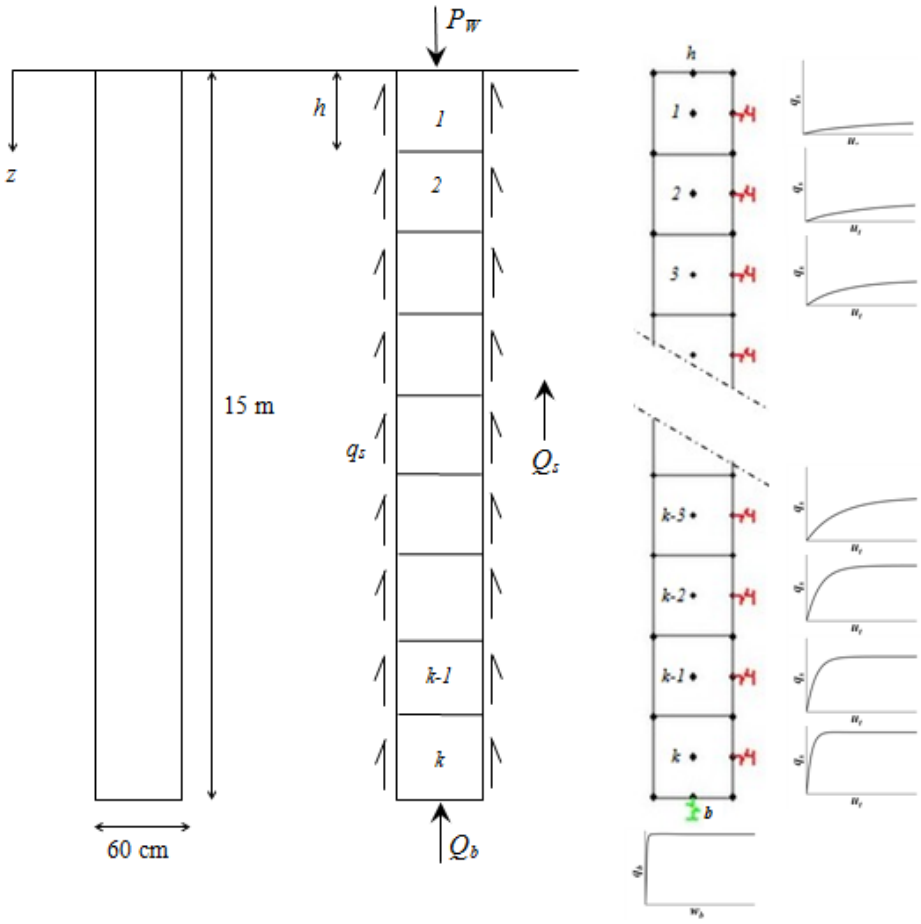

Figure 5.10 – Model schema using load transfer method

For the sake of clarity, downward movements of w are taken positive while upward movements are negative. Compressive stresses and forces are taken positive while tensile stresses and forces are negative according to the convention in soil mechanics. The response of the thermo-active pile over the cycles will be detailed in the following section, for both the free head pile and the restrained head pile. The behavior resulting

from load transfer analysis using the proposed *t–z* function is compared to the behavior resulting from 3D analysis using the Modjoin law.

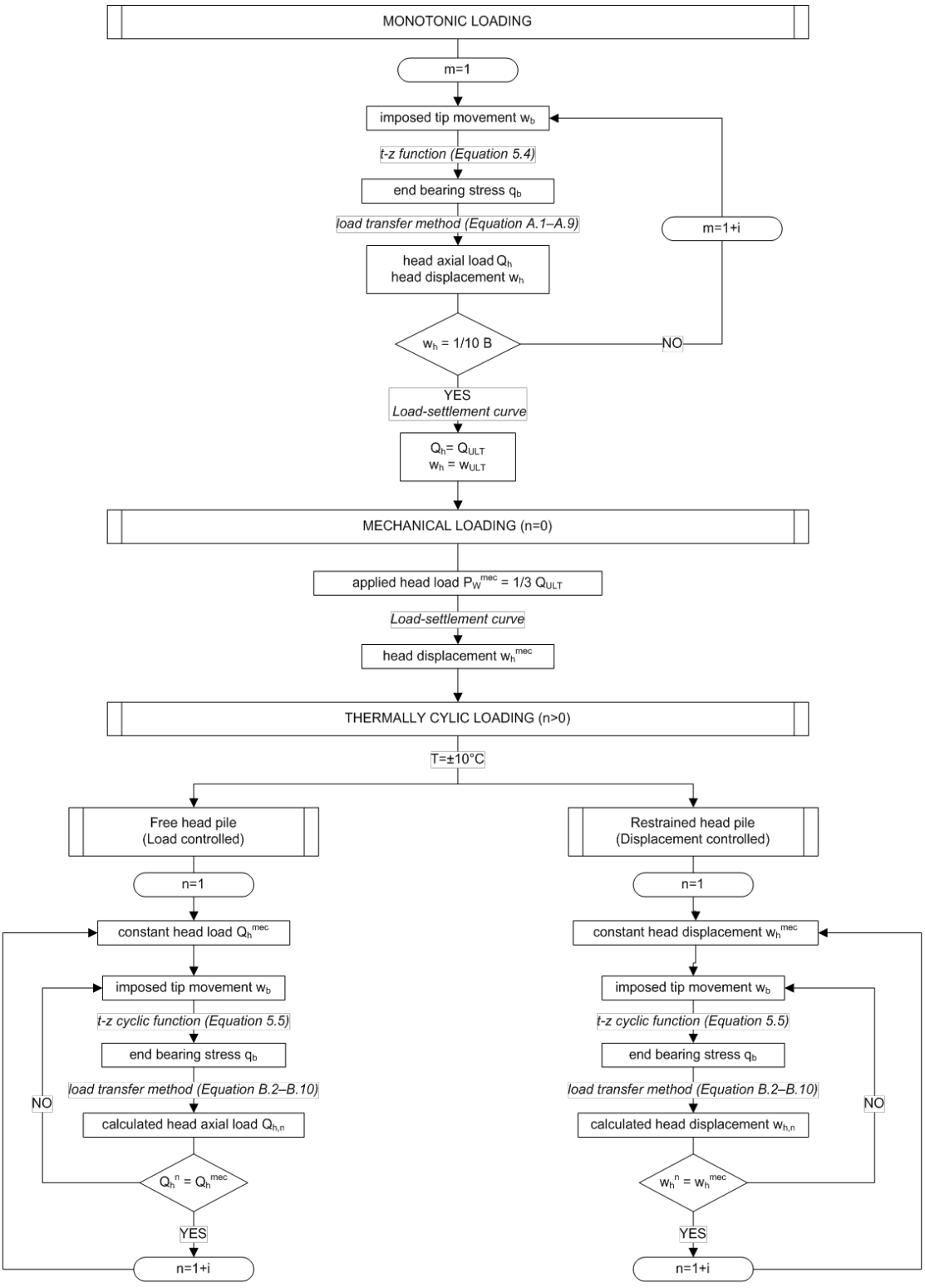

Figure 5.11 – Flowchart of numerical programming

5.3.2 Behavior of the free head pile

5.3.2.1 Change in pile head settlement

Figure 5.12 shows the change in pile head settlement relative to the initial response at the mechanical working stage of loading. The increase in pile head settlement for 1D and 3D analyses tends to have a similar tendency in the range between –5% of heave to +25% of settlement. To have a better vision, Figure 5.13 shows the increase in pile head settlement relative to the first thermal cycles, which shows that the increase in pile head settlement resulting from the 1D analysis is progressively linear. In contrast, the 3D analysis shows a tendency of nonlinear stabilization over the cycles due to the more refined and more complete analysis by modeling the soil mass surrounding the pile and the interface elements at the soil–pile contact zone.

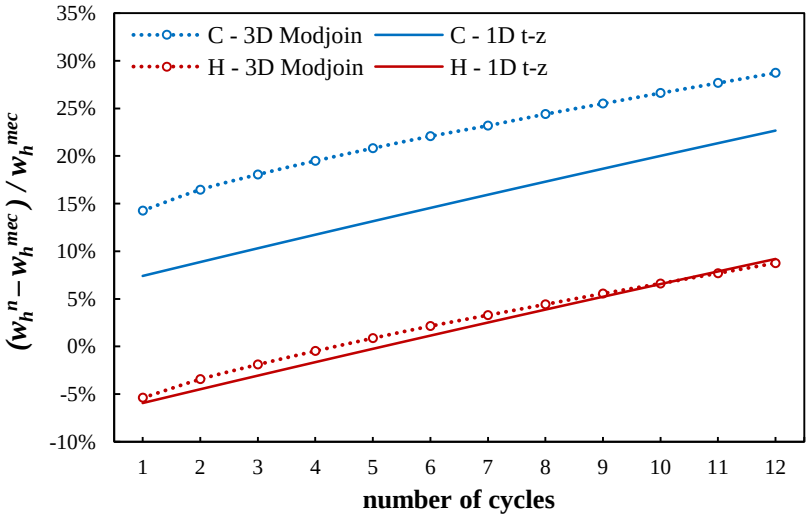

Figure 5.12 – Increase in head settlement relative to the mechanical loading stage

5.3.2.2 Distribution of normal force

Figure 5.14 shows the variation in normal force along the pile in the beginning of thermal cycles and in the end of thermal cycles as well. A decrease in normal force is found in the first cooling phase due to the pile shortening. The changes in normal force increase with the number of cycles, with the values of change in cooling phases are smaller than those in heating phases. The increase in normal force with the cycles is

caused by the degradation of interface and soil properties during cyclic loading. Variation in normal force resulting from 1D analysis and 3D analysis show a similar response in rendering cyclic fatigue effects.

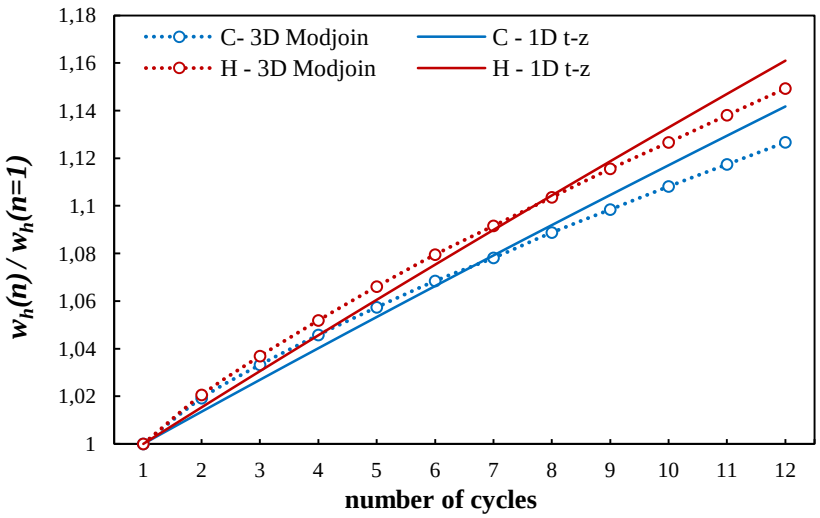

Figure 5.13 – Cyclic hardening in head settlement relative to the first thermal cycle

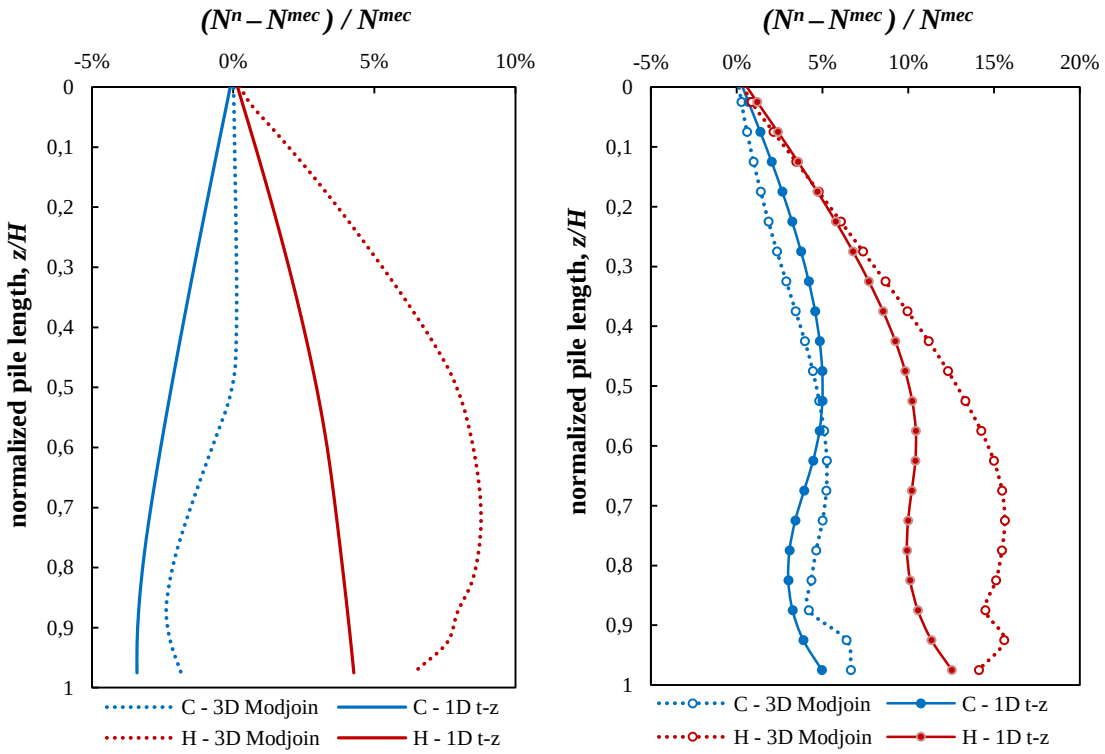

(a) in the beginning of thermal cycles *(b) in the end of thermal cycles*

Figure 5.14 – Change in normal force compared to 3D model

5.3.2.3 Change in shaft friction and tangential displacement at the soil–pile interface

In the case of free head pile, the distribution of shaft friction shows an opposite response at the upper part and the lower part of pile with respect to the opposite profile of thermal axial displacement. In cooling phases, the bearing stress decreases while the shaft friction increases due to the pile shortening. On the contrary, heating phases bring out an increase in bearing stress and a decrease in shaft friction relative to the expansion of pile.

The variation of local friction vs. local tangential displacement points out the cyclic fatigue phenomenon at the soil–pile interface for both models. Because of the choice of cyclic hardening/softening parameters in the models, a phenomenon of strain ratcheting appears (Figure 5.15). However, at the lower-half of the pile (Figure 5.15b), the degradation in interface capacity for the case of 3D model is smaller due to the presence of soil surrounding the pile which resists the stress mobilized. For the case of 1D model, the friction of interface tends to increase at the lower-half of the pile due to the boundary condition of the 1D model which limits the degradation in bearing stress.

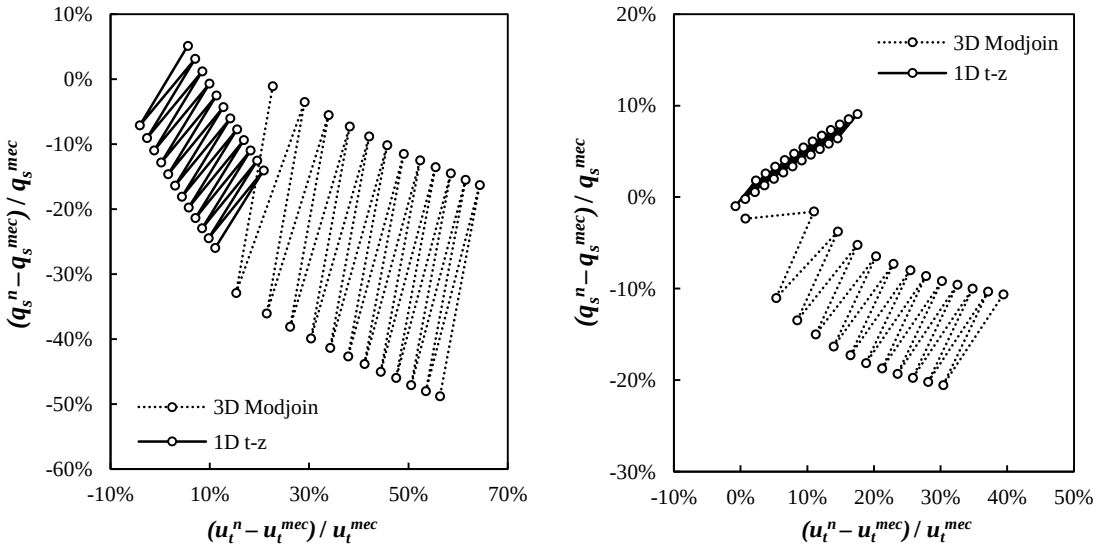

(a) at z = 0,2 H ***(b) at z = 0,8 H***

Figure 5.15 – Change in shaft friction and tangential displacement at different depths

5.3.3 Behavior of the restrained head pile

5.3.3.1 Change in head force

It is shown that under constant head displacement, the thermo-active pile in 1D model undergoes a decrease in head reaction force relative to the force at mechanical loading stage up to –20% during cooling phases and –35% during heating phases (Figure 5.16). The decrease resulting from 1D analysis is relatively greater than that of resulting from 3D analysis, which is possibly due to the absence of soil mass surrounding the pile. Figure 5.17 shows the decrease in head reaction force relative to the first thermal cycles which indicates the cyclic hardening. The response of the pile resulting from 3D analysis has a lower cyclic hardening thus tends to have a cyclic stabilization compared to the response resulting from 1D analysis.

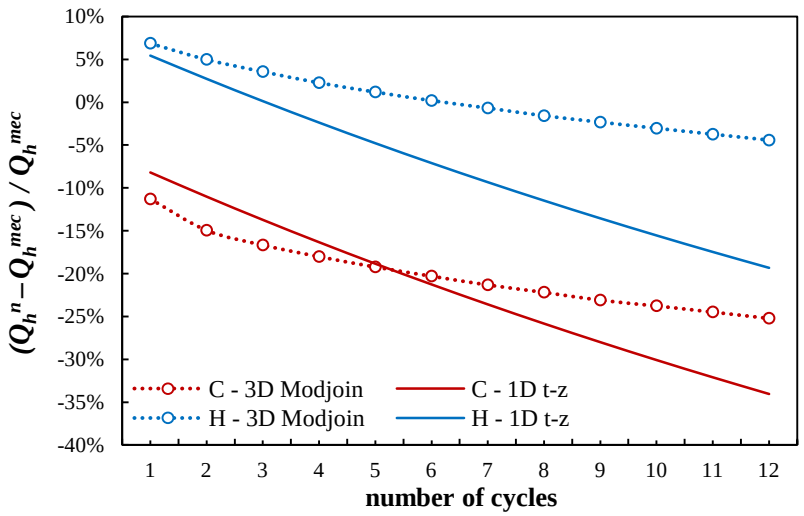

Figure 5.16 – Decrease in head force relative to mechanical loading stage

5.3.3.2 Distribution of normal force

The variation in normal force during thermal cycles is uniform along the entire pile length (Figure 5.18). In the beginning of cycles, the response of 1D analysis is very close to the response of 3D analysis. Both models present the contraction in the first cooling phase (i.e. decrease in normal force) and the expansion in the first heating phase (i.e. increase in normal force). Nevertheless, the variation in normal force continues to

decrease due to the degradation in soil–pile capacity over the cycles. In the end of thermal cycles, the decrease in normal force variation resulting from the 1D analysis is greater due to the higher cyclic hardening than that of 3D analysis.

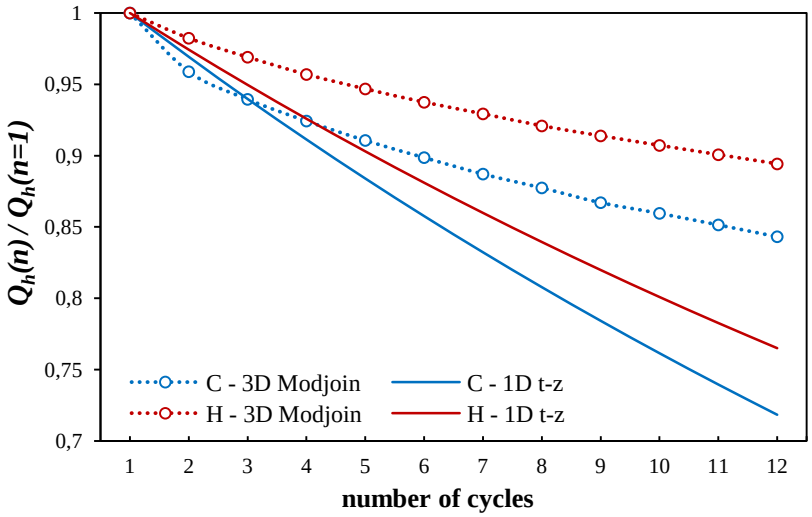

Figure 5.17 – Cyclic hardening in head force relative to the first thermal cycle

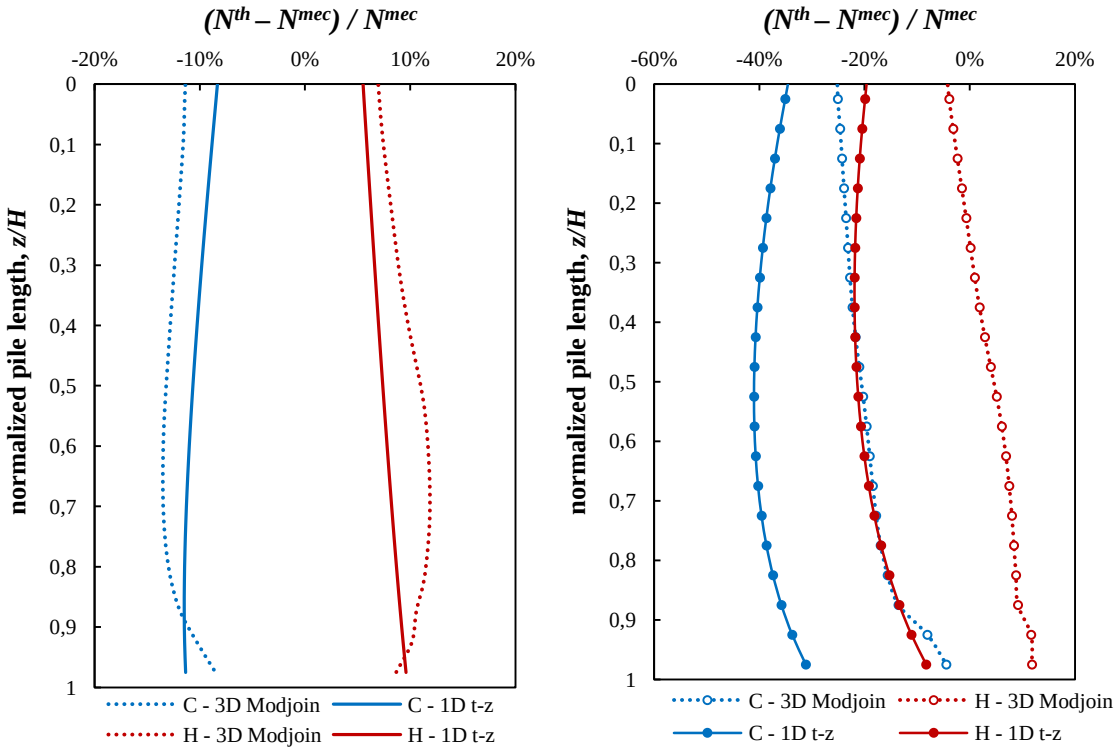

(a) in the beginning of thermal cycles *(b) in the end of thermal cycles*

Figure 5.18 – Change in normal force compared to 3D model

5.3.3.3 Change in shaft friction and tangential displacement at the soil–pile interface

In restrained head pile, shaft friction decreases gradually along the depth of pile. It is noted that the degradation of thermally-induced friction is higher in cooling phases than that in heating phases due to the decrease in base resistance when the pile base lifts up during contraction. Figure 5.19 points out a gradual diminution in shaft friction during thermal cycles, which shows a relaxation phenomenon. However, in the 1D model, the degradation in soil–pile interface is represented only by the gradual decrease in shaft friction and no increase in tangential displacement during cycles due to the absence of soil mass surrounding the pile. On the contrary, in the 3D model, the variation in tangential displacement is increasing due to the accumulation of tangential displacement at the Modjoin interfaces.

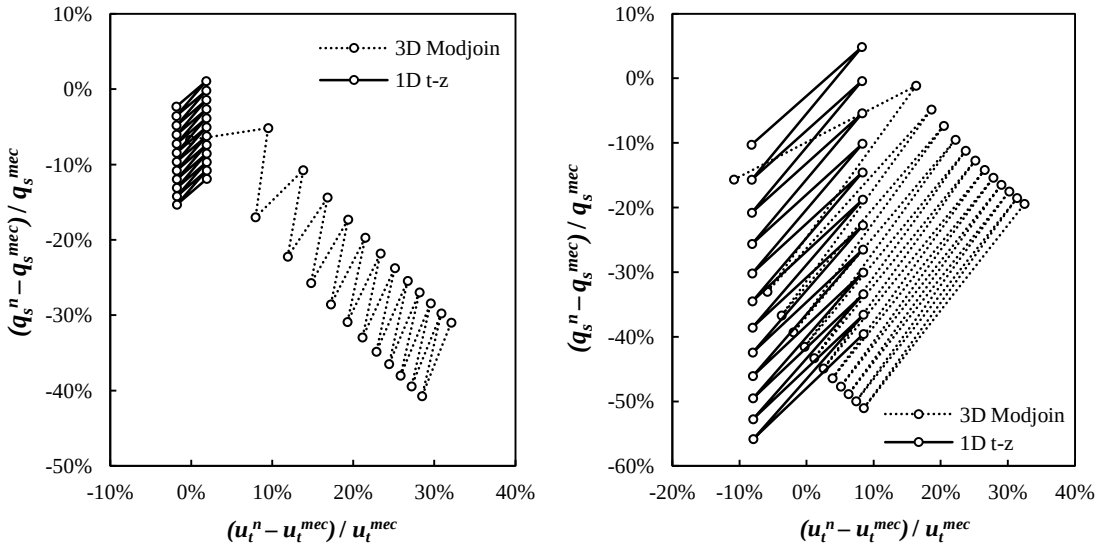

(a) at z = 0,2 H ***(b) at z = 0,8 H***

Figure 5.19 – Change in shaft friction and tangential displacement at different depths

5.4 Conclusion

This chapter presents a development of a theoretical *t–z* function for the soil–pile interface under two-way cyclic loading. The function is based on a series of results and

hypotheses of the previous field and laboratory investigations. The proposed function is able to describe the cyclic strain hardening/softening mechanism and the degradation phenomenon during cyclic loading including the cyclic fatigue effects such as stress relaxation and strain ratcheting. The function consists of nine parameters as follows:

- q_{s0} and α which describe the mobilization of friction under monotonic loading,
- β, δ, and γ which control the strain hardening/softening under monotonic loading (i.e. prior to peak and post–peak),
- Δq_s, ε, ρ, and ξ which take into account the cyclic strain hardening/softening.

This proposed *t–z* function is then employed to the load transfer method by creating a numerical program aiming to offer a practical engineering tool for the design and analysis of the thermo-active pile behavior.

Afterwards, the 1D analysis of a single thermo-active pile under combined axial mechanical and cyclic thermal loads is conducted by using the load transfer method with the proposed *t–z* function. The response of such pile resulting from 1D analysis is compared to that of resulting from the preceding 3D analysis using the Modjoin law. While the 1D load transfer *t–z* method permits to have a simplified and practical calculation with high time efficiency, the 3D model using the Modjoin law with finite difference code proposes a complete interaction analysis with higher numerical time consumption. The global response of the thermo-active pile in both models performs a good concordance. In comparison to the 1D model, the presence of the elastic soil surrounding the pile in the 3D model leads to a different local response at the soil–pile interface. Results from this study points out the capability of the two laws of soil–pile interface to render the cyclic fatigue effects in the thermo-active pile behavior. However, the proposed function still requires a parameter validation which is expected by the data of an ongoing in-situ loading test.

GENERAL CONCLUSION

This thesis presents a framework of understanding the thermo-active piles behavior by taking into account the interaction with the surrounding ground in various configurations. After general comprehension about the thermo–hydro–mechanical interaction phenomena in the entire system, the research is focused on analyzing the effect of temperature cycles on the geotechnical performance of such piles located in cohesionless soil. According to the soil type, the heat transfer within the system induces mainly change in pile mechanical behavior and no thermal volumetric change occurs in the grains of sand. Furthermore, since the ratio of the pile diameter to the pile length is small, the change in pile behavior in the radial direction is very small and thus ignored. Therefore, along this research study, analyses are conducted for the axially loaded piles in cohesionless soil, in which the transfer at the zone of contact between soil–pile (i.e. soil–pile interface) is very important. The characteristic of this research study lies on the use of the constitutive behavior law of interface under cyclic loading which is able to model cyclic fatigue effects and degradation phenomena, named the Modjoin law. Along this study, all properties of material (e.g. soil, concrete pile, and interface element) are assumed not to change with temperature.

Based on the results and analyses presented in this thesis, the following key conclusions can be drawn into three major categories as follows:

Numerical analysis of thermal diffusion

- Temperature at the soil–pile interface (or pile perimeter) is equal to the average temperature of the circulating fluid.
- Configuration of inlet–outlet pipes would be better in asymmetric position surround-

ing the pile in order to produce a homogeneous diffusion over the entire pile section.

- Due to the temperature diffusion to the surrounding soil, the equilibrium of ground temperature is disturbed and the annual mean ground temperature T_{ave} moves to a deeper depth.

Numerical analysis of soil–pile interaction

- The magnitude of variation in pile behavior induced by temperature is strongly related to the amount of mechanical working load coming from the permanent loads of the upper structure. The greater the working load is applied, the more rapid the cyclic fatigue occurs.
- Due to the group effects, the neighboring classic piles and the soil contained within the group are affected by cyclic thermal variations.
- Position of thermo-active piles in a pile group plays an important role in the distribution of thermal effects to the other neighboring piles.
- The change in pile group behavior induced by the presence of thermo-active piles in the group is dependent on the piles configuration and the raft rigidity.
- Group effect reduces the impact of temperature cycles on the pile behavior. This means that the values of thermally induced change in pile behavior for a single thermo-active pile case are the maximum values that could be produced.
- At the end of 12 years of thermal operation with a temperature change of ±10°C, the margin of change in pile behavior relative to the pile behavior at the mechanical loading stage is considerably below the failure limit.
- The thermo-active piles can still resist the additional forces induced by temperature variation and by cyclic fatigue when the design of such piles is based on the actual design code.

Load transfer analysis

- A development of theoretical *t–z* function under two-way cyclic loading is established in the framework of nonlinear elastoplastic with cyclic hardening rules.
- The proposed *t–z* function using the load transfer method is implemented in a computer program aiming to conduct a simplified and practical analysis for the de-

sign of thermo-active piles.

- The parameters chosen in this numerical study, both for the constitutive Modjoin law and the proposed *t–z* function, lead to the emergence of cyclic fatigue effects in the pile behavior, e.g. strain ratcheting and stress relaxation phenomena.

Recommendations

Instead of doubling the security factor, quantification of temperature-induced additional stress would help to justify rationally the design of thermo-active piles and establish a secure basis design method for the ultimate limit state (ULS) and the serviceability limit state (SLS), for example:

- The variation in pile head displacement during thermal cycles could be used to verify the serviceability limit states,
- The distribution of normal stress in the pile permits to control the compression and/or the tensile state in concrete,
- The evolution in local friction along the shaft allows calculating the margin of mobilized shaft resistance and mobilized base resistance during cyclic thermal loading and, thereby, estimating the required security factor.

The values of change induced by temperature could be included as variable load in the load combination design equivalent with the snow or wind loads.

Perspectives

The numerical models presented in this thesis focus on the axially loaded piles in cohesionless soil. However, the temperature-induced change in pile foundation behavior is dependent on many factors such as the soil types and the soil hydraulic gradient. Accordingly, further works are expected to be conducted such as:

- Validation of the parameters used in the two cyclic laws of interface behavior: the Modjoin law and the proposed *t–z* function by the data provided from the loading

tests of full-scale piles (within the ongoing project "GECKO" in which this PhD research takes part).

- Consideration of the groundwater flow within the thermo-active piles system in order to analyze the temperature-induced hydro-mechanical behavior of soil.
- Modeling the thin solid elements in the soil adjacent to the pile shaft for the analysis of the thermo-active piles behavior located in cohesive soil. Consideration of the cyclic fatigue effects will be provided with the sophisticated constitutive law of soil under cyclic loading, the Modsol law (Azar 1995) developed in the laboratory.

REFERENCES

Adam D. (2008). Tunnels and foundations as energy source–Practical applications in Austria. In *Deep Foundations on Bored and Auger Piles – BAP V: 5th International Symposium on Deep Foundations on Bored and Auger Piles*, van Impe WF and van Impe P (eds.). Taylor & Francis, pp. 337–342.

Adam D and Markiewicz R. (2009). Energy from earth-coupled structures, foundations, tunnels and sewers. *Géotechnique*, **59**(3): 229–236.

AFNOR. (2012). *Fondations profondes*, Norme française d'application nationale NF P 94-262. Paris.

Amatya B, Soga K, Bourne-Webb PJ *et al.* (2012). Thermo-mechanical behaviour of energy piles. *Géotechnique*, **62**(6): 503–519.

Bea RG, Audibert JME, and Dover AR. (1980). Dynamic response of laterally and axially loaded piles. Proceedings: *12th OTC Conference, Houston, TX*, **OTC 3749**, pp. 129–139.

Bjerrum L. (1973). Problems of soil mechanics and construction on soft clays and structurally unstable soils. Proceedings: *8th International Conference S.M. & F.E., Moscow, Rusia*, **13**, pp. 111–159.

Boënnec O. (2008). Shallow ground energy systems. *Proceedings of the ICE - Energy*, **161**(2): 57-61.

Boënnec O. (2009). Piling on the energy. In *GeoDrilling International*, March 2009: 150. Aspermont Media: London, pp. 25–28.

Boranyak S. (2013). International cooperation expands energy foundation technology. In *Deep Foundations: The Magazine of Deep Foundations Institute*, Mar/Apr 2013. DFI: Hawthorne, NJ, pp. 51–54.

Borel S. (2001). *Comportement et dimensionnement des fondations mixtes*. Etudes et recherches des Laboratoires des Ponts et Chaussées, Géotechnique et risques naturels. LCPC: Paris, 351 p.

Bourne-Webb PJ, Amatya B, and Soga K. (2013). A framework for understanding energy pile behaviour. *Proceedings of the ICE - Geotechnical Engineering*, **166**(GE2): 170-177.

Bourne-Webb PJ, Amatya B, Soga K *et al.* (2009). Energy pile test at Lambeth College, London: Geotechnical and thermodynamic aspects of pile response to heat cycles. *Géotechnique*, **59**(3): 237–248.

Bowles JE. (1997). *Foundation Analysis and Design* (5th edn). McGraw-Hill: Singapore, 1175 p.

Brandl H. (2006). Energy foundations and other thermo-active ground structures. *Géotechnique*, **56**(2): 81–122.

Brandl H. (2013). Thermo-active ground-source structures for heating and cooling. *Procedia Engineering*, **57**: 9–18.

Brown P. (1975). The significance of structure-foundation interaction. Proceedings: *2nd Australia-New Zealand Conference on Geomechanics, Australia*, pp. 79–82.

Brown P and Yu S. (1986). Load sequence and structure-foundation interaction. *Journal of Structural Engineering*, **112**(3): 481–488.

Burger A, Recordon E, and Bovet D. (1985). *Thermique des nappes souterraines*. Presses Polytchniques Romandes: Laussane, 255 p.

Campanella RG and Mitchell JK. (1968). Influence of temperature variations on soil behavior. *Journal of Soil Mechanics & Foundations Div.*, **94**(SM3): 709-734.

Cao J. (2010). *Modelisation numérique des problèmes d'interfaces sable-pieu pour les très grands nombres de cycles: Développement d'une méthode de sauts de cycles*. Doctoral thesis, University of Lille 1 Sciences and Technologies, Villeneuve d'Ascq, 139 p.

Cekerevac C and Laloui L. (2004). Experimental study of thermal effects on the mechanical behaviour of a clay. *International Journal for Numerical and Analytical Methods in Geomechanics*, **28**(3): 209–228.

Chin JT and Poulos HG. (1992). Cyclic axial pile loading analyses: A comparative study. *Computers and Geotechnics*, **13**: 137–158.

Choi JC, Lee SR, and Lee DS. (2011). Numerical simulation of vertical ground heat exchangers: Intermittent operation in unsaturated soil conditions. *Computers and Geotechnics*, **38**(8): 949–958.

Chow YK and Thevendran V. (1987). Optimisation of pile groups. *Computers and Geotechnics*, **4**(1): 43–58.

Clancy P and Randolph MF. (1993). An approximate analysis procedure for piled raft foundations. *International Journal for Numerical and Analytical Methods in Geomechanics*, **17**(12): 849–869.

Comodromos EM, Anagnostopoulos CT, and Georgiadis MK. (2003). Numerical assessment of axial pile group response based on load test. *Computers and Geotechnics*, **30**(6): 505–515.

Coyle HM and Reese LC. (1966). Load transfer for axially loaded piles in clay. *JSMFD, ASCE*, **92**(SM2): 1–26.

Coyle HM and Sulaiman IH. (1967). Skin friction for steel piles in sand. *JSMFD, ASCE*, **93**(SM6): 267–278.

Crawley J, Smith P, and Amis T. (2011). Ground soure heating and cooling for London complex. In *Deep Foundations: The Magazine of Deep Foundations Institute*, Spring 2011. DFI: Hawthorne, NJ, pp. 76–77.

De Gennaro V and Frank R. (2005). Modélisation de l'interaction sol-pieu par la méthode des éléments finis. In *Bulletin des Laboratoires des Ponts et Chaussées*: 256-257. Paris, pp. 107–133.

Deru MP and Kirkpatrick AT. (2001). Ground-coupled Heat and Moisture Transfer from Buildings Part 1: Analysis and Modeling. *American Solar Energy Society (ASES) National Solar Energy Conferences Forum, Washington D.C.*, pp. 1–9.

Desai C and Faruque M. (1984). Constitutive model for (geological) materials. *Journal of Engineering Mechanics*, **110**(9): 1391–1408.

Desai CS, Drumm EC, and Zaman MM. (1985). Cyclic testing and modelling of interfaces. *Journal of Geotechnical Engineering*, **111**(6): 793–815.

Desai CS and Fishman KL. (1991). Plasticity-based constitutive model with associated testing for joints. *International Journal of Rock Mechanics and Mining Sciences & Geomechanics Abstracts*, **28**(1): 15-26.

Devriendt M, Fairbairn T, Hirst J *et al.* (2012). One New Change. In *The Arup Journal*: 2/2012. ARUP: London, pp. 46–57.

Ennigkeit A and Katzenbach R. (2001). The double use of piles as foundation and heat exchanging elements. Proceedings: *15th International Conference on Soil Mechanics and Geotechnical Engineering (ICSMGE), Istanbul, Turkey*, **2**, pp. 893–896.

Fakharian K and Evgin E. (1997). Cyclic simple-shear behavior of sand-steel interfaces under constant normal stiffness condition. *Journal of Geotechnical and Geoenvironmental Engineering*, **123**(12): 1096–1105.

Fleming K, Weltman A, Randolph M *et al.* (2008). *Piling Engineering*. Taylor & Francis: Oxfordshire, UK, 408 p.

Frank R. (1995). *Fondations profondes*. Techniques de l'ingénieur Infrastructure de la construction. Techniques de l'ingénieur, 45 p.

Frank R and Zhao SR. (1982). Estimation par les paramètres pressiométriques de l'enfocement sous charge axiale de pieux forés dans des sols fins. *Bulletin de Liaison des Laboratoire des Ponts et Chaussées*, **119**: 17–24.

Fromentin A, Pahud D, Laloui L *et al.* (1999). Pieux échangeurs: conception et règles de pré-dimensionnement. *Revue française de génie civil*, **3**(6): 387–421.

Fung YYC and Tong P. (2001). *Classical and Computational Solid Mechanics*. Advanced Series in Engineering Science – Volume 1. World Scientific: Singapore, 930 p.

Gao J, Zhang X, Liu J *et al.* (2008). Thermal performance and ground temperature of vertical pile-foundation heat exchangers: A case study. *Applied Thermal Engineering*, **28**(17–18): 2295–2304.

Ghali A, Favre R, Badry M *et al.* (2002). Creep and shrinkage of concrete and relaxation of steel. In *Concrete Structures: Stresses and Deformations*. Taylor & Francis: London, pp. 1–19.

Goodman RE, Taylor RL, and Brekke TL. (1968). A model for the mechanics of jointed rock. *Journal of Soil Mechanics & Foundations Div*, **94**(SM3): 637–659.

Hadley WA and Eisenstadt R. (1955). Thermally actuated moisture migration in granular media. *Transactions–American Geophysical Union*, **36**: 615–623.

Hamada Y, Saitoh H, Nakamura M *et al.* (2007). Field performance of an energy pile system for space heating. *Energy and Buildings*, **39**(5): 517–524.

Herrmann LR. (1978). Finite element analysis of contact problems. *Journal of the Engineering Mechanics Division*, **104**(5): 1043–1057.

Hillel D. (2004). Soil Temperature and Heat Flow. In *Introduction to Environmental Soil Physics*. Elsevier Science, pp. 215–234.

Hofinger H, Markiewicz R, Adam D *et al.* (2010). Geothermal energy systems for major projects – design and construction / Geothermieanlagen bei Großprojekten – Planung und Umsetzung. *Geomechanics and Tunnelling*, **3**(5): 634–646.

Holmquist DV and Matlok H. (1976). Resistance-displacement relationships for axially-loaded piles in soft clay. Proceedings: *8th OTC Conference*, *Houston*, **OTC 2474**, pp. 554–569.

Hueckel T and Pellegrini R. (1989). Modeling of thermal failure of saturated clays. In *Proceeding of the 3rd International Symposium on Numerical Models in Geomechanics (NUMOG III)*, Pietruszczak S and Pande GN (eds.). Elsevier Applied Science, pp. 81–90.

ITASCA. (2005). FLAC3D Version 3.0 Theory and Background. Itasca Consulting Group, Inc., Minnesota, USA.

Jalaluddin and Miyara A. (2012). Thermal performance investigation of several types of vertical ground heat exchangers with different operation mode. *Applied Thermal Engineering*, **33–34**: 167–174.

Kaliakin VN and Li J. (1995). Insight into deficiencies associated with commonly used zero-thickness interface elements. *Computers and Geotechnics*, **17**(2): 225–252.

Katzenbach R, Ramm H, and Waberseck T. (2008). Economic and environment-friendly ways of designing and using deep foundations. In *The Application of Stress-wave Theory to Piles: Science, Technology and Practice - Proceedings of the 8th International Conference on the Application of Stress-Wave Theory to Piles : Lisbon, Portugal, 8-10 September 2008*, pp. 77-86.

Kavanaugh S. (2010). *Ground source heat pump system designer GSHPCalc Version 5.0 – An instruction guide for using a design tool for vertical ground-coupled, groundwater and surface water heat pumps systems*. Energy Information Services, Northport, AL.

Knellwolf C, Peron H, and Laloui L. (2011). Geotechnical analysis of heat exchanger piles. *Journal of Geotechnical and Geoenvironmental Engineering*, **137**(10): 890–902.

Kraft LM, Kagawa T, and Ray RP. (1981). Theoretical t–z curves. *Journal of Geotechnical Engineering*, **107**(GT11): 1543–1561.

Laboratory of Soil Mechanics EPFL. (2011). ThermoPile V.1 – Theorical Aspects. Swiss Federal Institute of Technology Lausanne, Lausanne.

Laloui L. (2001). Thermo-mechanical behaviour of soils. *Revue française de génie civil*, **5**(6): 809–843.

Laloui L and Di Donna A. (2011). Understanding the behaviour of energy geo-structures. *Proceedings of the ICE–Civil Engineering*, **64**(4): 184–191.

Laloui L, Moreni M, Fromentin A *et al.* (1999). Heat exchanger pile: Effect of the thermal solicitations on its mechanical properties. *Bulletin d'Hydrogéologie*, **17**.

Laloui L, Moreni M, and Vulliet L. (2003). Comportement d'un pieu bi-fonction, fondation et échangeur de chaleur. *Canadian Geotechnical Journal*, **40**(2): 388–402.

Laloui L, Nuth M, and Vulliet L. (2006). Experimental and numerical investigations of the behaviour of a heat exchanger pile. *International Journal for Numerical and Analytical Methods in Geomechanics*, **30**(8): 763–781.

Lemaitre J, Chaboche JL, Benallal A *et al.* (2009). *Mécanique des matériaux solides* (3ème edn). Dunod: Paris, 596 p.

Loveridge F and Powrie W. (2013). Pile heat exchangers: thermal behaviour and interactions. *Proceedings of the ICE–Geotechnical Engineering*, **166**(GE2): 178–196.

Lund J, Sanner B, Rybach L *et al.* (2004). Geothermal (Ground-Source) Heat Pumps – A World Overview. *GHC Bulletin*, **25**(3): 1–10.

Ma X and Grabe J. (2010). Efficiency increase of soil heat exchangers due to groundwater flow and air injection wells. *World Geothermal Congress 2010, Bali, Indonesia*.

Malvern LE. (1969). *Introduction to the Mechanics of a Continuous Medium*. Prentice Hall: Englewood Cliffs, New Jersey, 713 p.

Markiewicz R, Adam D, Hofinger J *et al.* (2005). Extraction of geothermal enegy from tunnels. Proceedings: *16th International Conference on Soil Mechanics and Geotechnical Engineering (ICSMGE), Osaka, Japan*, **3**, pp. 1629–1632.

Ménard L. (1975). *Règles d'utilisation des techniques pressiométriques et d'exploitation des résultats obtenus pour le calcul des fondations*, Notice génerale D.60. Paris.

Monnet A and Bernhardt V. (2000). Quelques propositions au sujet des fondations profondes. *Revue française de géotechnique*, **90**: 15–24.

Mortara G. (2008). Analysis of the interface behavior under cyclic loading. In *AIP Conference Proceedings of the 2008 Seismic Engineering Conference*

Commemorating the 1908 Messina and Reggio Calabria Earthquake, Santini A and Moraci N (eds.). AIP: Reggio Calabria, Italy, pp. 658–665.

Mortara G, Boulon M, and Ghionna VN. (2002). A 2-D constitutive model for cyclic interface behaviour. *International Journal for Numerical and Analytical Methods in Geomechanics*, **26**(11): 1071–1096.

Mortara G, Mangiola A, and Ghionna VN. (2007). Cyclic shear stress degradation and post-cyclic behaviour from sandsteel interface direct shear tests. *Canadian Geotechnical Journal*, **44**(7): 739–752.

Navayogarajah N, Desai C, and Kiousis P. (1992). Hierarchical single-surface model for static and cyclic behavior of interfaces. *Journal of Engineering Mechanics*, **118**(5): 990–1011.

Ng CWW, Simons N, and Menzies B. (2004). *A Short Course in Soil-Structure Engineering of Deep Foundations, Excavations and Tunnels*. Thomas Telford Publishing: London, 408 p.

Pahud D and Hubbuch M. (2007a). Measured Thermal Performances of the Energy Pile System of the Dock Midfield at Zürich Airport. *European Geothermal Congress 2007, Unterhaching, Germany*.

Pahud D and Hubbuch M. (2007b). *Mesures et optimisation de l'installation avec pieux énergétiques du Dock Midfield de l'aéroport de Zürich*, Projet DIS no 37'373 contrat DIS no 77'133, Rapport final. Office féderale de l'énergie, Ittigen, Switzerland.

Parlange MB, Cahill AT, Nielsen DR *et al.* (1998). Review of heat and water movement in field soils. *Soil and Tillage Research*, **47**(1–2): 5–10.

Parry RHG. (2004). *Mohr Circles, Stress Paths and Geotechnics* (2nd edn). Taylor & Francis: London, 280 p.

Philip JR and de Vries DA. (1957). Moistrure Movement in Porous Materials under Temperature Gradients. *Transactions—American Geophysical Union*, **38**: 222–232.

Piechowski M. (1999). Heat and mass transfer model of a ground heat exchanger: Theoretical development. *International Journal of Energy Research*, **23**(7): 571–588.

Potts DM and Zdravkovic L. (2001). *Finite Element Analysis in Geotechnical Engineering: Volume Two – Application*. Thomas Telford Publishing: London, 427 p.

Poulos HG. (1982). Influence of cyclic loading on axial pile response. Proceedings: *2nd International Conference on Numerical Methods in Offshore Piling, Austin, TX*, pp. 419–440.

Poulos HG. (1989). Pile behaviour – Theory and application. *Géotechnique*, **39**(3): 365–415.

Poulos HG and Davis EH. (1980). *Pile foundation analysis and design*. John Wiley & Sons: New York, 397 p.

Prakash S and Sharma HD. (1990). *Pile Foundations in Engineering Practice*. John Wiley & Sons: Danvers, Massachusetts, 768 p.

Randolph MF. (1986). *RATZ – Load transfer analysis of axially loaded piles*, Report No. Geo 86033, Research Report. Civil Engineering Department, University of Western Australia, Perth.

Randolph MF. (2003a). RATZ Manual Version 4-2 – Load transfer analysis of axially loaded piles. The University of Western Australia.

Randolph MF. (2003b). Science and empiricism in pile foundation design. *Géotechnique*, **53**(10): 847–875.

Randolph MF and Wroth CP. (1978). Analysis of deformation of vertically loaded piles. *Journal of Geotechnical Engineering*, **104**(GT12): 1465–1488.

Reese LC, Isenhower WM, and Wang S-T. (2006). Geotechnical Design of Driven Piles under Axial Loads. In *Analysis and Design of Shallow and Deep Foundations*. John Wiley & Sons: New Jersey, pp. 270–305.

Reese LC and O'Neill MW. (1987). *Drilled Shafts: Construction Procedures and Design Methods*. US Department of Transportation, Federal Highway Administration, Virginia.

Riederer P, Evars G, Gourmez D *et al.* (2007). *Conception de fondations geothermiques*, Rapport final ESE/ENR no 07.044RS, Rapport d'étude. Centre Scientifique et Technique du Bâtiment, Sophia-Antipolis, France.

Rouissi K, Krarti M, and McCartney JS. (2012). Analysis of Thermo-Active Foundations With U-Tube Heat Exchangers. *Journal of Solar Energy Engineering*, **134**(2): 021008-1-8.

Said I. (2006). *Comportement des interfaces et modélisation des pieux sous charge axiale*. Doctoral thesis, Ecole Nationale des Ponts et Chaussées, Champs-sur-Marne, 274 p.

Saner B. (2001). Shallow geothermal energy. *GHC Bulletin*, **22**(4): 19–25.

Schofield AN and Wroth CP. (1968). *Critical state soil mechanics*. McGraw Hill: London, 310 p.

Shahrour I and Rezaie F. (1997). An elastoplastic constitutive relation for the soil-structure interface under cyclic loading. *Computers and Geotechnics*, **21**(1): 21–39.

Suryatriyastuti ME, Mroueh H, and Burlon S. (2012). Understanding the temperature-induced mechanical behaviour of energy pile foundations. *Renewable and Sustainable Energy Reviews*, **16**(5): 3344–3354.

Uesugi M and Kishida H. (1991). Discussion of 'Cyclic axial loading analysis of piles in sand' by Poulos. *Journal of Geotechnical Engineering*, **117**(9): 1435–1457.

Xia Z, Kujawski D, and Ellyin F. (1996). Effect of mean stress and ratcheting strain on fatigue life of steel. *International Journal of Fatigue*, **18**(5): 335–341.

APPENDIX A: LOAD TRANSFER CALCULATION UNDER MONOTONIC LOADING

The procedure described below is used for the calculation of load–transfer of a pile under monotonic loading. The pile is divided into *k* segments shown in Figure 5.10, for segment n^o *1* indicates the segment at the top of the pile and segment n^o *k* indicates the segment at the bottom of the pile.

(1) Assume an initial value of the tip movement w_b at the bottom segment *k*

(2) Search the value of the end-bearing stress q_b at the pile base with the imposed w_b by using Equation 5.4 of the proposed *t*–*z* function

$$q_b = q_{b0}\left(1 - e^{-\frac{u_t}{\alpha_b}}\right) + \beta_b {u_t}^{\delta_b} e^{-\left(\frac{u_t}{\gamma_b}\right)^{\delta}}$$

(3) Calculate the end-bearing resistance

$$Q_b = q_b\left(\frac{1}{4}\pi B^2\right) \tag{A.1}$$

(4) Calculate the elastic deformation at the lower half of segment *k*

$$\varepsilon_b^e = \frac{Q_b}{\frac{1}{4}\pi B^2 E_M} \tag{A.2}$$

(5) Calculate the midpoint movement at segment *k*

$$w_k = w_b + \frac{1}{2} h_k \varepsilon_b^e \tag{A.3}$$

(6) By applying the estimated midpoint movement at segment *k*, search the value of shaft friction at segment *k*, using Equation 5.4 of the proposed *t*–*z* function

$$q_s = q_{s0}\left(1 - e^{-\frac{u_t}{\alpha_s}}\right) + \beta_s {u_t}^{\delta_s} e^{-\left(\frac{u_t}{\gamma_s}\right)^{\delta}}$$

(7) Calculate the axial load at the midpoint of segment *k*

$$Q_k = Q_b + \pi B \frac{1}{2} h_k q_{s\,k} \tag{A.4}$$

(8) Calculate the elastic deformation at the upper half of segment *k* and at the lower half of segment *k – 1*

$$\varepsilon_k^e = \frac{Q_k}{\frac{1}{4}\pi B^2 E_M} \tag{A.5}$$

(9) Calculate the midpoint movement at segment *k – 1*

$$w_{k-1} = w_k + \frac{1}{2}\left(h_k + h_{k-1}\right)\varepsilon_k^e \tag{A.6}$$

(10) Search the value of shaft friction at segment *k – 1*, using Equation 5.4 of the proposed *t*–*z* function

$$q_s = q_{s0}\left(1 - e^{-\frac{u_t}{\alpha_s}}\right) + \beta_s {u_t}^{\delta_s} e^{-\left(\frac{u_t}{\gamma_s}\right)^{\delta}}$$

(11) Calculate the axial load at the midpoint of segment *k – 1*

$$Q_{k-1} = Q_k + \pi B \frac{1}{2}\left(h_k + h_{k-1}\right) q_{s\,k-1} \tag{A.7}$$

(12) Do the iteration from the lower half of segment *k – 2* until the midpoint of top segment by repeating step 8–11

(13) For the upper half of segment *1*, calculate the response of the pile head

$$w_h = w_1 + \frac{1}{2} h_1 \varepsilon_1^e \tag{A.8}$$

$$Q_h = Q_1 + \pi B \frac{1}{2} h_1 q_{s1} \tag{A.9}$$

APPENDIX B:
LOAD TRANSFER CALCULATION UNDER CYCLIC THERMAL LOADING

This following calculation procedure is done during cyclic thermal loading in this study, for both free head pile and restrained head pile. The procedure is repeated for each load cycle. The division of pile segments is shown in Figure 5.10, for segment n^o *1* indicates the segment at the top of the pile and segment n^o *k* indicates the segment at the bottom of the pile.

(1) Boundary conditions of model:
- for free head pile under constant load $Q_h{}^n \cong Q_h{}^{mec}$
- for fully restrained head pile under constant displacement $w_h{}^n \cong w_h{}^{mec}$

(2) Delta temperature ±10°C from the ground temperature is applied uniformly along the pile. Calculate the thermal deformation induced by temperature variations:

$$\varepsilon^{th} = \alpha_T \Delta T \tag{B.1}$$

(3) Assume an initial value of the tip movement $w_b{}^n$ at the bottom segment *k*

(4) Search the value of the end-bearing stress $q_b{}^n$ at the pile base with the imposed $w_{b,}{}^n$ by using Equation 5.5 of the proposed *t–z* function

$$q_b = q_{bi} + A(-1)^{n+1}\left[\begin{array}{c}\left(q_{b0} + \Delta q_b\left(1 - e^{-\frac{u_{ts}}{\varepsilon_b}}\right)\right)\left(1 - e^{-R_b\left|\frac{u_t - u_{ti}}{\alpha_b}\right|}\right) \\ + \beta_b e^{-\frac{u_{ts}}{\varepsilon_b}}\left|u_t - u_{ti}\right|^{\delta_b} e^{-\left(\frac{u_t - u_{ti}}{\gamma_b}\right)^2}\end{array}\right]$$

(5) Calculate the end-bearing resistance

$$Q_b{}^n = q_b{}^n \times \frac{1}{4}\pi B^2 \tag{B.2}$$

(6) Calculate the elastic deformation at the lower half of segment *k*

$$\varepsilon_b^{e\,n} = \frac{Q_b{}^n}{\frac{1}{4}\pi B^2 E_M} + \varepsilon^{th} \tag{B.3}$$

(7) Calculate the midpoint movement at segment *k*

$$w_k{}^n = w_b{}^n + \frac{1}{2} h_k \varepsilon_p^{e\,n} \tag{B.4}$$

(8) By applying the estimated midpoint movement at segment *k*, search the value of shaft friction using Equation 5.5 of the proposed *t–z* function

$$q_s = q_{si} + A(-1)^{n+1}\left[\left(q_{s0} + \Delta q_s\left(1 - e^{-\frac{u_{ts}}{\varepsilon_s}}\right)\right)\left(1 - e^{-R_s\left|\frac{u_t - u_{ti}}{\alpha_s}\right|}\right) + \beta_s e^{-\frac{u_{ts}}{\varepsilon_s}}\left|u_t - u_{ti}\right|^{\delta_s} e^{-\left(\frac{u_t - u_{ti}}{\gamma_s}\right)^2}\right]$$

(9) Calculate the axial load at the midpoint of segment *k*

$$Q_k{}^n = Q_b{}^n + \pi B \frac{1}{2} h_k q_{s\,k}{}^n \tag{B.5}$$

(10) Calculate the elastic deformation at the upper half of segment *k* and at the lower half of segment *k* – 1 with the additional thermal deformation included

$$\varepsilon_k^{e\,n} = \frac{Q_k{}^n}{\frac{1}{4}\pi B^2 E_M} + \varepsilon^{th} \tag{B.6}$$

(11) Calculate the midpoint movement at segment *k* – 1

$$w_{k-1}{}^n = w_k{}^n + \frac{1}{2}\left(h_k + h_{k-1}\right)\varepsilon_k^{e\,n} \tag{B.7}$$

(12) Search the value of shaft friction at segment *k* – 1, using Equation 5.5 of the proposed *t–z* function

(13) Calculate the axial load at the midpoint of segment *k* – 1

$$Q_{k-1}{}^n = Q_k{}^n + \pi B \frac{1}{2}\left(h_k + h_{k-1}\right) q_{s\,k-1}{}^n \tag{B.8}$$

(14) Do the iteration from the lower half of segment k – 2 until the midpoint of top segment by repeating step 10–13

(15) For the upper half of segment 1, calculate the response of the pile head

$$w_h{}^n = w_1{}^n + \frac{1}{2} h_1 \varepsilon_1^{e\,n} \tag{B.9}$$

$$Q_h{}^n = Q_1{}^n + \pi B \frac{1}{2} h_1 q_{s1}{}^n \tag{B.10}$$

(16) Repeat step 3–15 until the limit conditions are achieved

APPENDIX C: PUBLICATIONS

The materials presented in this thesis have been, or are in the process of being, published elsewhere. The following sections provide details of these publications.

Book chapters:

[SUR 13b] Suryatriyastuti ME, Mroueh H, Burlon S, and Habert J. (2013). Numerical Analysis of the Bearing Capacity of Thermoactive Piles Under Cyclic Axial Loading. In *Energy Geostructures*, Laloui L and Di Donna A (eds.). John Wiley & Sons: Hoboken, NJ, pp. 139–155. doi: 10.1002/9781118761809.ch7

[SUR 13c] Suryatriyastuti ME, Mroueh H, and Burlon S. (2013). Impact of Transient Heat Diffusion of a Thermoactive Pile on the Surrounding Soil. In *Energy Geostructures*, Laloui L and Di Donna A (eds.). John Wiley & Sons: Hoboken, NJ, pp. 193–209. doi: 10.1002/9781118761809.ch10

Journal papers:

Suryatriyastuti ME, Mroueh H, and Burlon S. *(under review)*. Cyclic effects on the axial capacity of thermo-active piles. *Acta Geotechnica*.

[SUR 14] Suryatriyastuti ME, Mroueh H, and Burlon S. (2014). A load transfer approach for studying the cyclic behavior of thermo-active piles. *Computers and Geotechnics*, **55**: 378–391. doi: 10.1016/j.compgeo.2013.09.021

[SUR 12a] Suryatriyastuti ME, Mroueh H, and Burlon S. (2012). Understanding the temperature-induced mechanical behaviour of energy pile foundations. *Renewable and Sustainable Energy Reviews*, **16**(5): 3344–3354. doi: 10.1016/j.rser.2012.02.062

Conference papers:

[SUR 13d] Suryatriyastuti ME, Mroueh H, and Burlon S. (2013). Analyse de la portance des pieux géothermiques. Proceedings: *18th International Conference on*

Soil Mechanics and Geotechnical Engineering, 2–6 September, Paris, France, pp. 3407–3710.

[SUR 13a] Suryatriyastuti ME, Mroueh H, and Burlon S. (2013). Numerical analysis of thermo-active piles under cyclic thermal loads. *European Geothermal Congress 2013*, 4–6 June, Pisa, Italy.

[SUR 12c] Suryatriyastuti ME, Mroueh H, and Burlon S. (2012). Study of the performance of constitutive laws for interface soil-pile under cyclic solicitation. *10th International Congress on Advances in Cvil Engineering*, 17–19 October, Ankara, Turkey.

[SUR 12b] Suryatriyastuti ME, Mroueh H, and Burlon S. (2012). Modélisation numérique du comportement mécanique d'un pieu échangeur de chaleur. In *Acte des Journées Nationals de Géotechnique et de Géologie de l'Ingénieur JNGG 2012*, 4–6 July, Bordeaux, France, pp. 593–600.

[SUR 11b] Suryatriyastuti ME, Mroueh H, and Burlon S. (2011). Thermo-mechanics behaviour of energy piles subjeted by monotonic thermal loading. *20ème Congres Français de Mécanique – Colloque Euroméditerranée*, 28 August–2 September, Besançon, France.

[SUR 11a] Suryatriyastuti ME, Mroueh H, and Burlon S. (2011). Mechanical behaviour of energy piles in thermal regime. Proceedings: *12th International Conferences on Quality in Research*, 4–7 July, Bali, Indonesia, pp. 2184–2191.